

DESIGN OF MOVING TARGET INDICATION FILTERS WITH NON-UNIFORM PULSE
REPETITION INTERVALS

A THESIS SUBMITTED TO
THE GRADUATE SCHOOL OF NATURAL AND APPLIED SCIENCES
OF
MIDDLE EAST TECHNICAL UNIVERSITY

BY

MEHMET İSPİR

IN PARTIAL FULFILLMENT OF THE REQUIREMENTS
FOR
THE DEGREE OF MASTER OF SCIENCE
IN
ELECTRICAL AND ELECTRONICS ENGINEERING

JANUARY 2013

Approval of the thesis:

**DESIGN OF MOVING TARGET INDICATION FILTERS WITH
NON-UNIFORM PULSE REPETITION INTERVALS**

submitted by **MEHMET İSPİR** in partial fulfillment of the requirements for the degree of
**Master of Science in Electrical and Electronics Engineering Department, Middle
East Technical University** by,

Prof. Dr. Canan Özgen _____
Dean, Graduate School of **Natural and Applied Sciences**

Prof. Dr. İsmet Erkmek _____
Head of Department, **Electrical and Electronics Engineering**

Assoc. Prof. Dr. Çağatay Candan _____
Supervisor, **Electrical and Electronics Engineering Dept., METU**

Examining Committee Members:

Prof. Dr. Tolga Çiloğlu _____
Electrical and Electronics Engineering Dept., METU

Assoc. Prof. Dr. Çağatay Candan _____
Electrical and Electronics Engineering Dept., METU

Assoc. Prof. Dr. Ali Özgür Yılmaz _____
Electrical and Electronics Engineering Dept., METU

Assist. Prof. Dr. Umut Orguner _____
Electrical and Electronics Engineering Dept., METU

Dr. Alper Yıldırım _____
Chief Researcher, TÜBİTAK BİLGEM İLTAREN

Date: _____

I hereby declare that all information in this document has been obtained and presented in accordance with academic rules and ethical conduct. I also declare that, as required by these rules and conduct, I have fully cited and referenced all material and results that are not original to this work.

Name, Last Name: MEHMET İSPİR

Signature :

ABSTRACT

DESIGN OF MOVING TARGET INDICATION FILTERS WITH NON-UNIFORM PULSE REPETITION INTERVALS

İspir, Mehmet

M.Sc., Department of Electrical and Electronics Engineering

Supervisor : Assoc. Prof. Dr. Çağatay Candan

January 2013, 102 pages

Staggering the pulse repetition intervals is a widely used solution to alleviate the blind speed problem in Moving Target Indication (MTI) radar systems. It is possible to increase the first blind speed on the order of ten folds with the use of non-uniform sampling. Improvement in blind speed results in passband fluctuations that may degenerate the detection performance for particular Doppler frequencies. Therefore, it is important to design MTI filters with non-uniform interpulse periods that have minimum passband ripples with sufficient clutter attenuation along with good range and blind velocity performance.

In this thesis work, the design of MTI filters with non-uniform interpulse periods is studied through the least square, convex and min-max filter design methodologies. A trade-off between the contradictory objectives of maximum clutter suppression and minimum desired signal attenuation is established by the introduction of a weight factor into the designs. The weight factor enables the adaptation of MTI filter to different operational scenarios such as the operation under low, medium or high clutter power.

The performances of the studied designs are investigated by comparing the frequency response characteristics and the average signal-to-clutter suppression capabilities of the filters with respect to a number of defined performance measures. Two further approaches are considered to increase the signal-to-clutter suppression performance. First approach is based on a modified min-max filter design whereas the second one focuses on the multiple filter implementations. In addition, a detailed review and performance comparison with the non-uniform MTI filter designs from the literature are also given.

Keywords: MTI Radar, Non-uniform PRF, Non-uniform Filtering, Clutter Suppression, Blind Speed

ÖZ

DÜZENSİZ DARBE TEKRARLAMA ARALIKLARINA SAHİP HAREKETLİ HEDEF BELİRTİSİ SÜZGEÇLERİ TASARIMI

İspir, Mehmet

Yüksek Lisans, Elektrik Elektronik Mühendisliği Bölümü

Tez Yöneticisi : Doç. Dr. Çağatay Candan

Ocak 2013, 102 sayfa

Darbe tekrarlama aralıklarını değiştirmek, Hareketli Hedef Belirtisi (MTI) radar sistemlerinde kör hız problemini azaltmak için yaygın olarak kullanılan bir çözümdür. Düzgün olmayan örnekleme ile ilk kör hızın yaklaşık olarak on kat artırılması mümkündür. Kör hızdaki iyileşme, belirli Doppler frekanslarındaki tespit performansını azaltabilecek geçirme kuşağı salınımlarına neden olmaktadır. Bu nedenle en küçük geçirme kuşağı dalgalanmasına sahip ve yeterli kargaşa bastırımının yanında, iyi mesafe ve kör hız performansı olan, değişken aralıklı MTI süzgeç tasarımı önemlidir.

Bu tez çalışmasında, değişken aralıklı MTI süzgeç tasarımı en küçük kareler, konveks ve en küçük-en büyük süzgeç tasarımı metodolojileri kullanılarak çalışılmıştır. Tasarımlara ağırlık faktörü eklenmesi ile, çakışan en büyük kargaşa bastırımı ve en küçük istenen sinyal bastırımı amaçları arasında ilişki oluşturulmuştur. Ağırlık faktörü MTI süzgecinin düşük, orta ve yüksek güçlü kargaşa ortamlarında işleyiş gibi farklı operasyonel senaryolara adaptasyonuna olanak sağlamaktadır.

Çalışılan tasarımların performansları, süzgeçlerin frekans cevap karakteristikleri ve ortalama sinyal-kargaşa bastırımı yetenekleri tanımlanan birkaç performans ölçütüne göre karşılaştırılarak incelenmiştir. Sinyal-kargaşa bastırımını artırmak için ilaveten iki yaklaşım değerlendirilmiştir. İlk yaklaşım değiştirilmiş en küçük-en büyük süzgeç tasarımına dayanmakta iken, ikincisi ise önerilen süzgeç tasarımlarının çoklu süzgeçler olarak uygulamasına odaklanmaktadır. Ek olarak, literatürdeki düzensiz MTI süzgeç tasarımları ile de detaylı bir gözden geçirme ve performans karşılaştırması verilmiştir.

Anahtar Kelimeler: MTI Radar, Düzensiz DTF, Düzensiz Süzgeçleme, Kargaşa Bastırımı, Kör Hız

To My Family

ACKNOWLEDGMENTS

By the completion of this thesis work, I have the opportunity to express my sincere gratitudes to several people for their support and guidance.

I am truly indebted and thankful to my supervisor Assoc. Prof. Dr. Çağatay Candan for his valuable suggestions, criticism and guidance throughout the thesis work. The theoretical discussions with him was very informative and guided me to the right direction all the time. He always allocated time to clarify my questions and doubts, despite his busy schedules. I feel very lucky to find the chance to work with him for my Master's degree.

I would like to thank my family for their constant encouragement and support.

I also wish to thank to my colleagues at TÜBİTAK BİLGEM İLTAREN for their help and kindness. I gained a lot from their inputs and experience.

TABLE OF CONTENTS

ABSTRACT	v
ÖZ	vii
ACKNOWLEDGMENTS	x
TABLE OF CONTENTS	xi
LIST OF TABLES	xiii
LIST OF FIGURES	xv
CHAPTERS	
1 INTRODUCTION	1
2 BACKGROUND	5
2.1 Moving Target Indication (MTI) Radar	5
2.1.1 Operation of a Coherent MTI Radar	6
2.2 MTI Filtering	8
2.2.1 Delay Line Cancellers	9
2.2.2 FIR Type MTI Filters	11
2.2.3 Recursive MTI Filters	13
2.3 MTI Improvement Factor	13
2.4 Blind Speed Problem	16
2.5 Staggered PRI Design	17
3 NON-UNIFORM MTI FILTER DESIGN	21
3.1 Non-uniform FIR Filter Design	21
3.2 Performance Measures of Staggered MTI Filter	23
3.3 Least Square Design	25
3.4 Convex Design	31
3.5 Min-Max Design	35
3.6 Numerical Comparison with Selected Filter Designs	43
3.6.1 Binomial Filter	43
3.6.2 Prinsen's Filter	43
4 CLUTTER SUPPRESSION PERFORMANCE OF FILTER DESIGNS	51
4.1 Characteristics of Clutter	51
4.2 Comparison of Designed Filters with Optimal MTI Filter	54
4.3 Min-Max Filter Design with Optimum Improvement Factor	59
4.4 Multiple Filter Design with Time Varying Coefficients	64

5	COMPARISON OF FILTER DESIGNS WITH SELECTED STUDIES	81
5.1	Hsiao's Design	81
5.2	Jacomini's Design	85
5.3	Ewell's Design	88
5.4	Zuyin's Design	91
6	CONCLUSION	95
6.1	Results and Conclusion	95
6.2	Future Work	96
	REFERENCES	97
APPENDICES		
A	FILTER WEIGHTS FOR COMPARISON WITH SELECTED STUDIES . . .	101

LIST OF TABLES

TABLES

Table 2.1	Filter Weights for First 5 <i>N-pulse Cancellers</i>	13
Table 2.2	First Blind Speeds for Different Radar Bands [1]	17
Table 3.1	Performance Measures of Least Square Design for Different \mathcal{W} Values	29
Table 3.2	Performance Measures of Convex Design for Different \mathcal{W} Values	33
Table 3.3	Performance Measures of Min-Max Design for Different \mathcal{W} Values	37
Table 3.4	Performance Measures for Min-max Design for Different Initial Filter Coefficients with Same \mathcal{W} Values	40
Table 3.5	Performance Measures of Min-Max Design for Different Stopband Attenuation Requirement with Different Initial Conditions and \mathcal{W} Values	42
Table 3.6	Performance Measures for Comparison of Designed Filters with Binomial and Prinsen’s Filter with Same Stopband Attenuation Requirement	46
Table 3.7	Performance Measures for Comparison of Designed Filters with Binomial and Prinsen’s Filter with Smaller Cutoff Frequency	47
Table 3.8	Performance Measures for Comparison of Designed Filters with Binomial and Prinsen’s Filter with Bigger Cutoff Frequency	48
Table 3.9	Performance Measures for Comparison of Designed Filters with Binomial and Prinsen’s Filter with Larger Velocity Band	49
Table 4.1	Used Clutter Models and Related Values of Parameters	54
Table 4.2	Performance Measures for Comparison of Designed Filters with Prinsen’s Filter	56
Table 4.3	Improvement Factor Values for Comparison of Designed Filters with Prinsen’s Filter with Gaussian Clutter PSD	57
Table 4.4	Improvement Factor Values for Comparison of Designed Filters with Prinsen’s Filter with Gaussian Clutter PSD with Larger Doppler Spread	58
Table 4.5	Performance Measures of the Comparison of Minmax-IF Filter with Other Filter Designs	61
Table 4.6	Improvement Factor Values for Comparison of Designed Filters with Gaussian Clutter	62
Table 4.7	Improvement Factor Values for Comparison of Designed Filters with Gaussian Clutter with Larger Doppler Spread	63
Table 4.8	Performance Measures of Designed Filters for Stagger Ratio 16:20:17:22	68
Table 4.9	Improvement Factor Values of Designed Filters for Stagger Ratio 16:20:17:22	69
Table 4.10	Performance Measures of Total Power Response of Designed Filters for Stagger Ratio 16:20:17:22:16:20:17	70

Table 4.11 Improvement Factor Values of Designed Single Filters for Stagger Ratio 16:20:17:22:16:20:17	71
Table 4.12 Performance Measures of Designed Filters for Stagger Ratio 16:20:17:22 . . .	74
Table 4.13 Performance Measures of Designed Filters for Stagger Ratio 20:17:22:16 . . .	74
Table 4.14 Performance Measures of Designed Filters for Stagger Ratio 17:22:16:20 . . .	74
Table 4.15 Performance Measures of Designed Filters for Stagger Ratio 22:16:20:17 . . .	74
Table 4.16 Performance Measures of Designed Filters for Stagger Ratio 16:20:17:22 . . .	77
Table 4.17 Performance Measures of Designed Filters for Stagger Ratio 20:17:22:16 . . .	77
Table 4.18 Performance Measures of Designed Filters for Stagger Ratio 17:22:16:20 . . .	77
Table 4.19 Performance Measures of Designed Filters for Stagger Ratio 22:16:20:17 . . .	77
Table 4.20 Performance Measures of Designed Multiple Filters used for Stagger Ratio 16:20:17:22:16:20:17	78
Table 4.21 Improvement Factor Values of Designed Multiple Filters used for Stagger Ratio 16:20:17:22:16:20:17	79
Table 5.1 Performance Measures for Magnitude Response Comparison of Designed Fil- ters with Hsiao's Filter	83
Table 5.2 Improvement Factor Values of Designed Filters with Hsiao's Filter	84
Table 5.3 Performance Measures for Magnitude Response Comparison of Designed Fil- ters with Jacomini's Filter	86
Table 5.4 Improvement Factor Values of Designed Filters with Jacomini's Filter	87
Table 5.5 Performance Measures for Magnitude Response Comparison of Designed Fil- ters with Ewell's Filter	89
Table 5.6 Improvement Factor Values of Designed Filters with Ewell's Filter	90
Table 5.7 Performance Measures for Magnitude Response Comparison of Designed Fil- ters with Zuyin's Filter	92
Table 5.8 Improvement Factor Values of Designed Filters with Zuyin's Filter	93
Table A.1 Staggered MTI Filter Weights for Comparison with Hsiao's Study	101
Table A.2 Staggered MTI Filter Weights for Comparison with Jacomini's Study	101
Table A.3 Staggered MTI Filter Weights for Comparison with Ewell's Study	102
Table A.4 Staggered MTI Filter Weights for Comparison with Zuyin's Study	102

LIST OF FIGURES

FIGURES

Figure 2.1	Simplified Block Diagram of A Coherent MTI System [2]	6
Figure 2.2	MTI Processing of Received Echos from Successive Transmitted Pulses	8
Figure 2.3	Filter Structure of the Single Delay Line Canceller	9
Figure 2.4	Magnitude Response of Single Delay Line Canceller	10
Figure 2.5	Filter Structure of the Double Delay Line Canceller	10
Figure 2.6	Magnitude Response Comparison of Single and Double Delay Line Cancellers	11
Figure 2.7	Magnitude Response Comparison of Cascaded Single Delay Line Cancellers	11
Figure 2.8	General Structure of a Uniform FIR Filter	12
Figure 2.9	Double Delay Line Canceller Representation as a Transversal Filter Structure	12
Figure 2.10	IIR Filter Structure	14
Figure 2.11	Magnitude Response of Different Types of Shaped MTI Filters [3]	14
Figure 2.12	Magnitude Response Comparison of MTI Filter with Uniform and Staggered PRI	18
Figure 3.1	Non-uniform FIR Filter Structure	22
Figure 3.2	Regions for the MTI Filter Design	22
Figure 3.3	Performance Measures of the Staggered PRF MTI Filter Design	24
Figure 3.4	Frequency Response of Desired Highpass Filter	25
Figure 3.5	Frequency Response of Least Square Design with Different \mathcal{W} Values	29
Figure 3.6	Effect of \mathcal{W} on MSA, SA, MPE and MD for Least Square Design	30
Figure 3.7	Frequency Response of Convex Design with Different \mathcal{W} Values	33
Figure 3.8	Effect of \mathcal{W} on MSA, SA, MPE and MD for Convex Design	34
Figure 3.9	Frequency Response of Min-Max Design with Different \mathcal{W} Values	37
Figure 3.10	Effect of \mathcal{W} on MSA, SA, MPE and MD for Min-max Design for Same Initial Coefficients	38
Figure 3.11	Frequency Response of Min-Max Design for Different Initial Conditions with the Same \mathcal{W} Values	40
Figure 3.12	Effect of Initial Filter Coefficients on Performance Measures of Min-Max Design for Same \mathcal{W} Values	41
Figure 3.13	Min-Max Design for Different Stopband Attenuation Requirement with Dif- ferent Initial Conditions and \mathcal{W} Values	42
Figure 3.14	Comparison of Designed Filters with Binomial and Prinsen's Filter with Same Stopband Attenuation Requirement	46

Figure 3.15 Comparison of Designed Filters with Binomial and Prinsen's Filter with Smaller Cutoff Frequency	47
Figure 3.16 Comparison of Designed Filters with Binomial and Prinsen's Filter with Bigger Cutoff Frequency	48
Figure 3.17 Comparison of Designed Filters with Binomial and Prinsen Filter's with Larger Velocity Band	49
Figure 4.1 Gaussian Clutter Power Spectrum Density Model	52
Figure 4.2 Comparison of Optimum MTI Filters with Different Clutter PSD's	53
Figure 4.3 Frequency Response Comparison of Designed Filters with Prinsen's Filter	56
Figure 4.4 Improvement Factor Comparison of Designed Filters with Prinsen's Filter with Gaussian Clutter PSD	57
Figure 4.5 Improvement Factor Comparison of Designed Filters with Prinsen's Filter with Gaussian Clutter PSD with Larger Doppler Spread	58
Figure 4.6 Frequency Response Comparison of Minmax-IF Filter with Other Filter Designs	61
Figure 4.7 Improvement Factor Comparison of Designed Filters with Gaussian Clutter	62
Figure 4.8 Improvement Factor Comparison of Designed Filters with Gaussian Clutter with Larger Doppler Spread	63
Figure 4.9 Processing of Received Pulses with Multiple Filter Structure with Time Varying Coefficients	65
Figure 4.10 Frequency Response of Designed Filters for Stagger Ratio 16:20:17:22 (Single Filter)	68
Figure 4.11 Improvement Factor Plots of Designed Filters for Stagger Ratio 16:20:17:22 (Single Filter)	69
Figure 4.12 Total Power Response of Designed Time Invariant Single Filters for Stagger Ratio 16:20:17:22:16:20:17 (Multiple Filter)	70
Figure 4.13 Improvement Factor Plots of Designed Time Invariant Single Filters for Stagger Ratio 16:20:17:22:16:20:17 (Multiple Filter)	71
Figure 4.14 Passband Response of Designed Single Filters for Stagger Ratios 16:20:17:22, 20:17:22:16, 17:22:16:20, 22:16:20:17	72
Figure 4.15 Stopband Response of Designed Single Filters for Stagger Ratios 16:20:17:22, 20:17:22:16, 17:22:16:20, 22:16:20:17	73
Figure 4.16 Passband Response of Designed Filters for Stagger Ratios 16:20:17:22, 20:17:22:16, 17:22:16:20, 22:16:20:17	75
Figure 4.17 Stopband Response of Designed Filters for Stagger Ratios 16:20:17:22, 20:17:22:16, 17:22:16:20, 22:16:20:17	76
Figure 4.18 Total Power Response of Designed Multiple Filters used for Stagger Ratio 16:20:17:22:16:20:17 (Multiple Filter)	78
Figure 4.19 Improvement Factor Plots of Designed Multiple Filters used for Stagger Ratio 16:20:17:22:16:20:17	79
Figure 5.1 Magnitude Response Comparison of Designed Filters with Hsiao's Filter	83
Figure 5.2 Improvement Factor Plots of Designed Filters with Hsiao's Filter	84

Figure 5.3	Magnitude Response Comparison of Designed Filters with Jacomini's Filter	86
Figure 5.4	Improvement Factor Plots of Designed Filters with Jacomini's Filter	87
Figure 5.5	Magnitude Response Comparison of Designed Filters with Ewell's Filter . .	89
Figure 5.6	Improvement Factor Plots of Designed Filters with Ewell's Filter	90
Figure 5.7	Magnitude Response Comparison of Designed Filters with Zuyin's Filter . .	92
Figure 5.8	Improvement Factor Plots of Designed Filters with Zuyin's Filter	93

CHAPTER 1

INTRODUCTION

Detection of moving targets in strong clutter has been one of the most important tasks of the radar systems throughout the history. Through the evolution of radar systems a number of techniques and methods are developed in order to increase the target detection capability of the radar systems in strong clutter. One of the basic methods is the usage of Moving Target Indication (MTI) signal processor. As the name implies, it is used to indicate the presence of moving targets in heavy clutter by discriminating the component of the return echo due to moving targets from stationary background.

First MTI designs were based on the analog delay line cancellers, which are used for cancelling stationary clutter by subtracting the successive returns in order to improve the detection of the target component. With the introduction of digital systems, digital filters are developed and improvements in performance have been attained.

Design of the MTI processor is mainly based on the design of filter structure for clutter attenuation. For stationary clutter attenuation, simple highpass filters provide sufficient attenuation, whereas higher order filters can be required to sufficiently attenuate clutter with significant Doppler spread.

Digital implementation of the MTI signal processor filter has a periodic characteristic due to uniform sampling with constant pulse repetition frequency (PRF). Because of the periodic nature, the moving targets having Doppler frequencies which are integer multiples of PRF are cancelled by the MTI filter along with the background clutter. Therefore, these moving targets are not seen by the radar. Velocities that correspond to the undetected frequencies are called *blind speeds* [4]. There are different approaches for the solution of this problem in the literature. One of them is staggering the interpulse durations, that is the usage of different interpulse periods instead of a single one [5].

The usage of staggered interpulse durations improves the blind speed performance in MTI radars. It should be noted that the improvement in blind speed comes at almost no additional computational cost. An important disadvantage of non-uniform sampling is the passband ripples which are much larger in comparison to uniform PRI systems. Due to these ripples, the fluctuations of signal power at the MTI filter output may degrade the detection performance for particular Doppler frequencies. Therefore, it is important to design MTI filters by considering the detection probability and performance of the radar system for the specific Doppler frequencies.

Design of staggered MTI filters depends upon the radar system parameters that are related

to the detection probability and clutter attenuation. Based upon these parameters, staggered MTI filter design comprises on the optimization of two sets of parameters: the interpulse time durations and the filter coefficients. The unambiguous range and velocity specifications impose constraints on the interpulse periods. The desired clutter attenuation affects the values of filter coefficients [6].

Our goal in this thesis is to apply classical uniform filter design techniques and present flexible solution to the non-uniform MTI filter design for a *given* set of interpulse durations. Designed filters can be adopted to different scenarios having different clutter attenuation and Doppler frequency band of interest specifications. The presented designs provide the opportunity for the selection of the best interpulse periods from a set of suitable candidates by satisfying the unambiguous range-velocity constraints.

In the present work, we study three widely adopted FIR filter design techniques, the least square, convex and min-max filter design. The systematic design of each approach is described. A number of performance measures are defined and comparison between different filters is given for the various scenarios. Obtained results indicate that it is possible to design non-uniform filters according to different cutoff frequencies and clutter attenuation values. One can optimize the filter response by defining the clutter attenuation, cutoff frequency and interested Doppler frequency band and selecting a suitable weight factor.

A possible novelty of the present work is the design of a min-max MTI filter based upon improvement factor of the optimum filter. This design technique is different from the previously stated min-max filter design and uses the information of improvement factor of optimum filter response for a specified clutter power spectrum density.

Throughout the thesis work, a literature survey related to design of staggered MTI filters is given and a detailed description of the mentioned filter design approaches are presented with specific algorithm steps and performance comparisons for several parameters. Available designs in the literature are implemented and numerical comparisons with these are given.

The organization of thesis is as follows: In Chapter 2, the background information related to MTI filter is given. Different configurations of the MTI filters are given along with their frequency response characteristics. The blind speed problem is explained and the staggered PRF MTI filter solution is given.

In Chapter 3, the design of three different types of non-recursive staggered PRF MTI filters are given. First, the properties and design constraints of the non-uniform FIR filter design are explained. Later, three types of design approaches are presented in relation with the non-uniform FIR filter design. Finally a numerical comparison between previously designed filters are made.

In Chapter 4, the clutter attenuation is taken into account for the designed filters. First, the definition and the properties of clutter are presented. The effect of clutter on the earlier designs are discussed and the results are compared with respect to a number of figures of merits. Later, a novel min-max filter design approach is explained based upon the improvement factor of optimum filter. Finally, the multiple filter approach is described with time varying filter coefficients.

In Chapter 5, the simulation results of the designed filters with the designs in the literature are given. For each design in the literature, the design approach is explained with examples and

comparisons of the designed filters with respect to performance measures and improvement factor are given.

In Chapter 6, concluding remarks are presented, obtained results are summarized and the related future work is described.

CHAPTER 2

BACKGROUND

2.1 Moving Target Indication (MTI) Radar

It is difficult to distinguish a moving target in the presence of ground-clutter or sea-clutter environment due to strong clutter echos. Detection of moving targets in these conditions is performed using Moving Target Indication (MTI) radar. The MTI radar is a type of pulse radar that uses the non-zero Doppler shift of moving targets for their detection [5] by cancelling the stationary background clutter.

There are different types of MTI Radars classified according to operation modes, environments and used signal processing algorithms. *Coherent MTI Radar* is the type in which a moving target is detected as a result of pulse-to-pulse change in echo phase relative to the phase of a coherent reference oscillator [7]. In other words, it is a system that uses the phase difference resulting from Doppler effect to separate the moving targets from stationary background clutter. Pulses are transmitted and received echos are compared with the signal produced by the coherent reference oscillator. Due to Doppler shift, moving target component of the received echo has a phase difference in comparison to the reference oscillator signal and can be discriminated from clutter.

Another type of MTI radar that uses the clutter echo as the reference signal to discriminate the Doppler-shifted information of target echo is known as *Non-Coherent MTI* or *externally Coherent MTI* [5]. This type of MTI is simpler than coherent MTI; but it requires the presence of clutter for detecting the moving targets. Due to clutter dependence, *Non-Coherent MTI* implemented as a mode and can be switched on or off depending on the presence or absence of strong clutter reference. [5].

MTI Radars used in airborne applications named as *Airborne MTI* or *AMTI*. Operation principle of this type is similar to the *Coherent MTI*; however, compensation for the moving radar platform is necessary. The Doppler shift of the received echos change depending on the relative motion of the moving radar platform and target. After the compensation of relative motion between platforms, moving targets can be detected by suppressing the stationary clutter.

Adaptive MTI Radar is another type of MTI radar that adapts itself to the clutter. According to change in clutter characteristics, the coefficients of the MTI filter are changed on time basis. Adaptation to the clutter can be achieved by different estimation techniques for clutter covariance matrix [8].

Different from other MTI techniques, *Area MTI* radar does not use Doppler shift directly and compares the envelope-detected outputs of successive scans to detect the targets that move in range or azimuth between scans [5].

2.1.1 Operation of a Coherent MTI Radar

The operation of a *Coherent* MTI Radar is based upon discrimination of the radar return by comparing the phases of all echoes with reference (coherent) phase. Simplified structure of a *Coherent* MTI Radar is illustrated in Figure 2.1.

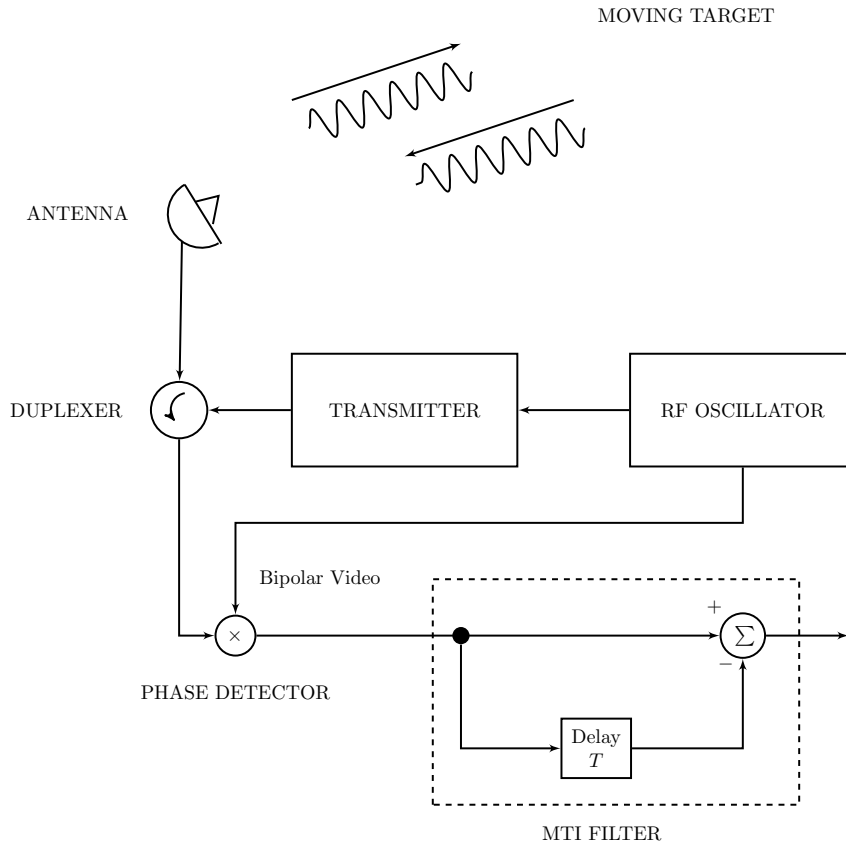


Figure 2.1: Simplified Block Diagram of A Coherent MTI System [2]

Here RF oscillator is used in the transmitter and also as reference for the received echos for phase comparison [2]. Duplexer is used for switching between transmission and reception operations. A radar return usually contains two components; target component and clutter component [9]. Clutter component signal arises due to stationary background objects and has much stronger than the target component signal, in general. Discrimination of the target and clutter components made by comparing successive received echos in terms of phase properties and filtering the stationary background clutter. The phase change due to target motion results in a component changing from pulse to pulse, whereas the clutter component stays the same. This provides a way to discriminate the clutter and target components by evaluating the phases of successive return echos. Phase comparison is implemented by delaying the previous echo

and subtracting from the current one. In frequency domain, the operation of the MTI filter corresponds to the attenuation of frequencies associated with the clutter spectrum without a significant (hopefully) reduction of the Doppler frequencies of moving targets. This shows that MTI filter is a highpass filter.

Figure 2.2 shows the operation of MTI. An examination of Figure 2.2 reveals that the magnitude response of the received echos stays same from pulse to pulse mostly. By looking at the successively received returns, it is not easy to extract the moving targets components from clutter component. However it is seen that, by subtracting the successive returns with MTI filter, the moving target component can be easily differentiated from the clutter. This result can be seen from the last sub plot given in Figure 2.2.

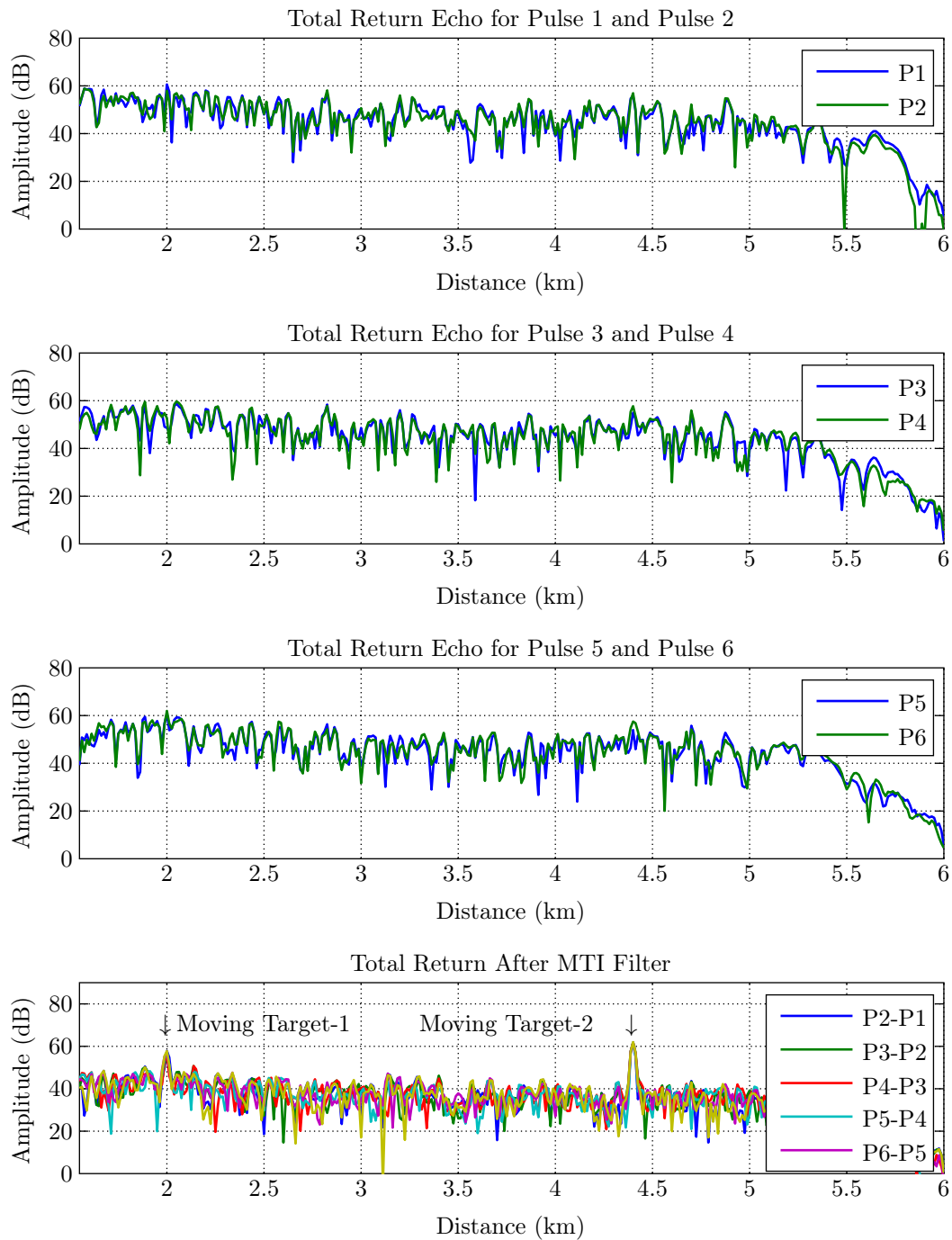


Figure 2.2: MTI Processing of Received Echos from Successive Transmitted Pulses

2.2 MTI Filtering

Different types of MTI filters are developed and have been used through the radar history. These filters are designed according to hardware specifications and the operation constraints of the radar system. A typical MTI filter has a highpass filter characteristics that is designed

for rejecting zero or small Doppler frequencies and passing higher frequencies corresponding to the moving targets. MTI filters can be classified in three main categories as follows.

2.2.1 Delay Line Cancellers

The delay line canceller is an analog technique used in the first MTI signal processor design. The operation is based on subtracting two consecutive radar returns. The structure of single delay line canceller can be given in Figure 2.3.

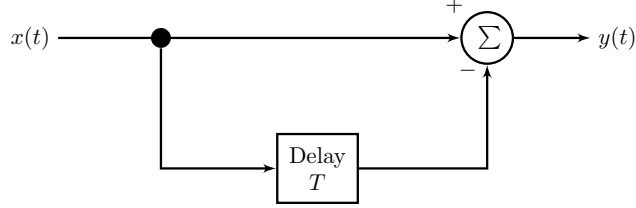


Figure 2.3: Filter Structure of the Single Delay Line Canceller

Time domain difference equation of the single delay line canceller with pulse repetition interval (PRI) T is given in (2.1)

$$y(t) = x(t) - x(t - T) \quad (2.1)$$

The frequency response characteristics of the single delay line canceller can be written by taking the Fourier Transform (\mathbf{F}) of the time domain difference equation as in (2.2)

$$\begin{aligned} \mathbf{F}\{y(t)\} &= \mathbf{F}\{x(t) - x(t - T)\} \\ Y(f) &= X(f)(1 - e^{-j2\pi fT}) \\ H_{sdlc}(f) &= \frac{Y(f)}{X(f)} = e^{-j2\pi fT/2}(e^{j2\pi fT/2} - e^{-j2\pi fT/2}) \\ &= 2j \sin(2\pi fT/2)e^{-j2\pi fT/2} \\ &= 2j \sin(\pi fT)e^{-j\pi fT} \end{aligned} \quad (2.2)$$

The magnitude of the frequency response of the single delay line canceller with the pulse repetition interval of T is given in (2.3) and plotted in Figure 2.4.

$$|H_{sdlc}| = 2 \sin(\pi fT) \quad (2.3)$$

Single delay line canceller rejects the stationary clutter which has zero Doppler shift. When the clutter has spread in the spectrum, then the performance of the single delay line canceller decreases and the clutter residue resides at the filter output, especially at small Doppler frequencies. When slow moving targets are present, then the detection performance of these targets are affected by the clutter residue. In other words, insufficient clutter attenuation decreases the performance of the single delay line canceller. Due to this reason, the single delay line canceller is not sufficient for the rejection of clutter with large spread in spectrum.

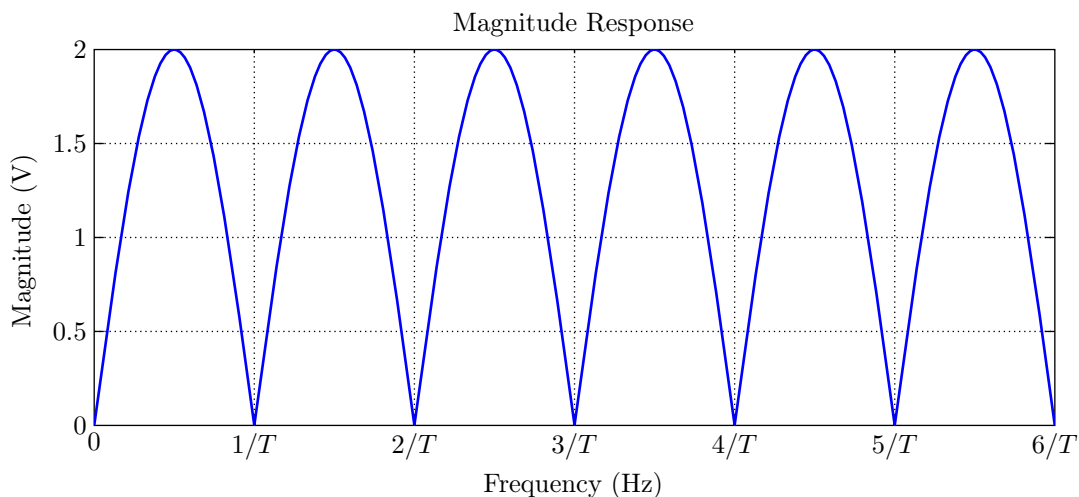


Figure 2.4: Magnitude Response of Single Delay Line Cancellor

As a solution to this problem, the usage of cascaded single delay line cancellers are proposed. By cascading two single delay line cancellers the double delay line canceller is formed. Figure 2.5 shows the filter structure of the double delay line canceller.

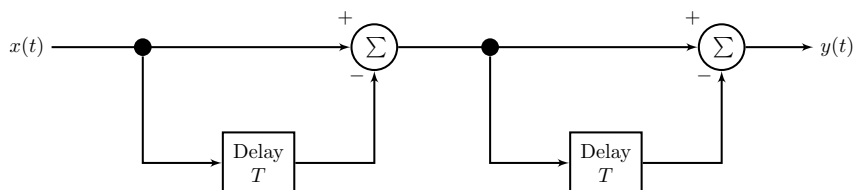


Figure 2.5: Filter Structure of the Double Delay Line Cancellor

The magnitude response of the double delay line canceller can be calculated using the single delay line canceller response as in (2.4) and pointed out in Figure 2.6 together with the single delay line canceller magnitude response for the purpose of comparison.

$$|H_{ddl}(f)| = |H_{sdl}(f)|^2 = (2|\sin(\pi fT)|)^2 = 4 \sin^2(\pi fT) \quad (2.4)$$

As seen from Figure 2.6, the double delay line canceller performance is greater in terms of the attenuation of non-zero spread clutter spectrum. By increasing the number of cascaded single delay line cancellers, an improved response in terms of attenuating finite width clutter can be obtained. Figure 2.7 indicates the response of cascaded single cancellers. The responses of the cascaded single cancellers can be calculated by taking the N th power of the single delay line canceller response as in (2.5). Here N represents the number of single delay line cancellers that are cascaded.

$$|H_{Ndl}(f)| = (2|\sin(\pi fT)|)^N \quad (2.5)$$

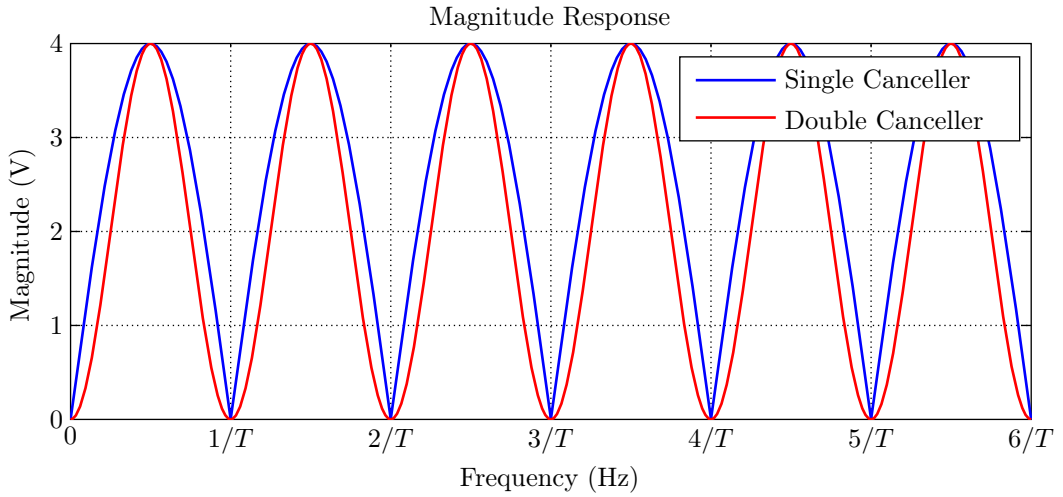


Figure 2.6: Magnitude Response Comparison of Single and Double Delay Line Cancellers

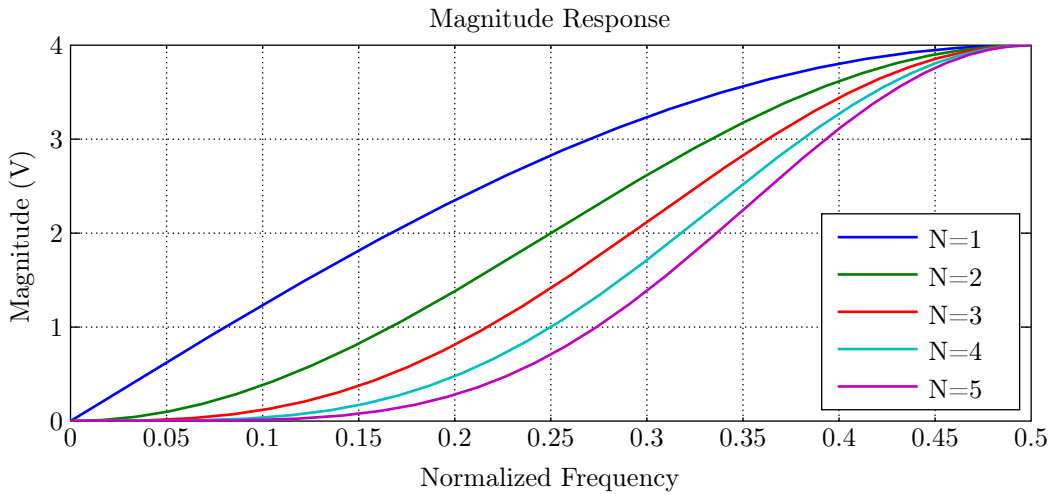


Figure 2.7: Magnitude Response Comparison of Cascaded Single Delay Line Cancellers

2.2.2 FIR Type MTI Filters

Finite-Impulse-Response (FIR) filters can be used for MTI processing if the filter weights are chosen in order to obtain a highpass filter characteristics. General structure of the FIR filters for uniform pulse repetition interval are given in Figure 2.8.

One of the simplest and widely used uniform FIR type MTI filter is the *Binomial* MTI filter whose coefficients are formed by binomial numbers. This method corresponds to the cascade of single delay line cancellers. As an example, the double delay line canceller can be arranged as FIR type in Figure 2.9.

These cascade arrangements of the single delay line cancellers as transversal filter structure is

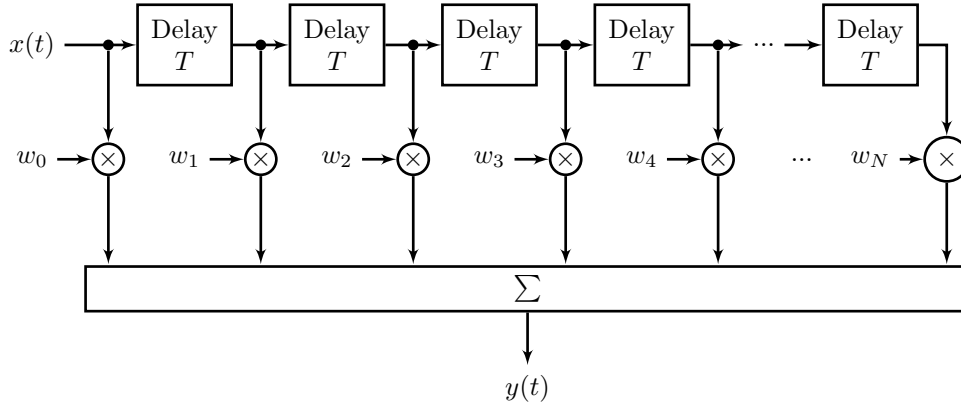


Figure 2.8: General Structure of a Uniform FIR Filter

called as *N-pulse cancellers* since N pulse is processed for $N - 1$ cascaded single cancellers. For example, a double delay line canceller named as 3-pulse canceller can be represented as an FIR filter as in Figure 2.9.

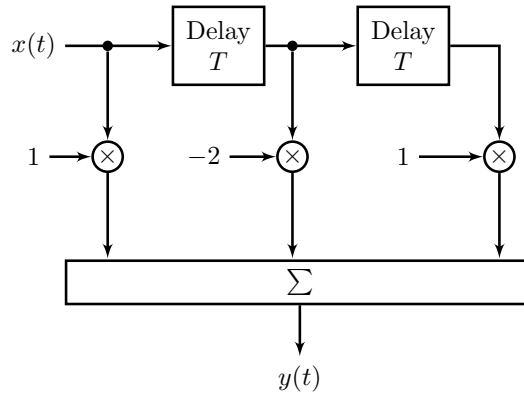


Figure 2.9: Double Delay Line Canceller Representation as a Transversal Filter Structure

For cascaded single delay line cancellers, z-transform of the time domain difference equation can be written as

$$H_{Ndlc}(z) = (1 - z^{-1})^N \quad (2.6)$$

If the equation (2.6) is expanded, the coefficients are the binomial numbers with alternating signs. Corresponding filter weights of the *N-pulse cancellers* can be calculated using the following equation:

$$w_i = (-1)^{i-1} \frac{N!}{(N - i + 1)!(i - 1)!}, \quad i = 1, 2, \dots, N + 1 \quad (2.7)$$

For the first 5-pulse canceller structures, filter weights are given in Table 2.1. Usage of the binomial coefficients lead to naming of *N-pulse Cancellers* as *MTI Filter with Binomial Weights* in the literature.

Table 2.1: Filter Weights for First 5 *N-pulse Cancellers*

N-pulse Canceller	Filter Weights
2-pulse	[1,-1]
3-pulse	[1,-2,1]
4-pulse	[1,-3,3,-1]
5-pulse	[1,-4,6,-4,1]

Besides *Binomial* MTI filter, different techniques and designs are proposed in the literature for adjusting the coefficients of the FIR type MTI filters [10], [6], [11]. Most of the studies seek the optimum MTI filter for clutter rejection and propose different optimization techniques like quadratic programming for calculating the filter weights [10]. The constraints of these designs are based on minimization of output clutter and attenuation of stationary clutter.

2.2.3 Recursive MTI Filters

Recursive filters are also used as an MTI signal processor. They are utilized to shape the stopband response. Recursive filters have the feedback coefficients and feedforward coefficients. An example direct-form structure is given in Figure 2.10. Using recursive filters, stopband of the filter can be shaped more easily due to additional degrees of freedom that comes from feedback coefficients. However, these filters have poor transient response. This type of filters can be designed using classical z-transform theory and pole-zero analysis [3], [12]. Z-domain transfer function of a recursive filter is given in (2.8). As an example, magnitude responses of three different shaped MTI filters are given in Figure 2.11.

$$H(z) = \frac{\beta_0 + \beta_1 z^{-1} + \beta_2 z^{-2} + \dots + \beta_M z^{-M}}{1 + \alpha_1 z^{-1} + \alpha_2 z^{-2} + \dots + \alpha_N z^{-N}} \quad (2.8)$$

After the examination of three types of MTI filters, we present the design criteria for the MTI filters. There are different figures of merit for the performance comparison of the MTI filters. These are stated as MTI Improvement Factor, subclutter visibility, MTI gain, MTI response, clutter attenuation, clutter visibility factor and cancellation ratio in [4]. The most commonly used and accepted measure is the MTI Improvement factor whose definition includes the effect of clutter attenuation and MTI gain.

2.3 MTI Improvement Factor

MTI Improvement Factor is a performance measure for the clutter attenuation. It is defined as “the signal-to-clutter power ratio at the output of the MTI filter to the signal-to-clutter power ratio at the input, averaged uniformly over all target velocities of interest.” [7]. It can be expressed as

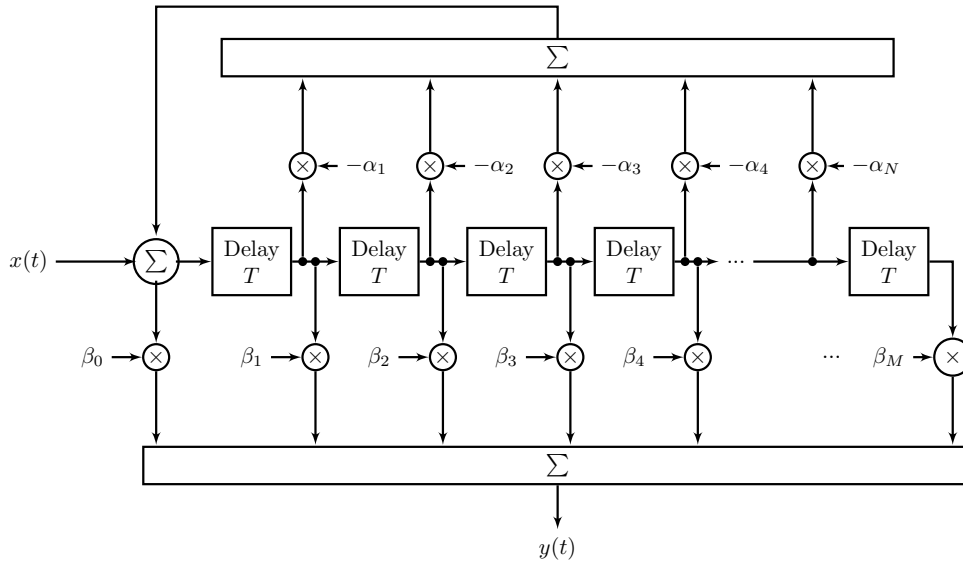


Figure 2.10: IIR Filter Structure

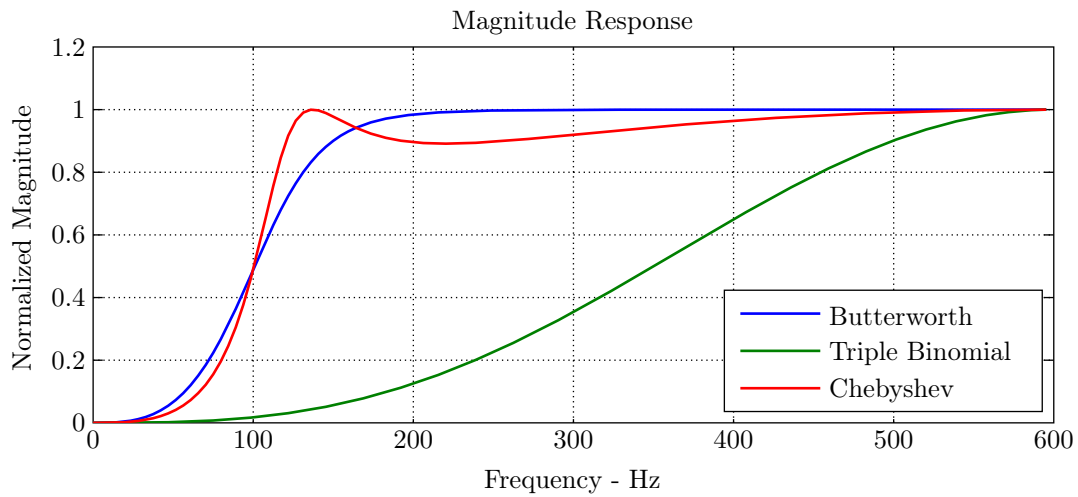


Figure 2.11: Magnitude Response of Different Types of Shaped MTI Filters [3]

$$\text{Improvement Factor} = IF = \frac{(SCR)_{out}}{(SCR)_{in}} \quad (2.9)$$

where SCR_{out} and SCR_{in} represent average signal-to-clutter ratio at the output and input of the MTI filter respectively. Improvement factor can be thought of average SCR improvement of the MTI filter, not at a particular frequency. The improvement factor can be further described as follows. If the received signal is

$$\mathbf{r} = \mathbf{s}(\theta) + \mathbf{c} \quad (2.10)$$

where \mathbf{r} , $\mathbf{s}(\theta)$ and \mathbf{c} are $N \times 1$ column vectors that represent the received signal, clutter component and signal component of the received echo respectively. θ is phase change in PRI seconds corresponding to Doppler effect. Average power at the input can be written as the addition of signal and clutter power if the signal and clutter are assumed to be zero mean and uncorrelated. It is given by

$$\begin{aligned} P_i &= \mathbf{E}\{\|\mathbf{s}(\theta) + \mathbf{c}\|^2\} \\ &= \mathbf{E}\{\mathbf{s}(\theta)^H \mathbf{s}(\theta)\} + \mathbf{E}\{\mathbf{c}^H \mathbf{c}\} \end{aligned} \quad (2.11)$$

where the first and second terms represent signal and clutter powers at the input respectively.

After filtering the input signal with an FIR MTI filter with $N \times 1$ coefficient vector $\boldsymbol{\alpha}$, power of the filtered signal can be written as follows:

$$\begin{aligned} P_o &= \mathbf{E}\{\|\boldsymbol{\alpha}^H [\mathbf{s}(\theta) + \mathbf{c}]\|^2\} \\ &= \mathbf{E}\{\boldsymbol{\alpha}^H \mathbf{s}(\theta) \mathbf{s}^H(\theta) \boldsymbol{\alpha}\} + \mathbf{E}\{\boldsymbol{\alpha}^H \mathbf{c} \mathbf{c}^H \boldsymbol{\alpha}\} \end{aligned} \quad (2.12)$$

Similar to the input power case, the first and second terms represent the signal and clutter powers at the output of the MTI filter respectively.

Using (2.11) and (2.12), SCR_{in} and SCR_{out} can be written as follows

$$SCR_{out} = \frac{\mathbf{E}\{\boldsymbol{\alpha}^H \mathbf{s}(\theta) \mathbf{s}^H(\theta) \boldsymbol{\alpha}\}}{\mathbf{E}\{\boldsymbol{\alpha}^H \mathbf{c} \mathbf{c}^H \boldsymbol{\alpha}\}} \quad (2.13)$$

$$SCR_{in} = \frac{\mathbf{E}\{\mathbf{s}(\theta)^H \mathbf{s}(\theta)\}}{\mathbf{E}\{\mathbf{c}^H \mathbf{c}\}} \quad (2.14)$$

By putting SCR equations in (2.9), improvement factor can be rewritten as in (2.15)

$$\begin{aligned} IF(\theta) &= \frac{\mathbf{E}\{\boldsymbol{\alpha}^H \mathbf{s}(\theta) \mathbf{s}^H(\theta) \boldsymbol{\alpha}\}}{\mathbf{E}\{\mathbf{s}(\theta)^H \mathbf{s}(\theta)\}} \times \frac{\mathbf{E}\{\mathbf{c}^H \mathbf{c}\}}{\mathbf{E}\{\boldsymbol{\alpha}^H \mathbf{c} \mathbf{c}^H \boldsymbol{\alpha}\}} \\ &= \frac{\boldsymbol{\alpha}^H \mathbf{R}_s \boldsymbol{\alpha}}{\boldsymbol{\alpha}^H \mathbf{R}_c \boldsymbol{\alpha}} \end{aligned} \quad (2.15)$$

where \mathbf{R}_c and \mathbf{R}_s are normalized clutter and signal covariance matrices respectively.

By using the obtained improvement factor equation, MTI improvement factor for the coherent MTI case with FIR type filter can be expressed as in (2.16) by assuming uniform distribution

for Doppler frequencies of the signal.

$$IF = \int_0^{2\pi} IF(\theta)d\theta = \frac{\sum_{j=0}^{N-1} \alpha_j^2}{\sum_{j=0}^{N-1} \sum_{k=0}^{N-1} \alpha_j \alpha_k \rho(j, k)} \quad (2.16)$$

where α_j, α_k 's are the MTI's real weights, $\rho(j, k)$ is the correlation coefficient of clutter returns between the j 'th and k 'th pulses. and N is the number of pulses processed by the MTI.

As seen from the improvement factor relation, the improvement factor depends upon filter coefficients and clutter covariance matrix. Hsiao [13] shows that optimal MTI filter depends upon clutter covariance matrix and weights of the optimal MTI are given by the elements of the eigenvector that corresponds to the minimum eigenvalue of the clutter covariance matrix.

2.4 Blind Speed Problem

One of the main disadvantages of the usage of uniform interpulse duration in digital MTI filters is that moving targets with Doppler frequencies that are integer multiples of the PRF will be cancelled together with clutter because of periodic sampling of Doppler frequency. The nulls that result from the periodic sampling characteristics of the system are given by:

$$f_d = \frac{n}{PRI} = n \times PRF \quad (2.17)$$

The speeds correspond to these undetected Doppler frequencies are named as *blind speeds* ([9]) and can be calculated as in (2.18) .

$$V_{blind} = n \times \lambda/2 \times PRF = \frac{n \times c \times PRF}{2f} \quad (2.18)$$

where λ is wavelength and PRF is pulse repetition frequency and f is the operating frequency. As an example, an X-Band radar that has 500 μs uniform PRI exhibits blind speeds at 300 m/s , 600 m/s , 900 m/s , \dots

Table 2.2 illustrates widely used frequency bands. For high frequency bands, first blind speeds can have smaller values, typically not sufficient to detect possible targets of interest for these bands. Therefore it is essential to increase the value of first blind speed for the designated radar frequency bands.

Considering the blind speed equation (2.18), four methods are proposed in order to increase the first blind speed of a radar system [5]. These methods can be stated as

- Usage of lower center frequencies for operation frequency of radar system
- Increasing the pulse repetition frequency
- Usage of multiple pulse repetition intervals

Table 2.2: First Blind Speeds for Different Radar Bands [1]

PRF (Hz)		10000	1000	250		
Maximum Range (km)		15.00	150.00	600.00		
	Band					
Frequency	US	UK	ECM	First Blind Speeds (m/s)		
600 MHz	UHF	UHF	C	2500.00	250.00	62.5
1300 MHz	L	L	D	1153.85	115.38	28.85
3000 MHz	S	S	E..F	500.00	50.00	12.50
5500 MHz	C	C	G	272.73	27.27	6.82
10000 MHz	X	X	I	150.00	15.00	3.75
16000 MHz	Ku	J	J	93.75	9.38	2.34
30000 MHz	Ka	Q	K	50.00	5.00	1.25

- Usage of multiple frequencies for operation frequency of radar system

Suggested solutions can be used together or individually. However each one of the solutions have some negative effects on the operation of the radar system.

Operation with a lower center frequencies results in a decrease in range and angle resolutions of the radar. Lower frequency band is used in civil applications. Therefore, lowering the frequency is not a desirable choice for many of radar systems. Increasing the pulse repetition frequency decreases the unambiguous range and causes range ambiguities. Usage of more than one PRF's increases first blind speed of the radar system whereas multiple-time-around clutter echoes will fold into different ranges. Operating the radar at more than one frequency causes stress on transmitter and is not desirable within the usual frequency bands allocated [5].

Widely used solution to blind speed problem in MTI filters is the usage of non-uniform (staggered) PRI [9]. With this method the first blind speed is increased with respect to a uniform PRI MTI system. Two main staggering approaches utilized generally: pulse to pulse and block to block staggering. Pulse to pulse staggering is performed by changing the interpulse period from pulse to pulse. This method is suitable for MTI processing and resistant to electronic jamming. On the other hand, block-to-block staggering is utilized by changing the interpulse period after transmitting a group of pulses with same PRI and used widely in pulse-Doppler radars.

2.5 Staggered PRI Design

Staggered PRI design is based upon defining the interpulse durations according to range and velocity specifications of the radar system. If N interpulse durations denoted as $T_1, T_2, T_3, \dots, T_N$ is taken into account, the period of the stagger pattern is given by

$$T_p = \sum_{i=1}^N T_i \quad (2.19)$$

Each interpulse duration can be expressed as multiple of greatest common factor of the set of interpulse durations.

$$T_i = k_i T_{gcd} \quad (2.20)$$

Here k_i 's are integers that define the stagger ratio of the corresponding interpulse durations and T_{gcd} is the greatest common divisor of the time durations set.

The coefficient k_i define the improvement of the first blind speed of the staggered system which is given by average interpulse duration

$$T_{av} = \frac{1}{N} \sum_{i=1}^N k_i T_{gcd} \quad (2.21)$$

As an example, for a 2-PRI system with $T_1 = 3T$ and $T_2 = 5T$, the frequency response of the staggered system with T_1 and T_2 is compared with non-staggered system with uniform PRI of $4T$ is shown in Figure 2.12.

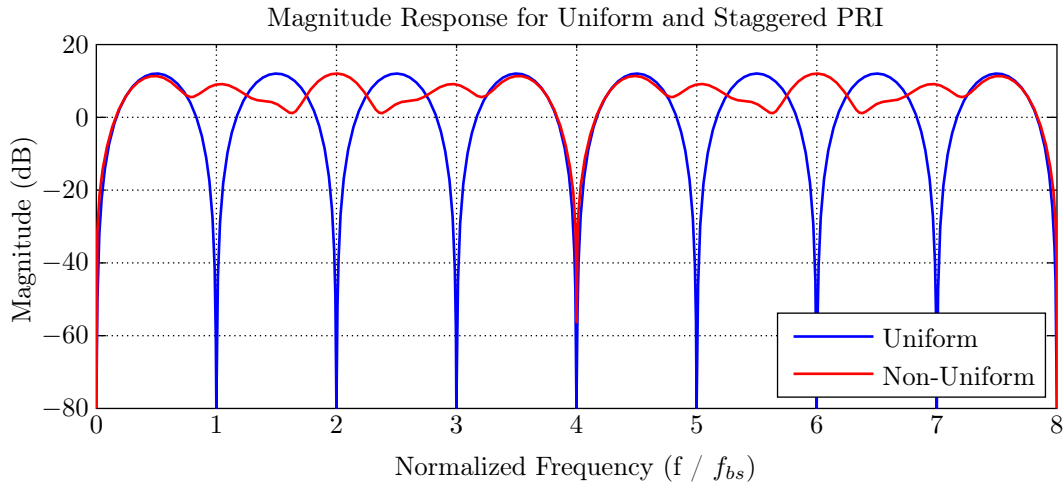


Figure 2.12: Magnitude Response Comparison of MTI Filter with Uniform and Staggered PRI

As it is seen from Figure 2.12, by using two different PRI values, first blind speed of the staggered system increased 4 times with respect to non-staggered system with PRI of $4T$.

Usage of PRI staggering improves blind speed, but because of the non-uniform sampling the frequency response fluctuates in the passband which results in degradation in the improvement factor. It is important to provide a flat passband response for an equally probable target detection over the velocity band of interest. In addition, adjustment of interpulse durations is important in terms of minimum unambiguous range and dwell time. Therefore, it is necessary to optimize the stagger periods according to the other specifications.

Different stagger patterns are given in the literature. One of the simplest techniques is adding integer values to the desired multiple of the first blind speed [2]. For example, for a four and five-period stagger schemes $-3,2,-1,3$ and $-6,5,-4,4,1$ integer groups are used respectively. If a

14 times and 57 times blind speed increase is desired, the corresponding stagger ratios will be 11 : 16 : 13 : 17 and 51 : 62 : 53 : 61 : 58.

It is also discussed to use stagger periods according to analytical patterns. Interpulse durations can be changed according to linear, sinusoidal, symmetric, wobulated and random manner [14], [15]. Small deviations from the average interpulse period are also implemented [16]. As a different approach, choosing the stagger intervals according to frequency response of non-uniform transversal filter is discussed in [17].

Other solutions for stagger optimization pursue analytical methods through of searching and obtaining the best possible stagger scheme with respect to different constraints [18], [19], [20], [21], [22]. To this aim, an algorithmic solution can be described as follows.

- Define a cost function
- Define an initial stagger scheme
- Calculate cost function
- Change stagger intervals
- Recalculate the cost function
- If the cost function improved, choose new stagger values

Along with the stagger interval adjustment, coefficients of the MTI filter that process staggered pulses must be optimized in terms of satisfactory clutter attenuation and system performance. The goal of the MTI filter design is to provide maximum amount of clutter suppression concurrently with the least amount desired signal suppression (flat passband). Design of staggered MTI filter can be implemented in terms of two general cases. After the selection of the interpulse durations according to range-velocity constraints, coefficients of the non-uniform filter can be selected to satisfy the required clutter attenuation and improvement factor as studied in [11], [18], [6], [23], [24]. Alternatively, optimization of the stagger intervals and filter coefficients are carried out together by considering range-velocity and clutter attenuation constraints [19], [25], [20].

CHAPTER 3

NON-UNIFORM MTI FILTER DESIGN

In this chapter staggered MTI filter designs are studied from the perspective of filter design with non-uniform samples. First, properties and constraints of the non-uniform FIR filter design is presented. Second, designed filters for non-uniform MTI processing explained in detail with defined performance measures. Finally, a comparison of designed filters with the selected designs is given in terms of the performance measures.

3.1 Non-uniform FIR Filter Design

Non-uniform sampling and filtering have been frequently used in several applications in the processing of acoustic, image and radio frequency signals [26], [27], [28], [29], [30], [31], [32], [33], [34]. The studies mostly focus on decreasing the total sampling time, reconstruction of the non-uniformly sampled signals, and improving the system performance. Most of the studies focus on FIR type implementations ([29], [27], [28], [31], [32]), but IIR type designs are also considered ([30], [35]).

The general filter structure of the discrete non-uniform FIR type filter is illustrated in Figure 3.1. The output signal is obtained by summation of the linear combination of the non-uniformly sampled input signal. The impulse response of this transversal filter is expressed by the following relation

$$h(t) = \sum_{n=0}^{N-1} \alpha_n \delta(t - t_n) \quad (3.1)$$

where α_n are the filter coefficients and t_n are the sampling times given by

$$t_n = \begin{cases} \sum_{i=0}^{n-1} T_i, & n \geq 1 \\ 0, & n = 0 \end{cases} \quad (3.2)$$

where T_i 's are the interpulse periods.

The corresponding frequency response of the filter is given by

$$H(f) = \sum_{i=0}^{N-1} \alpha_i e^{-j2\pi f t_i} \quad (3.3)$$

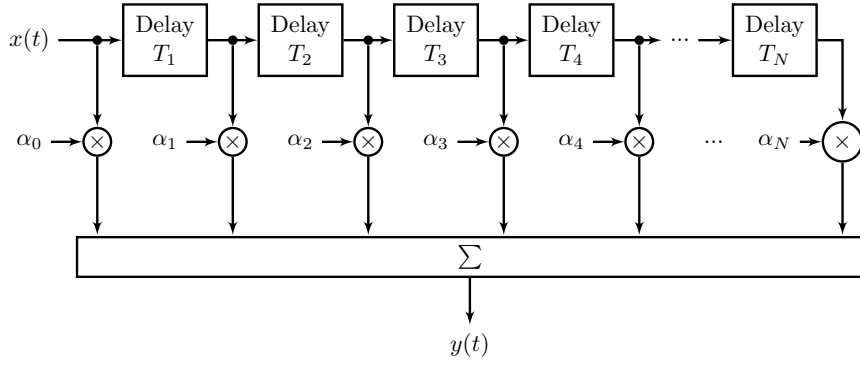


Figure 3.1: Non-uniform FIR Filter Structure

where f is the frequency of interest.

In this section, the design of non-uniform FIR filter is considered in terms of optimizing the staggered MTI filter frequency response. Design of staggered PRI MTI filter mainly relies on defining the frequency domain constraints and finding the optimal values for the interpulse periods T_i and filter coefficients α_i . The adjustments of these parameters are done by considering the ideal MTI filter response in Figure 3.2.

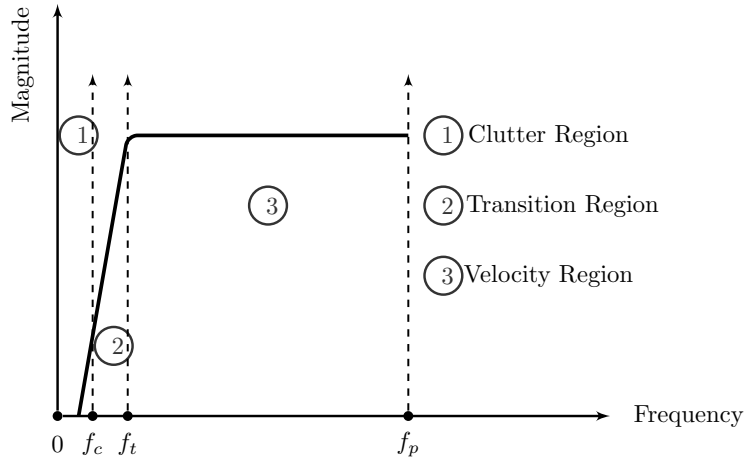


Figure 3.2: Regions for the MTI Filter Design

In Figure 3.2 Doppler spectrum of interest is divided into frequency regions [36]. *Clutter Region* indicates the region where clutter exist. This region starts from DC and goes up to the cutoff frequency of the designed filter and forms the stopband. *Transition Region* identifies the steepness of the filter to be designed and has no importance on the design. *Velocity region* is the region bounded by Doppler frequency of the interested targets and forms the passband of the filter to be designed.

The design criteria of the staggered MTI filter based upon defining the constraints in these

regions and there is often a compromise between these performance metrics [5]. Possible objectives of the MTI filter design can be listed as follows;

- All targets in the velocity interval of interest be equally detectable
- Clutter at the output of the filter be minimum
- Required MTI improvement factor for the clutter attenuation be satisfied
- The deepest null in the passband should not be excessive
- Passband ripple should be minimized and kept uniform

The described objectives above form the design constraints for the staggered MTI filter. In essence, the given objectives of the MTI filter can be condensed to

- Minimizing the passband ripple in velocity region
- Maximizing stopband attenuation in clutter region

It should be clear that both objectives can not be achieved simultaneously and a practical solution has to operate at a trade-off between these objectives. In order to obtain a flexible solution to these objectives; least square, convex and min-max filter design approaches are studied. Before the examination of these filter design methods, we would like to present a number of criterion that would be useful in the performance comparison of different designs.

3.2 Performance Measures of Staggered MTI Filter

Based on the stated constraints the design performance of the staggered MTI filter can be compared using the following criterion:

Mean Stopband Attenuation (MSA): This criteria indicates the clutter attenuation performance in clutter region. As the name implies it is the average of the *SCR* in the stopband region which is bounded by cutoff frequency f_c . It is given by

$$MSA = \frac{1}{f_c} \int_0^{f_c} |H(f)|^2 df \quad (3.4)$$

Stopband Attenuation @ f_c (SA): This is the value of filter magnitude response at the cutoff frequency f_c . Since the frequency values smaller than f_c ($0 \leq f \leq f_c$) are typically attenuated more than the value at the cutoff frequency, this value can be considered to represent the worst case signal attenuation in the stopband. It is given by

$$SA = |H(f_c)|^2 \quad (3.5)$$

Maximum Deviation (MD): This parameter indicates the maximum deviation from the ideal flat response in the velocity region. This value is commonly seen at near transition region and referred as *the depth of the first null*. It is given by

$$MD = \max |H_d(f) - H(f)|^2 \quad (3.6)$$

Mean Passband Error (MPE): This criteria is to measure the flatness of the filter in the velocity region. It is the average of the difference between ideal and designed filter responses in the passband and given by the following equation

$$MPE = \int_{f_t}^{f_p} |H_d(f) - H(f)|^2 df \quad (3.7)$$

where $H_d(f)$ and $H(f)$ are the frequency responses of the ideal and designed filters respectively. The limits of the integral are the lowest and highest frequency in the passband.

Schematic representation of the stated parameters is given in the Figure 3.3

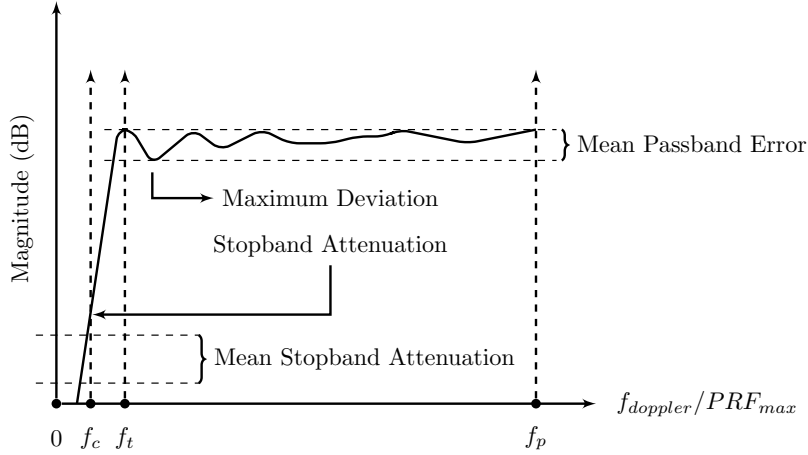


Figure 3.3: Performance Measures of the Staggered PRF MTI Filter Design

It must be noted that in order to compare the frequency response of different filters a normalization is necessary for quantifying the rejection capabilities of the filters. Unity noise gain assumption is used for normalization of the responses and the filter weights are normalized as in (3.8) before the comparison of the filter responses.

$$\alpha_{in} = \frac{\alpha_i}{\sqrt{\sum_{i=0}^{N-1} \alpha_i^2}} \quad (3.8)$$

Doppler frequency interval is normalized by maximum pulse repetition frequency in order to consider more general cases for specified stagger intervals, since maximum pulse repetition frequency determines the unambiguous range. Normalization with maximum pulse repetition frequency illustrates the increase with respect to minimum unambiguous range value and is convenient for the performance comparison with the studies in the literature.

It is also important to note that maximum desired passband frequency f_p must be smaller than $F_{max} - f_c$ for proper optimization that consider the periodicity of the frequency response of the staggered MTI filter. Here F_{max} represents the normalized first blind speed of MTI system with staggered PRI.

Based on the above criteria three main design approaches are studied in terms of optimizing the filter coefficients for the given interpulse periods. First a least square (LS) approach is examined, to obtain the filter coefficients that gives the near desired response in the sense of minimum squared average error. Second, a convex optimization method (CVX) is studied. Later, a min-max (Min-max) approach design is implemented. The details of these filter design approaches are explained in the following sections.

3.3 Least Square Design

The approach depends on minimizing the error between the desired filter and the designed filter. The standard cost function for a least square sense designed filter is given by (3.9)

$$J_{cost} = \int_0^{f_d} |H_d(f) - H_{ls}(f)|^2 df \quad (3.9)$$

where $H_d(f)$ and $H_{ls}(f)$ indicates the frequency responses of the desired and least square sense designed filter respectively.

$H_d(f)$ is the ideal highpass filter whose frequency domain definition given by (3.10) and plotted in Figure 3.4

$$H_d(f) = \begin{cases} 0 & \text{if } 0 \leq f \leq f_c, \\ 1 & \text{if } f_c \leq f \leq f_p, \end{cases} \quad (3.10)$$

Here f_c is the cutoff frequency used for adjusting the notch of the filter according to attenuation bandwidth and f_p is the bound for passband interval of Doppler frequency.

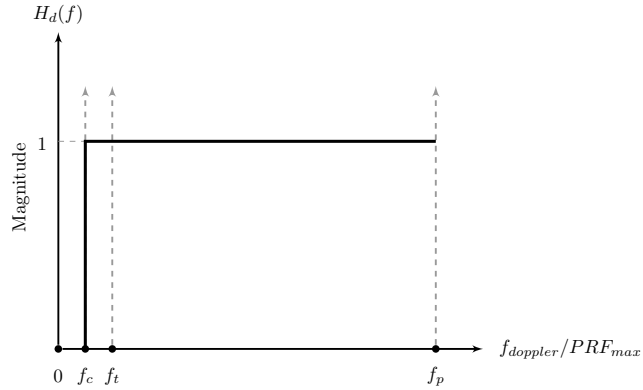


Figure 3.4: Frequency Response of Desired Highpass Filter

For non-uniform MTI filter, least square minimization problem can be stated as

$$\begin{aligned} & \text{minimize } ||H_d(f) - H_{ls}(f, \alpha_i)|| \\ & \text{subject to } \sum_{i=0}^{N-1} \alpha_i = 0, \quad x \in \Re \end{aligned}$$

Here the $\sum_{i=0}^{N-1} \alpha_i = 0$ constraint used to suppress the DC value and $\|\cdot\|$ is the Euclidean norm. It must be noted that with the inclusion of a linear constraint, least square design turns into a constraint least square design. By putting the equations in place, the cost function of the least square equation can be written as in (3.11). It must be noted that to simplify the presentation only the positive frequency band is used.

$$J_{cost}(\alpha, \lambda) = \int_0^{f_d} |H_d(f) - \sum_{i=0}^{N-1} \alpha_i e^{-j2\pi f t_i}|^2 df + \lambda \left(\sum_{i=0}^{N-1} \alpha_i \right) \quad (3.11)$$

The constraint equation is incorporated into the design via *Lagrangian Multiplier* λ . In order to minimize this cost function it is required that

$$\frac{\partial J_{cost}}{\partial \alpha_i} = 0 \quad (3.12)$$

By taking the partial derivatives of the cost function with respect to filter coefficients, we can get the following equation

$$\frac{\partial J_{cost}}{\partial \alpha_i} = \int_0^{f_d} \left(H_d(f) - \sum_{n=0}^{N-1} \alpha_n e^{-j\pi f t_n} \right) e^{j2\pi f t_i} df + N\lambda \quad (3.13)$$

By equating, the partial derivatives given in (3.13) to zero for $i = \{0, 1, \dots, N\}$, we can get the following linear equation system:

$$\mathbf{A}\boldsymbol{\alpha} = \mathbf{H}_d + \lambda \mathbf{1} \quad (3.14)$$

Here \mathbf{H}_d is a $N \times 1$ column vector with the k 'th entry

$$\mathbf{H}_d(k) = \int_{f_c}^{f_d} e^{j2\pi f t_k} df \quad (3.15)$$

and \mathbf{A} is a $N \times N$ matrix with the i 'th row and j 'th column entry

$$\mathbf{A}(i, j) = \int_0^{f_d} e^{-j2\pi f (t_j - t_i)} df \quad (3.16)$$

$\mathbf{1}$ is the $N \times 1$ column vector with entries of 1

$$\mathbf{1} = [1_1 \quad 1_2 \quad \dots \quad 1_N]^T \quad (3.17)$$

Finally, the vector $\boldsymbol{\alpha}$ in (3.14) is the vector of unknowns, that is the MTI filter coefficients.

In order to establish a trade-off between the objectives of clutter attenuation and passband ripple; we introduce a weight \mathcal{W} to control the contribution of stopband error to the cost function. The weight \mathcal{W} changes the cost given in (3.18) as follows

$$J_{cost}^{\mathcal{W}} = \mathcal{W} \int_0^{f_c} |H_d(f) - H_{ls}(f)|^2 df + \int_{f_t}^{f_d} |H_d(f) - H_{ls}(f)|^2 df + \lambda \left(\sum_{i=0}^{N-1} \alpha_i \right) \quad (3.18)$$

Optimization with the weighted cost function results in the following equation for the filter coefficients

$$(\mathcal{W} \times \mathbf{A}_{\text{stop}} + \mathbf{A}_{\text{pass}}) \boldsymbol{\alpha} = \mathbf{H}_d + \lambda \mathbf{1} \quad (3.19)$$

In the last equation, we have

$$\mathbf{A}_{\text{stop}}(i, j) = \int_0^{f_c} e^{-j2\pi f(t_j - t_i)} df \quad (3.20)$$

and

$$\mathbf{A}_{\text{pass}}(i, j) = \int_{f_t}^{f_p} e^{-j2\pi f(t_j - t_i)} df \quad (3.21)$$

It should be clear that by increasing \mathcal{W} , the contribution of the stopband error to the cost function is increased and therefore, the optimized filter provides more clutter suppression for higher \mathcal{W} values.

In order to find the least square MTI filter coefficients, *Lagrangian Multiplier* λ must be written in terms of other variables. By rewriting (3.19)

$$\boldsymbol{\alpha} = (\mathcal{W} \times \mathbf{A}_{\text{stop}} + \mathbf{A}_{\text{pass}})^{-1} (\mathbf{H}_d + \lambda \mathbf{1}) \quad (3.22)$$

Since $\mathbf{1}^T \boldsymbol{\alpha} = 0$, *Lagrangian Multiplier* λ found as

$$\mathbf{1}^T \boldsymbol{\alpha} = \mathbf{1}^T (\mathcal{W} \times \mathbf{A}_{\text{stop}} + \mathbf{A}_{\text{pass}})^{-1} \mathbf{H}_d + \mathbf{1}^T (\mathcal{W} \times \mathbf{A}_{\text{stop}} + \mathbf{A}_{\text{pass}})^{-1} \lambda \mathbf{1} = 0 \quad (3.23)$$

$$\lambda = \frac{\mathbf{1}^T (\mathcal{W} \times \mathbf{A}_{\text{stop}} + \mathbf{A}_{\text{pass}})^{-1} \mathbf{H}_d}{\mathbf{1}^T (\mathcal{W} \times \mathbf{A}_{\text{stop}} + \mathbf{A}_{\text{pass}})^{-1} \mathbf{1}} \quad (3.24)$$

As an example, frequency responses of least square design for different weight factors \mathcal{W} with the specified stagger ratio of 25 : 30 : 27 : 31 (which is taken from [5]) is plotted in Figure 3.5. As it is seen from the figure, an increase in the weight factor \mathcal{W} results in a bigger attenuation in the clutter region and bigger mean square error in the velocity region as expected. However the *MD* value does not depend upon weight factor linearly. This can be seen from the performance criterion given for different weight factors in Table 3.1. For $\mathcal{W} = 10^3$, *MD* takes the value of 25.4 dB whereas it is 19.569 dB when \mathcal{W} equals to 10^6 . Since maximum deviation of the response is important in terms of detection performance, \mathcal{W} value must be selected according to minimum deviation after providing the required stopband attenuation.

In order to see the effect of weight factor on the design parameters for a wider range, change of performance parameters with respect to \mathcal{W} values is plotted in Figure 3.6. The results indicate that the *MSA* and *SA* show monotonic property and reach a final value as weight factor increases. This means that for the specified stagger ratio, attenuation property of the LS design is bounded. In other words, since the LS design mainly focuses on minimizing the passband error, the attenuation capability is limited whereas it can be increased to some degree by increasing the weight factor \mathcal{W} .

Similarly, MPE reaches a final value as \mathcal{W} increases, however it is not monotonously decreasing. Therefore, when smaller stopband attenuation is satisfactory for the system requirements, small \mathcal{W} values can be selected for smaller average passband error.

As can be seen from the last sub figure in Figure 3.6, MD is the most sensitive criteria. As \mathcal{W} increases, MD fluctuates and poses a number of minimum values. For higher stopband attenuation values, it reaches a constant value similar to other performance measures.

After evaluating the responses of the each performance measure, it is reasonable to choose \mathcal{W} according to MD value.

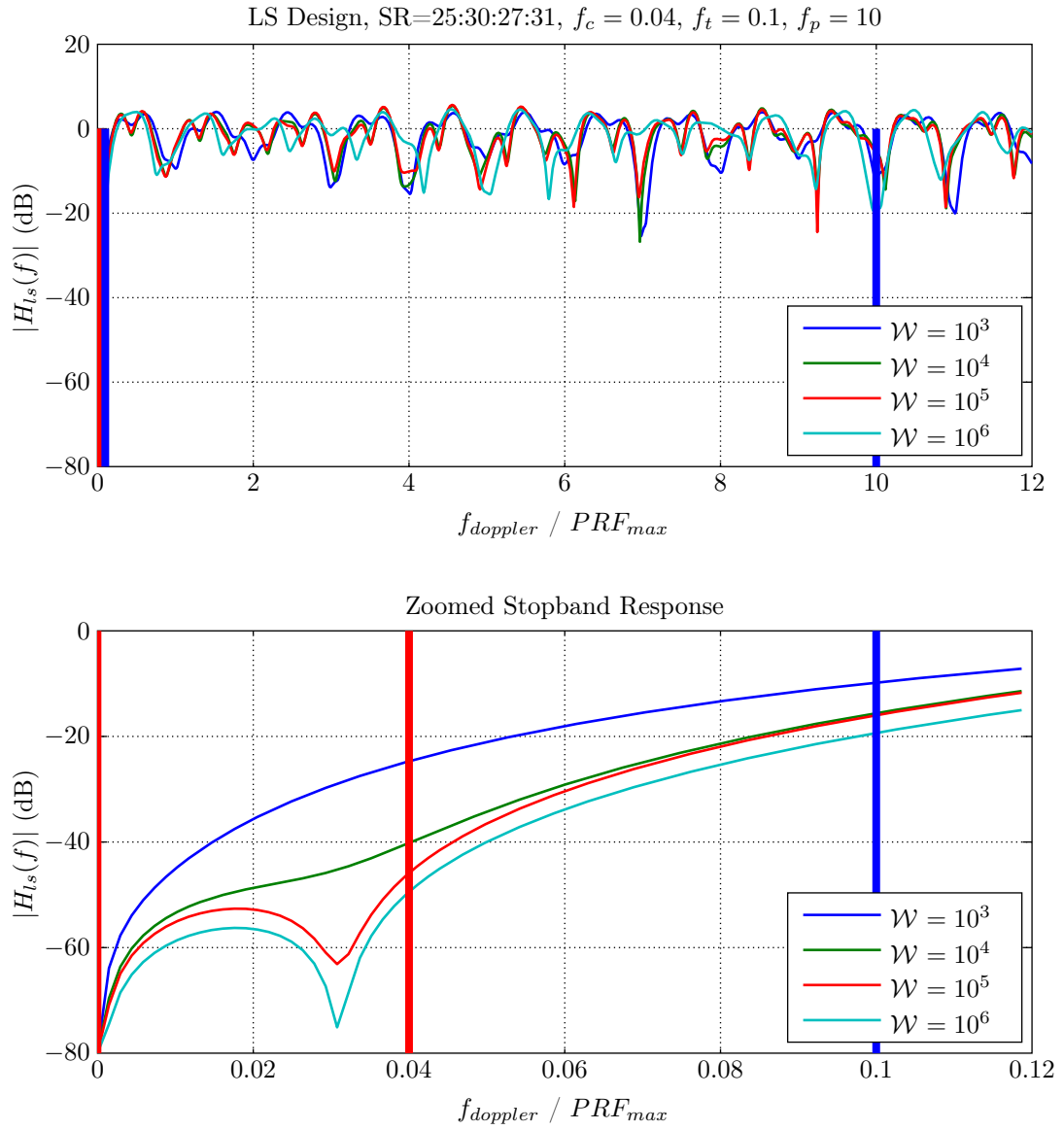


Figure 3.5: Frequency Response of Least Square Design with Different \mathcal{W} Values

Table 3.1: Performance Measures of Least Square Design for Different \mathcal{W} Values

\mathcal{W}	MSA (dB)	SA (dB)	MPE (dB)	MD (dB)
1000	-33.719	-24.884	-0.659	25.409
10000	-49.168	-40.470	-0.699	26.771
100000	-61.080	-46.445	-0.699	24.476
1e+06	-66.713	-50.030	-0.691	19.569

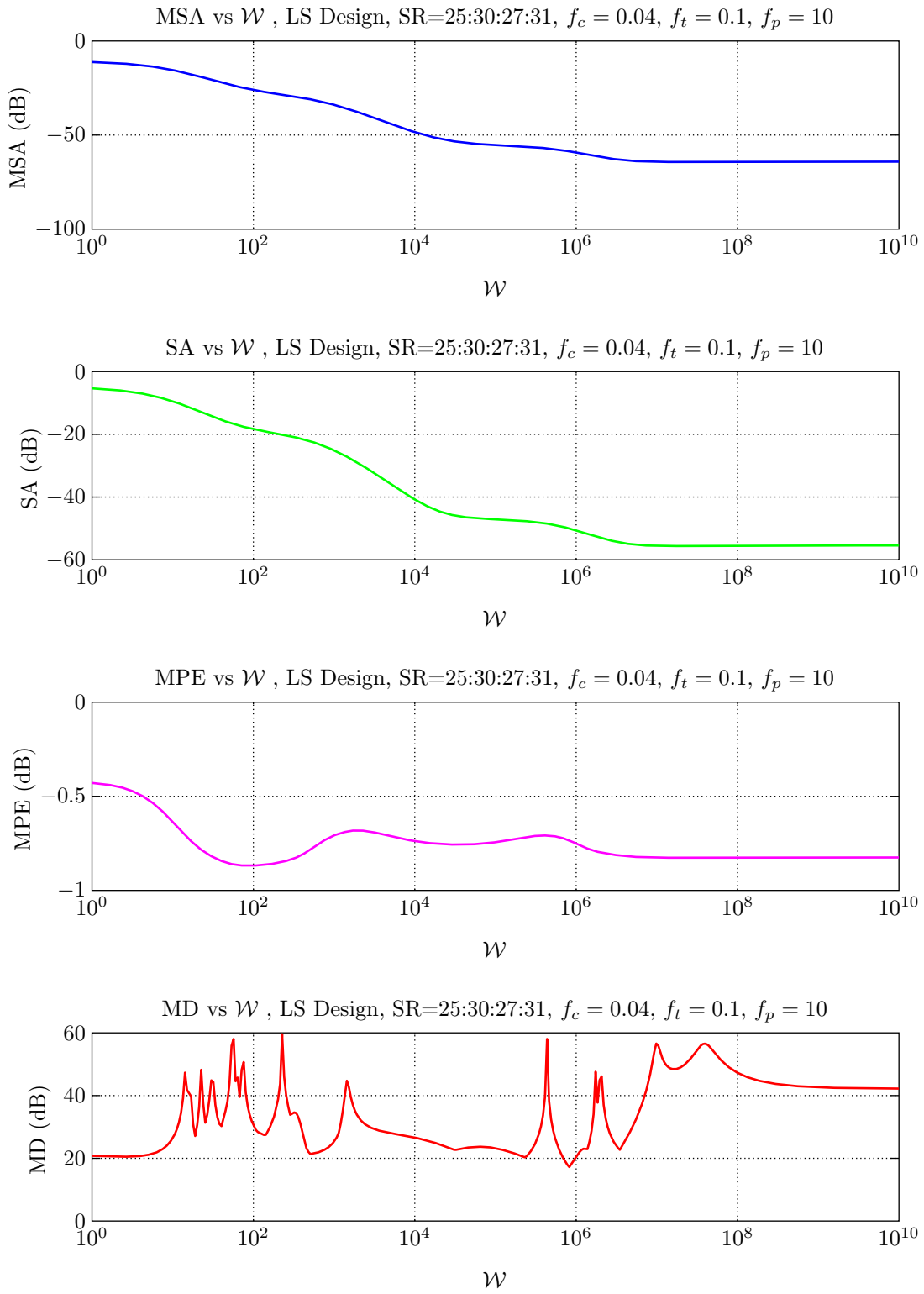


Figure 3.6: Effect of \mathcal{W} on MSA, SA, MPE and MD for Least Square Design

3.4 Convex Design

In convex filter design, staggered MTI filter design formulated as a convex optimization problem. A convex optimization problem can be stated as [37]

$$\begin{aligned} & \text{minimize} && f_0(x) \\ & \text{subject to} && f_i(x) \leq b_i, i = 1, \dots, m \end{aligned}$$

where the functions $f_0, \dots, f_m : \mathbf{R}^n \rightarrow \mathbf{R}$ are convex.

Convex design of non-uniform MTI filter starts with the formulation of design constraints as a convex optimization problem. Design constraints are based upon same approach as in least square sense design which is the minimization of the passband error and maximization of the stopband attenuation. Similar to the least square design, the passband ripple and the stopband attenuation goals are linked with the weight factor \mathcal{W} . Using the stated constraints, the optimization problem of the convex design can be stated as follows

$$\begin{aligned} & \text{minimize} && \delta \\ & \text{subject to} && |H(f, \alpha_i)| \leq \delta, f \in [0, f_c], \alpha_i \in \mathbf{R}, i \in \mathbf{N}_0 \\ & && |H(f, \alpha_i) - 1| \leq \mathcal{W}\delta, f \in [f_t, f_d], \alpha_i \in \mathbf{R}, i \in \mathbf{N}_0 \\ & && \sum_{i=0}^{N-1} \alpha_i = 0, \alpha \in \mathbf{R} \end{aligned}$$

The optimization variables are the filter weights α_i 's, N is the filter order, f_t, f_d is the lower and upper bound of normalized passband frequency respectively and f_c is the upper bound of normalized stopband frequency. It must be noted that weight factor \mathcal{W} affects the passband ripple directly, different from the least square design. In the least square design, the weight factor affects the clutter attenuation.

Using (3.3) and representing the stopband and passband separately, the convex optimization problem equation can be rewritten as

$$\begin{aligned} & \text{minimize} && \delta \\ & \text{subject to} && |\mathbf{A}_{\text{stop}}\boldsymbol{\alpha}| \leq \delta, f \in [0, f_c], \alpha_i \in \mathbf{R}, i \in \mathbf{N}_0 \\ & && |\mathbf{A}_{\text{pass}}\boldsymbol{\alpha} - \mathbf{1}| \leq \mathcal{W}\delta, f \in [f_t, f_d], \alpha_i \in \mathbf{R}, i \in \mathbf{N}_0 \\ & && \sum_{i=0}^{N-1} \alpha_i = 0, \alpha \in \mathbf{R} \end{aligned}$$

where

$$\mathbf{A}_{\text{stop}}(i, j) = \int_0^{f_c} e^{-j2\pi f(t_j - t_i)} df \quad (3.25)$$

and

$$\mathbf{A}_{\text{pass}}(i, j) = \int_{f_t}^{f_p} e^{-j2\pi f(t_j - t_i)} df \quad (3.26)$$

One must be careful in choosing the weight factor to minimize the passband error due to the constraint of $|\mathbf{A}_{\text{pass}}\boldsymbol{\alpha} - \mathbf{1}|$, since if $\mathbf{A}_{\text{pass}}\boldsymbol{\alpha}$ happens to a negative value, a large passband error can form. (This problem is remedied with min-max design presented later.)

The convex optimization problem solved by using CVX library, which is a MATLAB package developed for implementation of *disciplined convex programming* problems. It is possible to solve constrained minimization and maximization problems using CVX library. Part of the MATLAB code that uses the CVX library in the convex design of staggered MTI filter given as follows.

```

cvx_begin
    variable x(N)
    variable delta
    minimize delta
        subject to
            ones(1,N)*x==0
            abs(Astop*x) <= delta
            abs(Apass*x - 1) <= weight*delta
cvx_end

```

Figure 3.7 indicates the frequency response of the designed non-uniform MTI filter for different weight factors \mathcal{W} and Table 3.2 gives the related performance criteria of the design. The effect of weight factor on the performance measures are plotted in Figure 3.8.

Stagger ratio used for the convex design is 11 : 16 : 13 : 17 (taken from [5]). As seen from the Figure 3.7, the effect of \mathcal{W} on the stopband attenuation is similar to the least square design. The increase in \mathcal{W} provides better attenuation in stopband whereas the maximum deviation in the passband increases also. In order to obtain a more general opinion related to the effect of weight factor, Figure 3.8 must be examined. It shows that the increase in \mathcal{W} results in different effects on the performance measures. When the weight factor takes values between 10^4 and 10^7 , all the parameters change abruptly. However, four separate regions can be observed by examining the stopband attenuation value. Stopband attenuation value takes different values that stay constant for different \mathcal{W} intervals. Mean passband error nearly shows a decreasing pattern whereas maximum deviation does not have a predictable behaviour.

Looking at the effect of weight factor on performance measures, it is reasonable to choose the weight factor similar to the least square design case. Once the required stopband attenuation is specified, the weight factor that gives the satisfactory stopband attenuation with smaller maximum deviation can be selected.

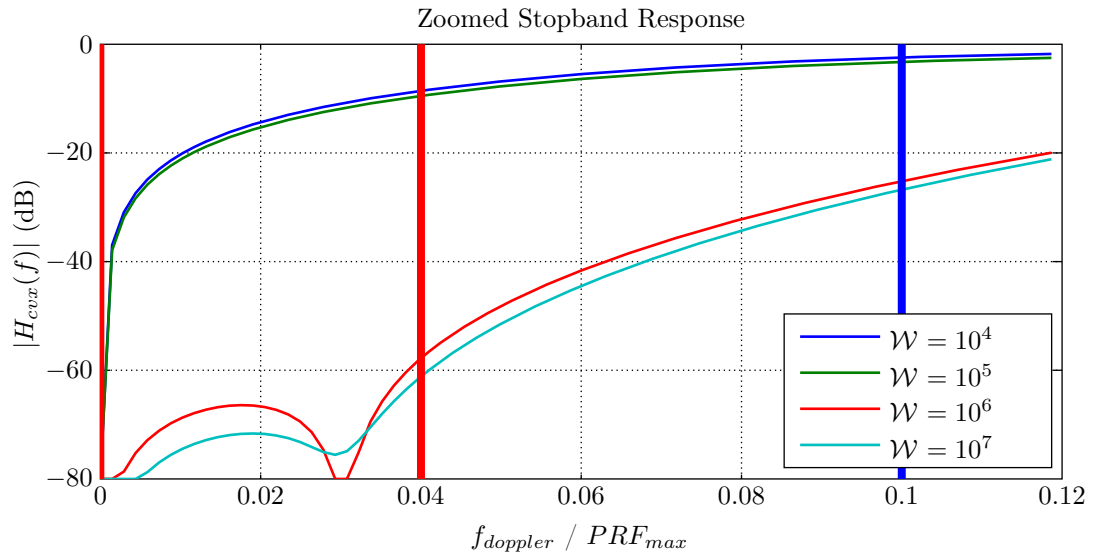
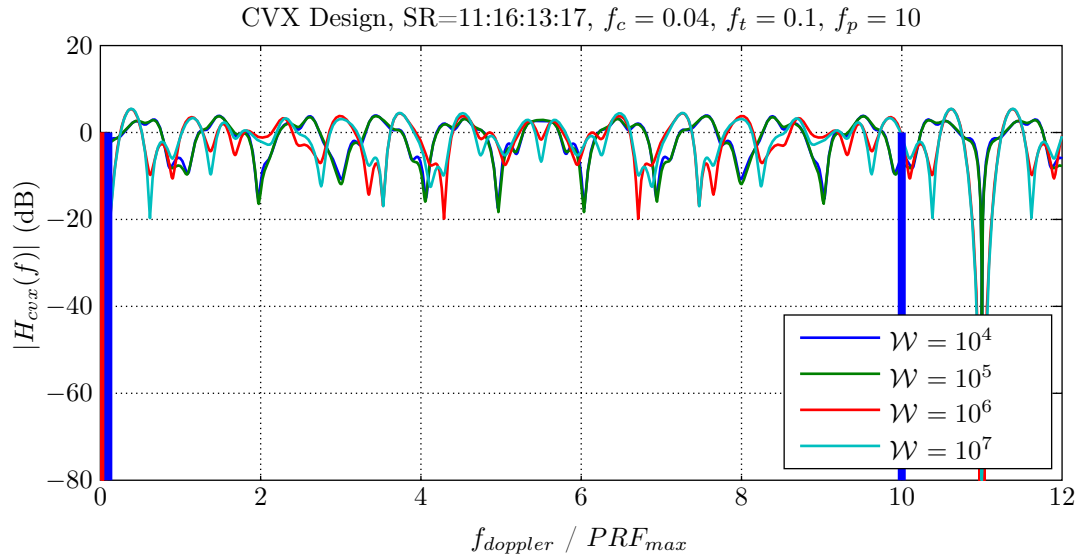


Figure 3.7: Frequency Response of Convex Design with Different \mathcal{W} Values

Table 3.2: Performance Measures of Convex Design for Different \mathcal{W} Values

\mathcal{W}	MSA (dB)	SA (dB)	MPE (dB)	MD (dB)
10000	-14.540	-8.659	-0.614	17.464
100000	-15.470	-9.584	-0.664	18.310
1e+06	-77.987	-58.366	-0.612	25.309
1e+07	-79.187	-61.712	-0.635	26.876

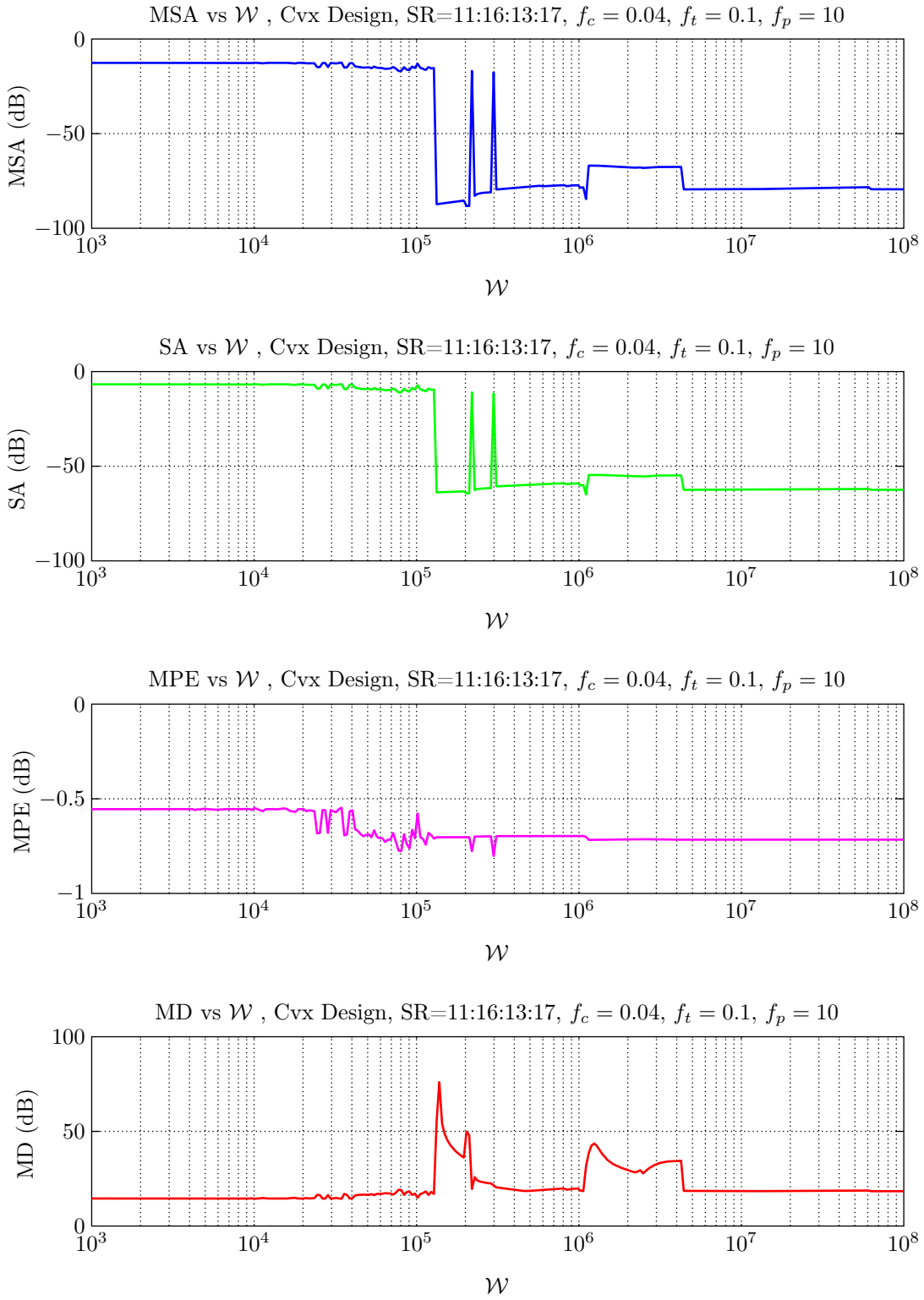


Figure 3.8: Effect of \mathcal{W} on MSA, SA, MPE and MD for Convex Design

3.5 Min-Max Design

In this section, we examine the min-max filter design method for non-uniform MTI filter design. The min-max filter design aims to select the filter coefficients to minimize the maximum deviation from the desired response in the passband. This method is different than the two previous methods. The earlier methods have a single optima which is the global one while this one has many local maximas. Therefore, this method requires a good initial filter coefficient set for a satisfactory performance. It is therefore necessary to experiment with different initial filter weights to determine the parameters that satisfy the required specifications. From the constraints perspective, this filter design also based on the minimization of the maximum passband ripple and maximization of the stopband attenuation. The optimization problem of the min-max design can be stated as follows

$$\begin{aligned}
 & \text{minimize} && \delta \\
 & \text{subject to} && |H_{mm}(f, \alpha_i)| \leq \delta, \quad f \in [0, f_c], \quad \alpha_i \in \mathbf{R}, \quad i \in \mathbf{N}_0 \\
 & && |1 - |H_{mm}(f, \alpha_i)|| \leq \mathcal{W}\delta, \quad f \in [f_t, f_p], \quad \alpha_i \in \mathbf{R}, \quad i \in \mathbf{N}_0 \\
 & && \sum_{n=0}^{N-1} \alpha_n = 0, \quad \alpha \in \mathbf{R}
 \end{aligned} \tag{3.27}$$

Here $H_{mm}(f, \alpha_i)$ is the frequency response of the min-max filter and the variable δ shows the maximum deviation from the desired characteristics (for $\mathcal{W} = 1$). The goal in this design is to minimize the maximum deviation from the desired highpass characteristic. The first and second constraints enforce the *magnitude deviation* be smaller than δ (for $\mathcal{W} = 1$) in the designated bands. The third constraint guarantees that the min-max design has a null at DC frequency.

Different from the LS design, there is no closed form mathematical relation from which the optimal min-max filter coefficients can be retrieved. The optimization has to be done numerically. The numerical implementation of the optimization problem requires the discretization of frequency band into a dense set of frequency points. Therefore, the constraints given in (3.27) are not evaluated for a continuum of points; but for a finitely many number of points.

Similar to the convex design, a weight factor \mathcal{W} is introduced to establish a trade-off between clutter attenuation and passband ripple objectives. It should also be noted that the min-max problem examined here is focused on minimizing the maximum deviation of the *magnitude* response from the desired response.

Figure 3.9 indicates the obtained frequency response for different weight factors and Table 3.3 gives the related performance measures of the design. The effect of weight factor, is given in Figure 3.10.

In these figures, the initial filter coefficients are kept constant and binomial coefficients are used in order to see the effect of the weight factor \mathcal{W} individually. The stagger ratio of 12 : 16 : 13 : 18 is used (taken from [38]). When the Figure 3.9 is examined, \mathcal{W} indicates the same effects as in least square and the convex designs. Larger values of \mathcal{W} result in increase in stopband attenuation and passband ripple. However, different from the previous designs, maximum deviation does not have a monotonous increase or decrease characteristic. To get a more general idea, it is necessary to examine the effect of \mathcal{W} in a much wider interval. Figure 3.10 indicates the effect of \mathcal{W} on the performance parameters. Examination of the figure

indicates that stopband attenuation parameters show a continuous increase whereas passband ripple fluctuates rapidly. In order to select the weight factor that gives a reasonable response in terms of stopband attenuation and passband ripple, smaller maximum deviation value must be selected for specified stopband attenuation.

It is important to remember that Figures 3.9 and 3.10 are plotted by using the same initial filter coefficients. Since the min-max optimization problem has local optima, it is necessary to see the effect of the initial filter coefficients on the response of the min-max sensed designed non-uniform MTI filter. Therefore, min-max design is evaluated with different initial coefficient sets which are selected randomly. Obtained results are presented in Figure 3.11, 3.12 and Table 3.4

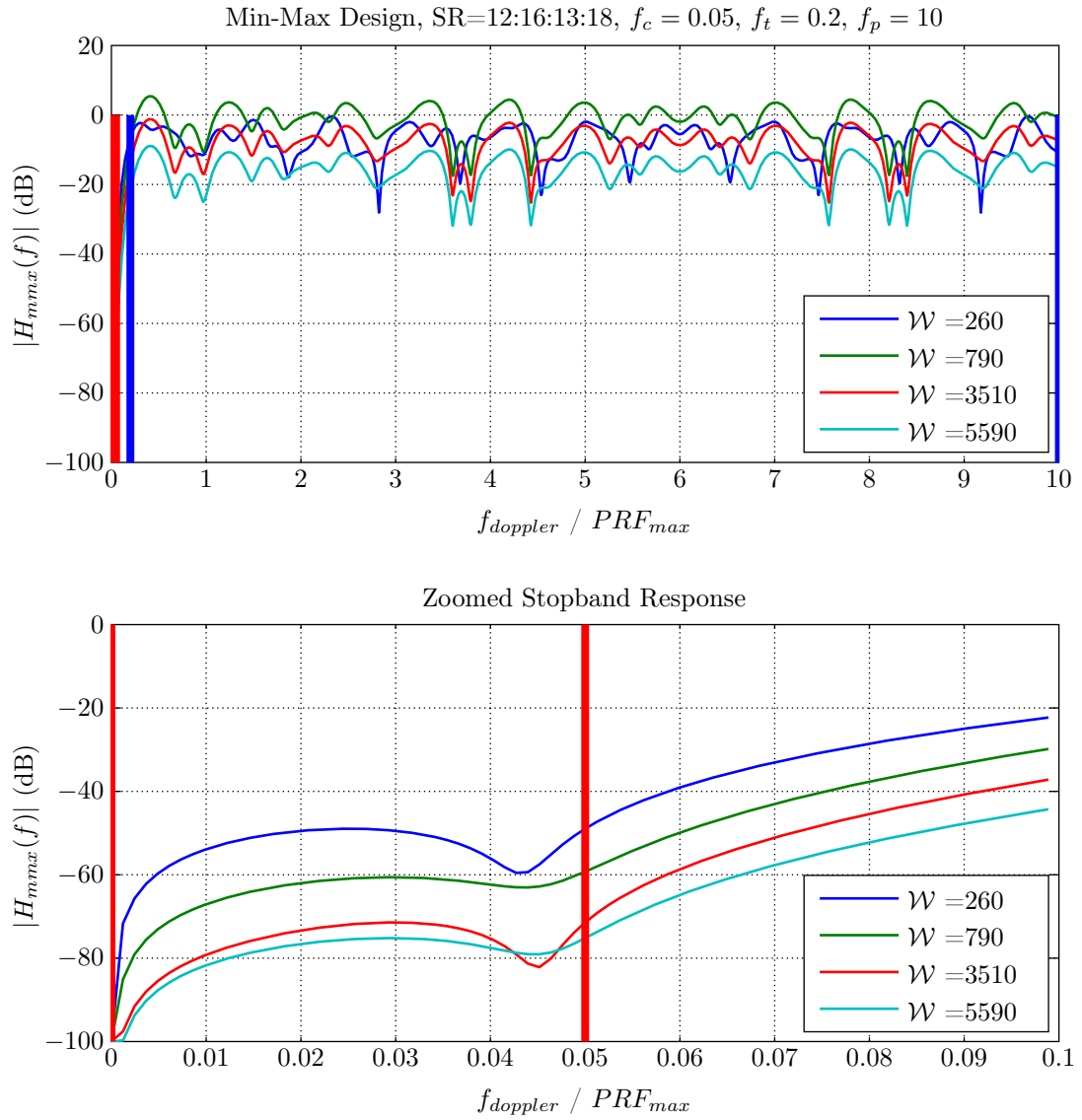


Figure 3.9: Frequency Response of Min-Max Design with Different \mathcal{W} Values

Table 3.3: Performance Measures of Min-Max Design for Different \mathcal{W} Values

\mathcal{W}	MSA (dB)	SA (dB)	MPE (dB)	MD (dB)
260	-55.042	-50.697	-6.285	28.071
790	-63.927	-60.375	-0.577	17.535
3510	-78.101	-73.861	-7.224	25.245
5590	-78.861	-76.513	-14.918	31.869

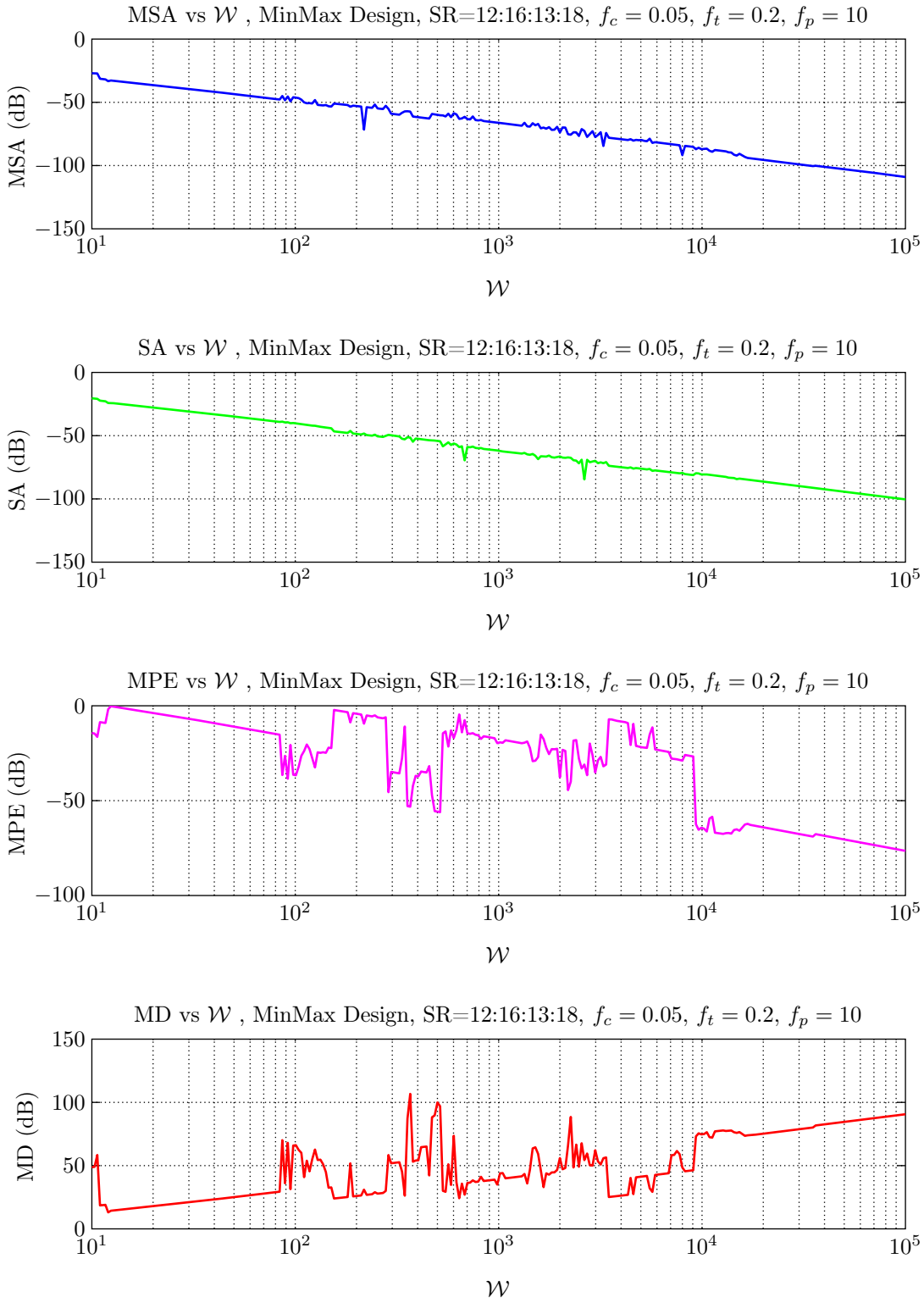


Figure 3.10: Effect of \mathcal{W} on MSA, SA, MPE and MD for Min-max Design for Same Initial Coefficients

Figure 3.11 indicates the response of min-max filter with four different initial coefficient sets and same weight factor. It is seen that several values in terms of stopband attenuation and passband ripple are obtained. This indicates the importance of the effect of the initial filter coefficients on the min-max design. Importance of the selection of the initial filter coefficients are derived from the nature of the min-max design, since the min-max design algorithm seeks the minimum deviation near the initial filter coefficient values. To see the effects of the initial filter coefficient on the performance measures, 300 different initial conditions are evaluated and the corresponding performance parameters are plotted in Figure 3.12.

Min-max design requires more computation compared to the previous least square and convex design methods. Initial filter coefficients and the weight factor must be selected appropriately in order to obtain the required response in terms of stopband attenuation and the passband ripple. The taken approach for the min-max design of non-uniform MTI filter requires two phases. First, the weight factor is determined according to the required stopband attenuation by using the binomial coefficients as the initial filter coefficients. After the weight factor selection, different initial conditions for specified number of iterations are tried and the coefficients that give the minimum deviation in the passband are selected. Using this approach four filters are designed and obtained results are presented in Figure 3.13. Stopband attenuation bound for these four filters are selected as 45 dB, 45 dB, 60 dB and 70 dB respectively. Obtained performance parameters are given in Table 3.5. Using this approach, it is possible to obtain desired stopband attenuation with improved maximum deviation by determining the initial filter coefficients and weight factor.

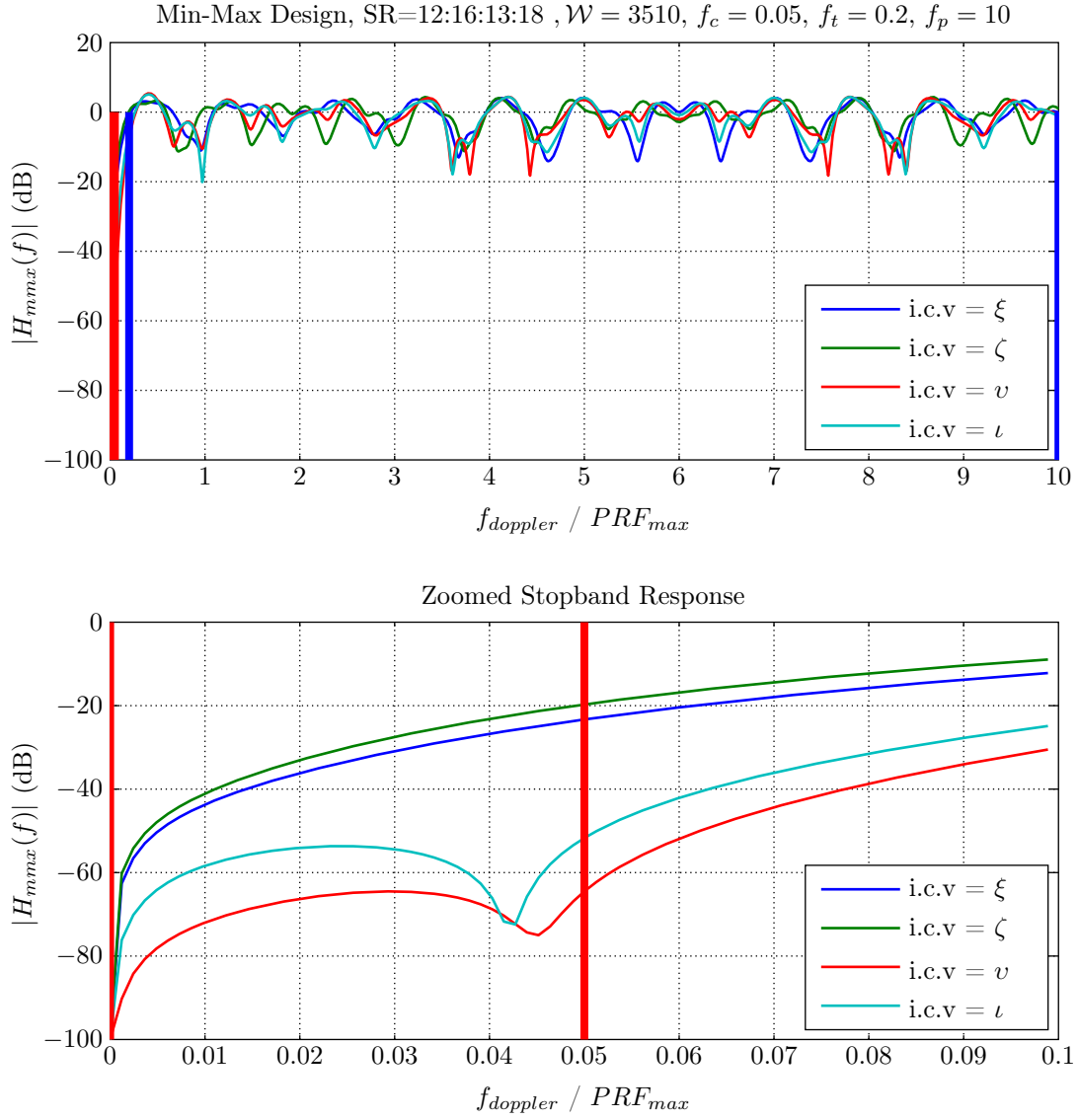


Figure 3.11: Frequency Response of Min-Max Design for Different Initial Conditions with the Same \mathcal{W} Values

Table 3.4: Performance Measures for Min-max Design for Different Initial Filter Coefficients with Same \mathcal{W} Values

Initial Coefficient Vector (i.c.v)	MSA (dB)	SA (dB)	MPE (dB)	MD (dB)
$\xi = [-0.53 \ -0.26 \ 1.72 \ -1.09 \ 0.16]$	-32.044	-23.682	-0.566	14.132
$\zeta = [0.57 \ 0.14 \ 2.22 \ -0.52 \ -2.42]$	-29.156	-20.073	-0.561	11.315
$\nu = [0.52 \ 1.20 \ -1.12 \ 0.74 \ -1.34]$	-71.135	-66.891	-0.614	18.262
$\iota = [0.18 \ 0.04 \ 0.53 \ -0.89 \ 0.15]$	-59.852	-53.433	-0.616	20.107

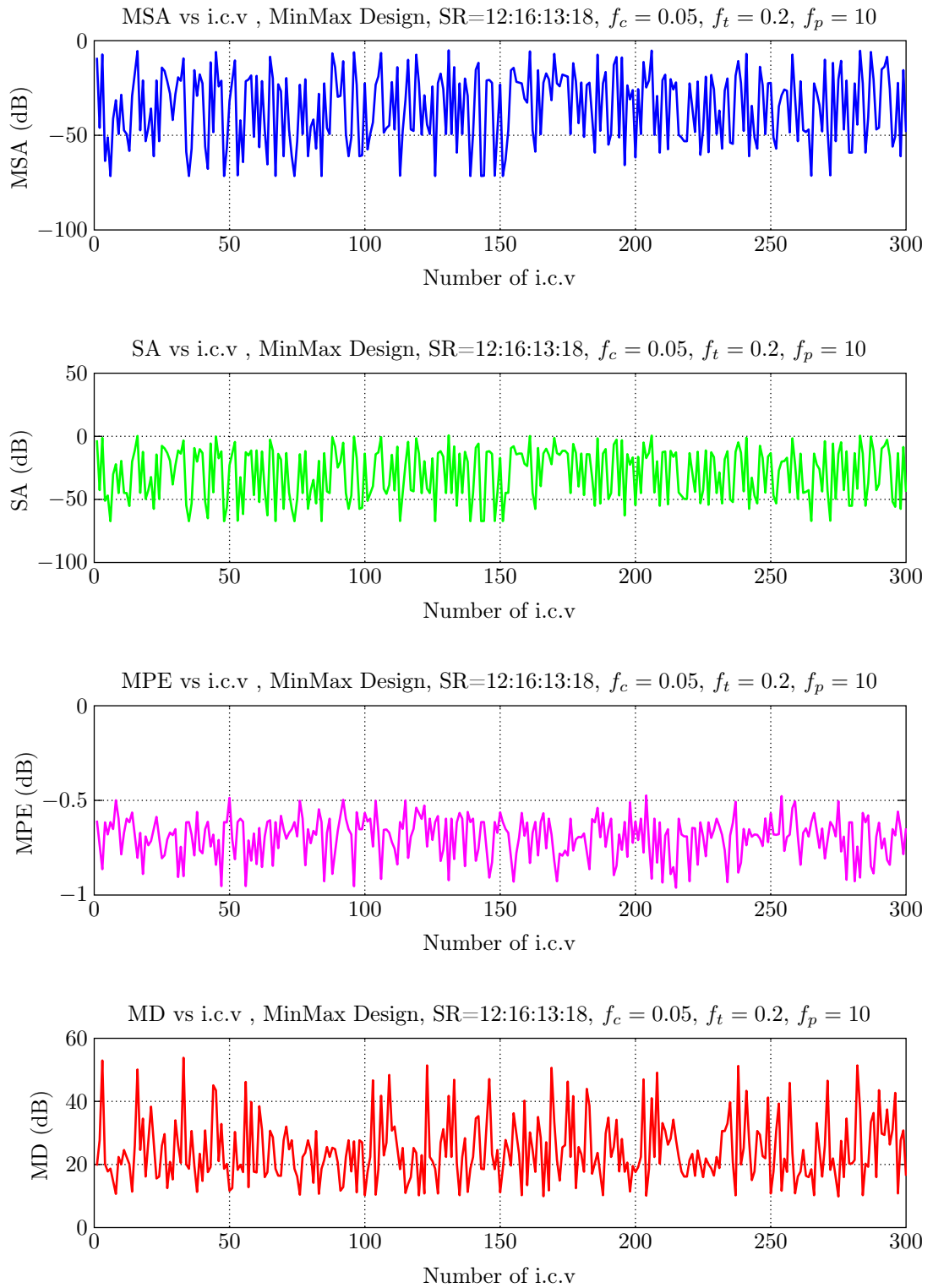


Figure 3.12: Effect of Initial Filter Coefficients on Performance Measures of Min-Max Design for Same \mathcal{W} Values

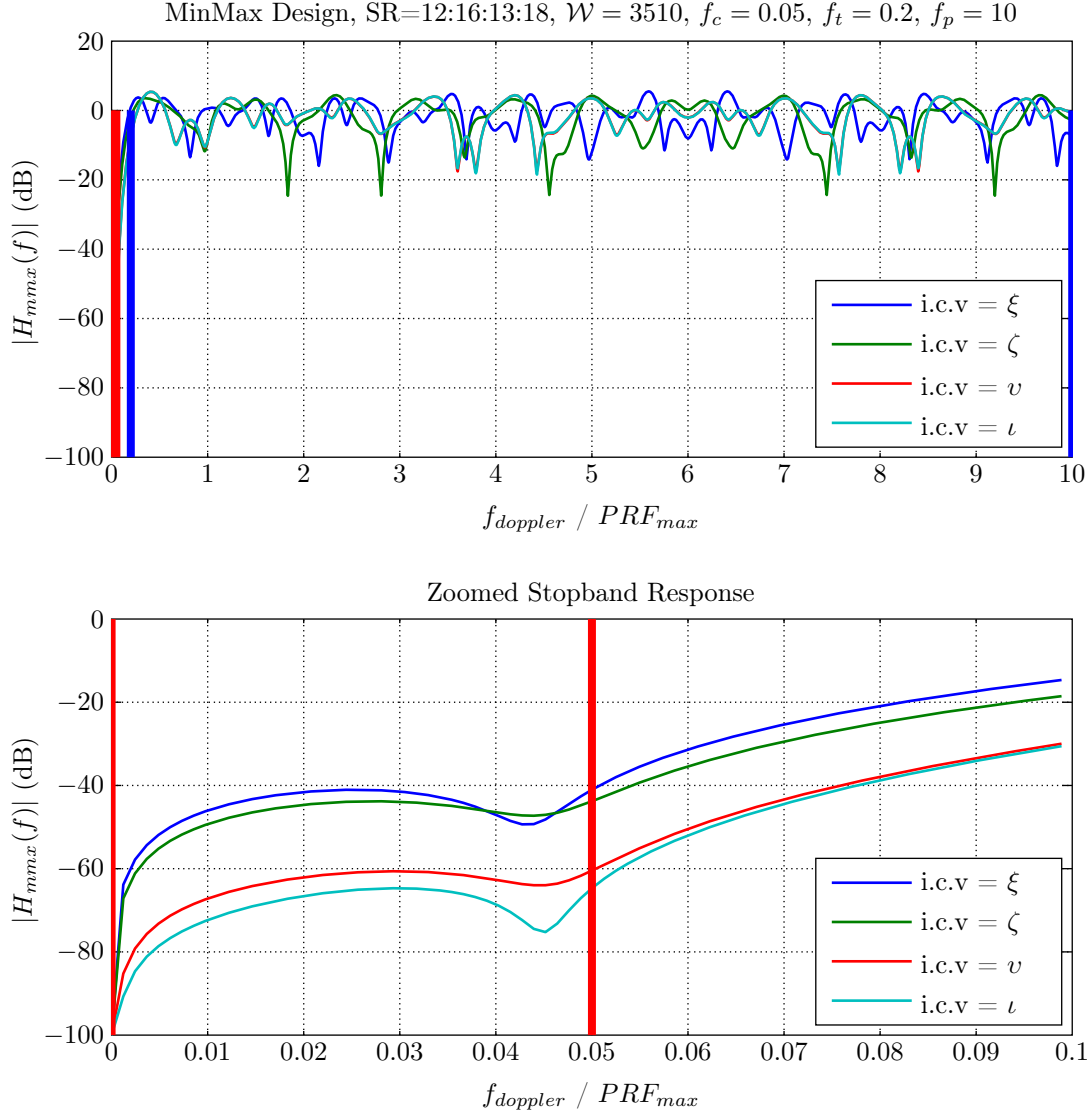


Figure 3.13: Min-Max Design for Different Stopband Attenuation Requirement with Different Initial Conditions and \mathcal{W} Values

Table 3.5: Performance Measures of Min-Max Design for Different Stopband Attenuation Requirement with Different Initial Conditions and \mathcal{W} Values

Initial Coefficient Vector (i.c.v)	MSA (dB)	SA (dB)	MPE (dB)	MD (dB)
$\xi = [-1.92 \ 0.63 \ 0.75 \ 0.21 \ 0.33]$	-46.910	-42.645	-0.691	15.978
$\zeta = [-0.94 \ -0.65 \ 0.28 \ -1.13 \ 2.44]$	-47.361	-44.824	-0.671	24.601
$v = [0.96 \ -0.34 \ -0.17 \ 0.62 \ -1.06]$	-64.175	-61.705	-0.613	17.565
$t = [-1.52 \ -1.07 \ -3.07 \ 0.52 \ 5.14]$	-71.357	-67.105	-0.614	18.488

3.6 Numerical Comparison with Selected Filter Designs

To this point designed filters are compared individually with different weight factors and initial coefficient sets. In this section filter designs will be compared among themselves and also with the similar filters in the literature.

3.6.1 Binomial Filter

As explained in previous chapter, *Binomial* filter is a filter that is derived by cascading single cancellers. These are simple FIR filters whose coefficients are selected as binomial numbers with alternating signs that are given by

$$w_i = (-1)^{i-1} \frac{N!}{(N-i+1)!(i-1)!}, \quad i = 1, 2, \dots, N+1 \quad (3.28)$$

where N is the order of the filter.

Binomial filters are widely used filters for performance comparison of MTI filters in the literature.

3.6.2 Prinsen's Filter

Prinsen developed a simple algorithm for staggered PRF MTI filters [11]. Design is based on the requirement for the maximally flat stopband characteristic at zero frequency. The filter design also a generalization to the *Binomial* filter. FIR filter equation for the MTI design is given in (3.29).

$$y(f) = \sum_{n=1}^{N-1} w_n e^{j2\pi f t_n} \quad (3.29)$$

where w_0, \dots, w_{N-1} are filter coefficients and t_0, \dots, t_{N-1} are the sampling times.

Theory of the design relies on making the first M coefficients of the Taylor series expansion of the filter response near zero frequency to be zero.

The Taylor expansion of $y(f)$ around $f = 0$ is given in following equations.

$$y(f) = y(0) + \frac{y'(0)}{1!} f + \frac{y''(0)}{2!} f^2 + \dots \quad (3.30)$$

$$y^{(k)}(0) = (j2\pi)^k \sum_{n=0}^{N-1} t_n^k w_n, \quad k = 0, 1, 2, \dots \quad (3.31)$$

Maximally flat stopband and a non-trivial solution requires that the first $N-1$ coefficients of $y^{(k)}(0)$, $k = 0, \dots, M-1$ in (3.31) to be zero. Matrix form of the $N-1$ equations are given as

$$\mathbf{T}\mathbf{w} = -w_0 \mathbf{u}_1 \quad (3.32)$$

where

$$\mathbf{T} = \begin{bmatrix} 1 & 1 & \dots & 1 \\ t_1 & t_2 & \dots & t_{N-1} \\ \vdots & \vdots & \ddots & \vdots \\ t_1^{N-2} & t_2^{N-2} & \dots & t_{N-1}^{N-2} \end{bmatrix}, \quad \mathbf{w} = \begin{bmatrix} w_1 \\ w_2 \\ \dots \\ w_{N-2} \end{bmatrix}, \quad \mathbf{u}_1 = \begin{bmatrix} 1 \\ 0 \\ \dots \\ 0 \end{bmatrix}$$

\mathbf{T} matrix is a Vandermonde matrix and \mathbf{T}^{-1} exists since $t_i \neq t_j$ for $i \neq j$. Simplified form of the equation is given in (3.33).

$$w_i = -w_0 \prod_{\substack{n=1 \\ n \neq i}}^{N-1} \frac{t_n}{t_n - t_i} \quad i = 1, \dots, N-1 \quad (3.33)$$

Designed filters are compared with *Binomial* and *Prinsen's* MTI filters under four different cases.

In the first case, the stopband attenuation (*SA*) is fixed. In Figure 3.14, the desired stopband attenuation value is selected as -60 dB. This means that, the magnitude of the filter responses is designed to better than 60 dB at the cutoff frequency f_c . By examining the performance measures given in Table 3.6, one can see that LS design does not provide the required attenuation. This is due to the stopband performance of the LS design. 56.228 dB is the maximum attenuation that LS design can achieve for the used stagger ratio. It must also be noted that the LS design has the smallest mean passband error.

If the performance of the CVX design is focused, it has good stopband attenuation and reasonable values in terms of passband ripple. The performance in stopband is related to the choice of the weight factor. By choosing a different weight factor better values could be obtained for passband ripple with decreased stopband attenuation performance.

The desired min-max design achieves least deviation value and provides required stopband attenuation. Response of Prinsen's filter is also satisfactory. Since it is designed for maximally flat stopband response, it gives better attenuation values. However the passband performance is not very satisfactory and it has large deviations from the ideal response. It has the worst maximum deviation compared to other filter designs.

In the second case, cutoff frequency f_c is reduced. Figure 3.15 indicates this case. As observed, all the responses are improved in terms of stopband attenuation and passband ripple. It should be noted that, the response of LS design is improved, but it does not provide same suppression level of other designs except the *Binomial* filter. It is also eye catching that, maximum deviation of the CVX design is improved nearly 10 dB compared to the previous case.

In the third case, a bigger cutoff frequency is examined. Figure 3.16 shows the response of filters when the cutoff frequency f_c is selected as 0.08. Expectedly, stopband attenuation performances of the filters are decreased. However passband performances do not worsen. On the contrary, better maximum deviation is obtained with min-max design.

The final case considers the response to the bigger velocity band. Figure 3.17 indicates the response of the filters when the passband bound is increased to ten times of the maximum PRF value. As compared with the Figure 3.14, Min-Max and CVX designs present better responses. However response of LS filter in terms of maximum deviation is degraded with

respect to the first case. Therefore, it can be concluded that the usage of wider velocity band exhibits different effects on the performance of the filter designs.

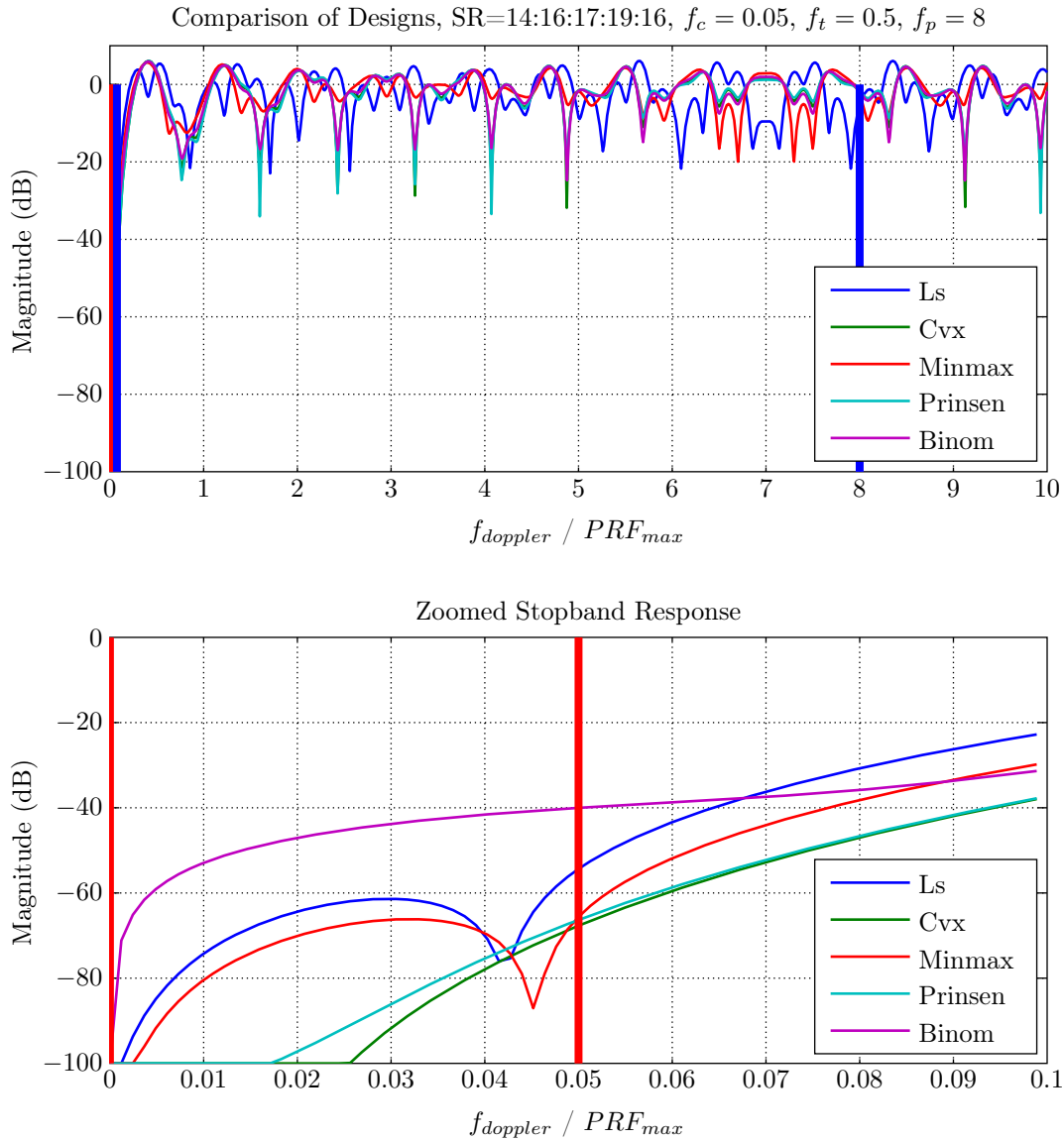


Figure 3.14: Comparison of Designed Filters with Binomial and Prinsen’s Filter with Same Stopband Attenuation Requirement

Table 3.6: Performance Measures for Comparison of Designed Filters with Binomial and Prinsen’s Filter with Same Stopband Attenuation Requirement

Designs	MSA (dB)	SA (dB)	MPE (dB)	MD (dB)
Ls	-65.918	-56.228	-1.128	22.974
Cvx	-84.256	-68.740	-0.807	31.856
Min-Max	-71.762	-68.536	-0.796	19.944
Prinsen	-81.606	-67.280	-0.800	34.047
Binom	-45.688	-40.175	-0.798	24.773

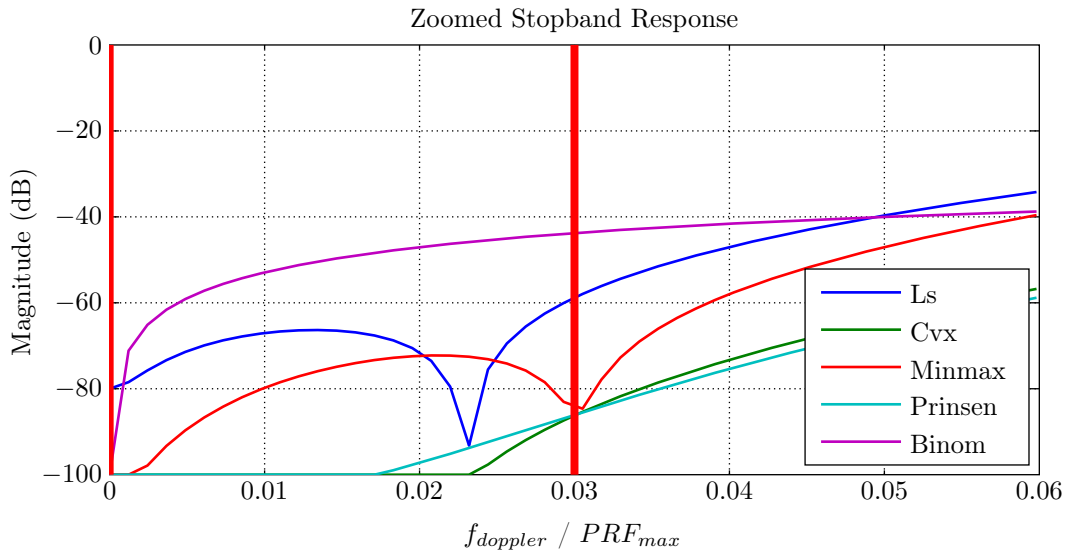
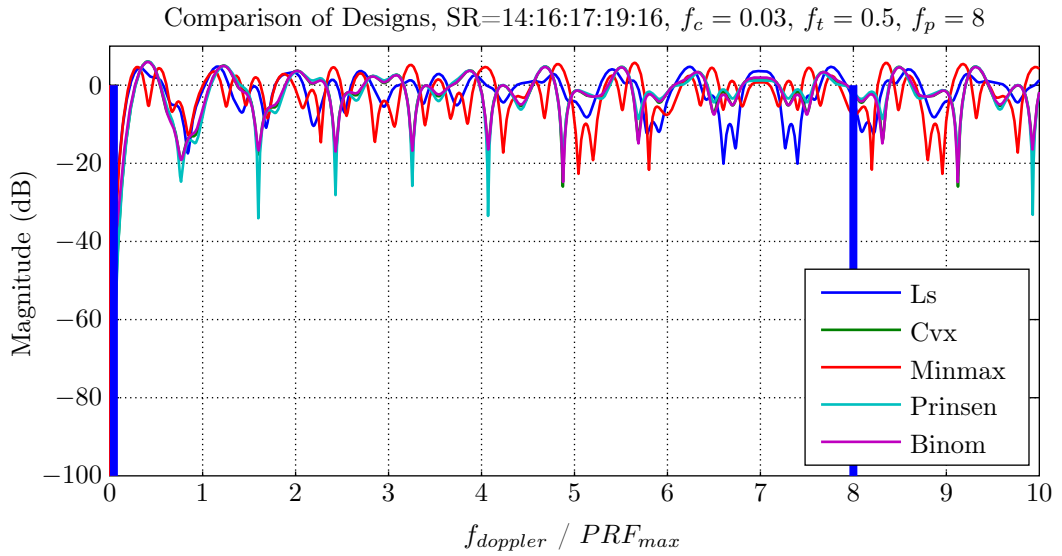


Figure 3.15: Comparison of Designed Filters with Binomial and Prinsen’s Filter with Smaller Cutoff Frequency

Table 3.7: Performance Measures for Comparison of Designed Filters with Binomial and Prinsen’s Filter with Smaller Cutoff Frequency

Designs	MSA (dB)	SA (dB)	MPE (dB)	MD (dB)
Ls	-68.928	-60.051	-0.768	20.098
Cvx	-102.017	-87.380	-0.806	25.971
Min-Max	-77.504	-83.057	-0.863	22.698
Prinsen	-98.145	-86.868	-0.800	34.047
Binom	-49.776	-43.951	-0.798	24.773

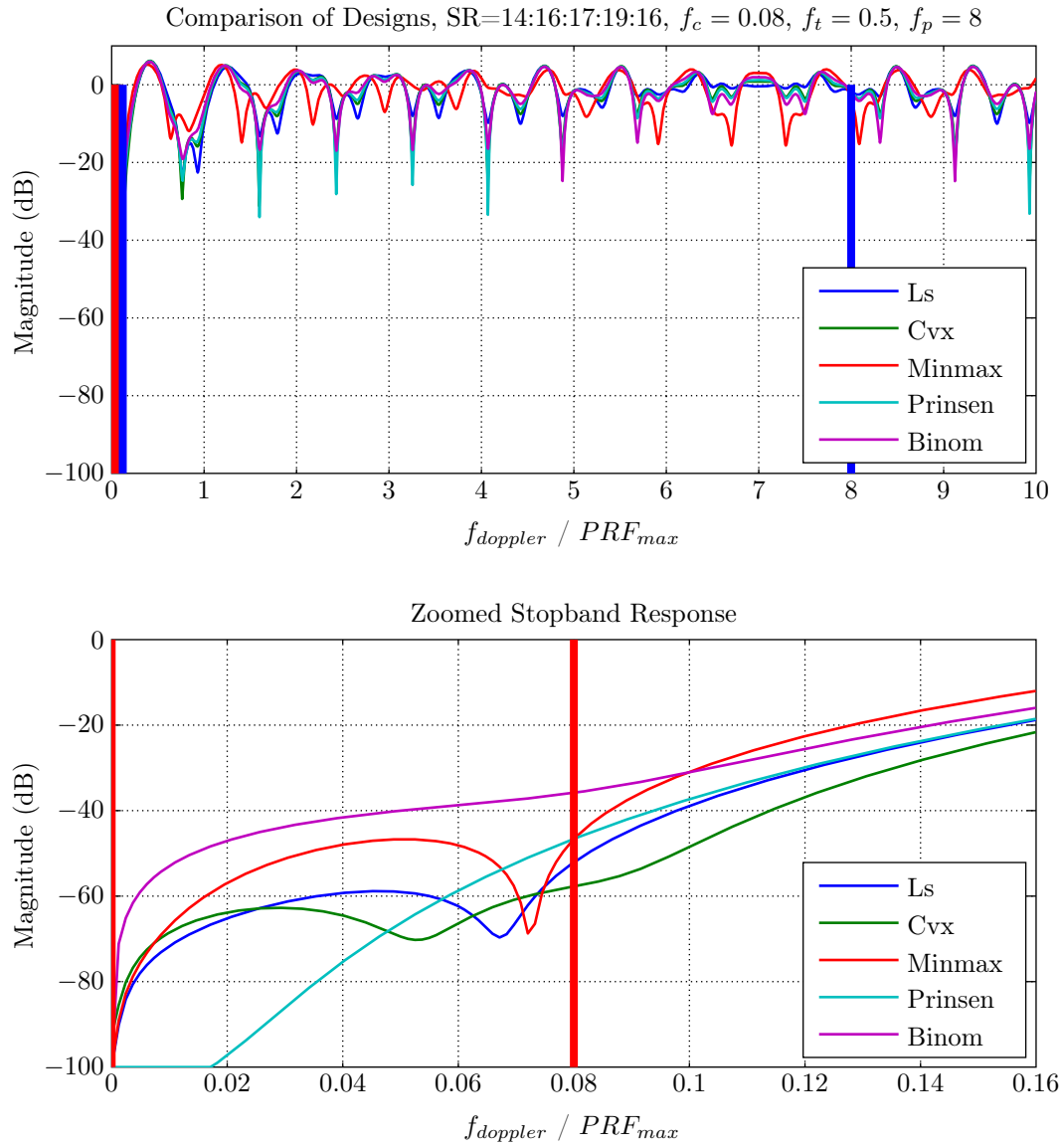


Figure 3.16: Comparison of Designed Filters with Binomial and Prinsen's Filter with Bigger Cutoff Frequency

Table 3.8: Performance Measures for Comparison of Designed Filters with Binomial and Prinsen's Filter with Bigger Cutoff Frequency

Designs	MSA (dB)	SA (dB)	MPE (dB)	MD (dB)
Ls	-62.313	-52.694	-0.762	24.395
Cvx	-64.628	-57.884	-0.803	31.225
Min-Max	-52.152	-47.638	-0.782	15.648
Prinsen	-61.969	-46.941	-0.800	34.047
Binom	-41.948	-35.948	-0.798	24.773

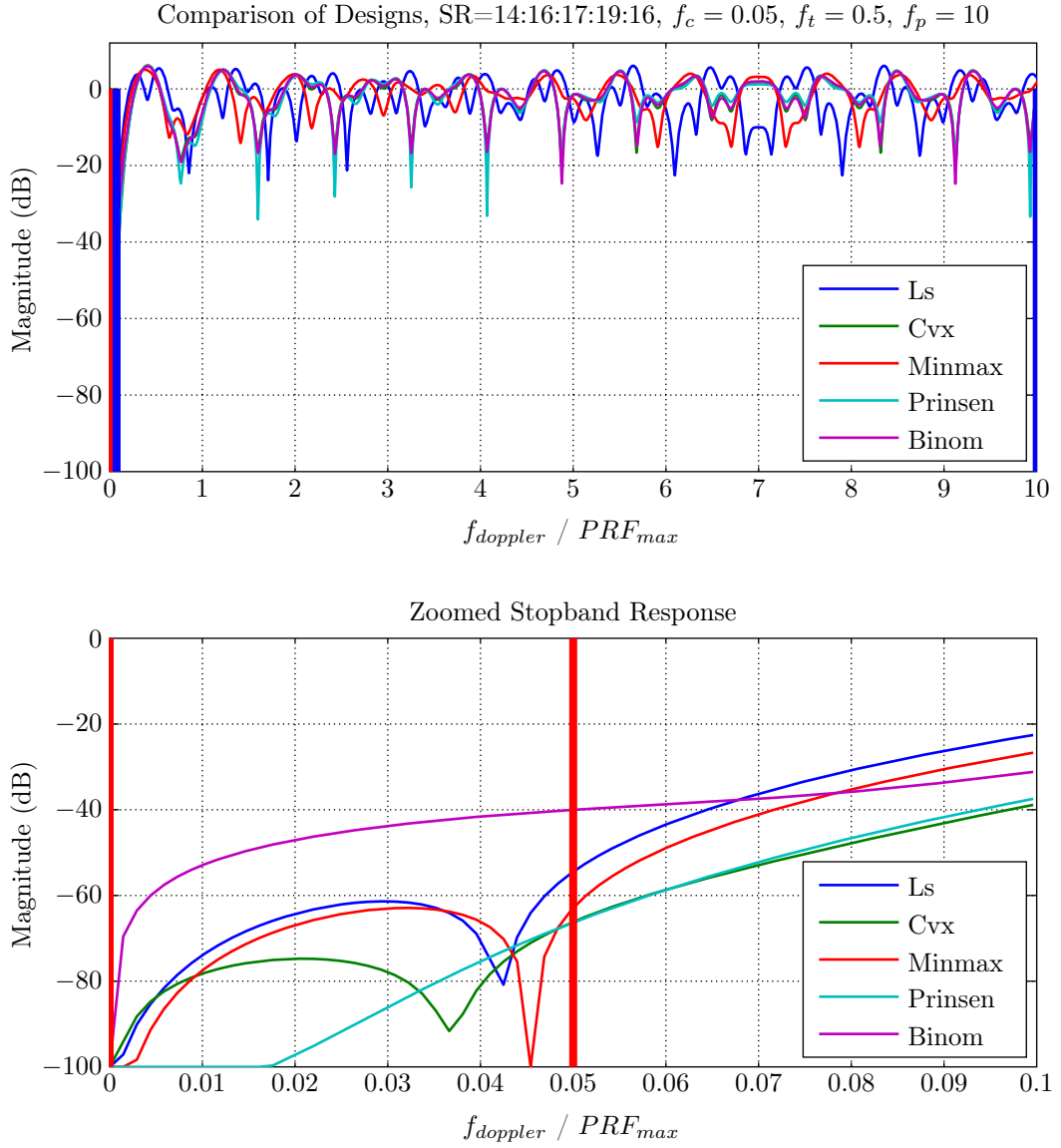


Figure 3.17: Comparison of Designed Filters with Binomial and Prinsen Filter's with Larger Velocity Band

Table 3.9: Performance Measures for Comparison of Designed Filters with Binomial and Prinsen's Filter with Larger Velocity Band

Designs	MSA (dB)	SA (dB)	MPE (dB)	MD (dB)
Ls	-65.499	-54.759	-1.032	23.855
Cvx	-76.607	-66.319	-0.913	19.634
Min-Max	-68.512	-63.361	-0.833	15.187
Prinsen	-80.774	-66.461	-0.891	34.104
Binom	-45.538	-40.038	-0.901	24.773

CHAPTER 4

CLUTTER SUPPRESSION PERFORMANCE OF FILTER DESIGNS

In this chapter clutter is taken into account for designing optimal staggered MTI filters. First, definition of the clutter and properties of the clutter covariance matrix are given. Second, optimal filters are studied for different types of clutter PSD's. Later, performances of the filter designs are compared according to MTI improvement factor and a modified min-max design is presented. Finally, time varying filter concept is explained and obtained results are discussed.

4.1 Characteristics of Clutter

Clutter is defined as non-wanted interference from land, sea or weather. Return from these, can block the target component of the radar echo signal. Therefore, it is important to reject clutter in radar signal processor units. In most cases the rejection of the clutter is used as a performance index such as clutter attenuation and subclutter visibility.

For MTI filter performance analysis, the effect of clutter is put into consideration by using clutter covariance matrix or clutter power spectrum density (PSD). Transformation between these metrics are carried out with Fourier transformation.

Widely used model for the clutter PSD is Gaussian Model with zero mean Doppler frequency ([3]):

$$C(f) = \frac{P_c}{\sqrt{2\pi}\sigma_g} \exp\left(\frac{-f^2}{2\sigma_g^2}\right) \quad (4.1)$$

Here P_c is the clutter power, f is the Doppler frequency and σ_g is the standard deviation of the clutter spectrum. An example of Gaussian Clutter model for several σ_g values are given in Figure 4.1.

Using the power spectral model, the elements of the normalized clutter covariance matrix can be found by

$$\begin{aligned} \mathbf{R}_{ij} &= \int_{-\infty}^{\infty} C(f) e^{j2\pi f(t_i - t_j)} df \\ &= e^{-2\pi^2 \sigma_g^2 (t_i - t_j)^2} \end{aligned} \quad (4.2)$$

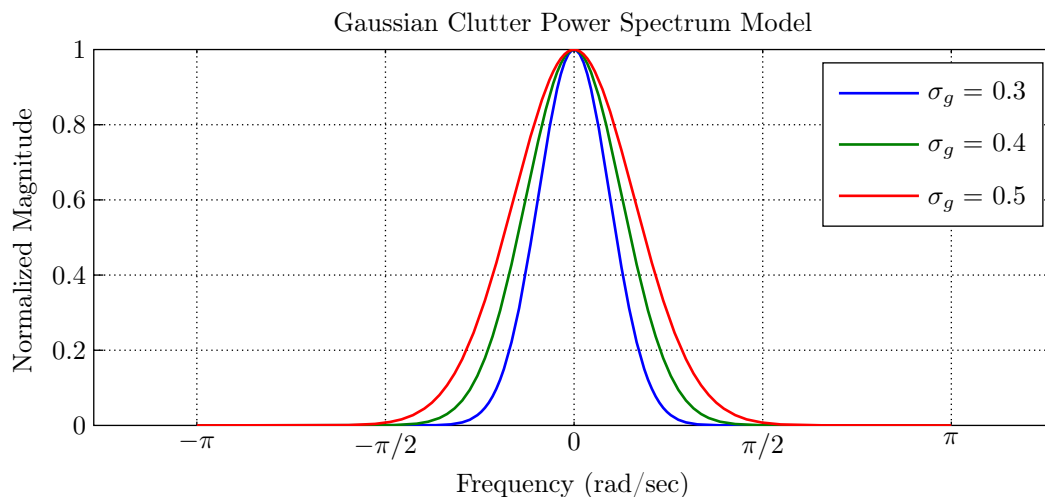


Figure 4.1: Gaussian Clutter Power Spectrum Density Model

Calculation of the optimal MTI filters is based upon clutter covariance matrix. Hsiao [13] shows that elements of the eigenvector that corresponds to the minimum eigenvalue of the clutter covariance matrix, are the coefficients of the optimum MTI filter.

Another optimum filter design comes from the matched filtering concept. The weights are calculated for each transmitted signal component in the sense of matching the received waveform. Optimal filter weights for each transmitted pulse are given by

$$\mathbf{w}_{\text{opt}} = \mathbf{R}^{-1}\mathbf{s} \quad (4.3)$$

Here \mathbf{w}_{opt} is the coefficient vector of optimum filter weights and \mathbf{s} is the signal vector. Figure 4.2 illustrates the performance comparison of optimal filters with different clutter PSD values. Here, optimal filter-2 represents the eigenfilter method of Hsiao's (the filter corresponds to eigenvector of $\mathbf{R}_{\mathbf{c}}$ with the smallest eigenvalue), whereas optimal filter-1 illustrates the match filter type optimal filter. The first sub figure is plotted with a Gaussian clutter PSD and the second sub figure is plotted with a Gaussian clutter PSD model with a large Doppler spread. For the first case, optimal filters show the same performance, whereas in the second case optimal filter-1 shows better response for all Doppler frequencies. It must be noted that the optimal filter-1 is unique for each frequency as seen from (4.3), whereas the optimal filter-2 is the same for all frequencies.

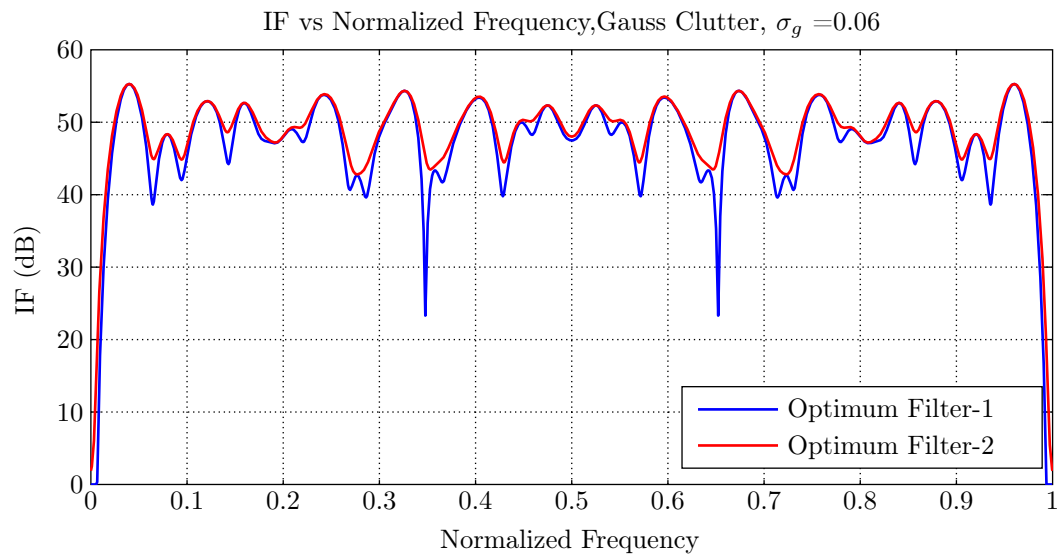
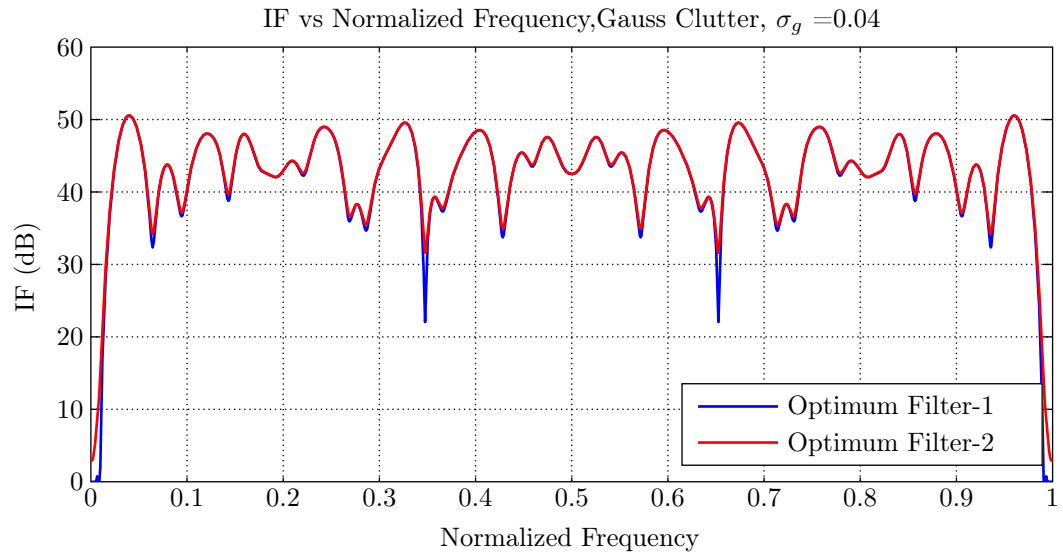


Figure 4.2: Comparison of Optimum MTI Filters with Different Clutter PSD's

4.2 Comparison of Designed Filters with Optimal MTI Filter

In the previous section, designed filters are compared in terms of magnitude response. In this section, the filters are compared in terms of MTI improvement factors. MTI improvement factor of the corresponding FIR filter designs can be calculated as follows;

$$IF = \frac{\mathbf{w}^H \mathbf{R}_s \mathbf{w}}{\mathbf{w}^H \mathbf{R}_c \mathbf{w}} \quad (4.4)$$

where the variables \mathbf{w} , \mathbf{R}_c and \mathbf{R}_s represent weight vector, clutter covariance matrix and signal covariance matrix respectively.

The comparisons related to improvement factor in the following figures and chapters, the effect of Doppler spread of clutter is investigated. The used clutter models and corresponding values of parameters are given in Table 4.1.

Table 4.1: Used Clutter Models and Related Values of Parameters

Antenna Type	Stationary Antenna	Rotary Antenna
Clutter Models	Gaussian Clutter	Gaussian Clutter
Doppler Spread ($f_{doppler}/PRF_{max}$)	0.02-0.08	0.02-0.08
SNR (dB)	10	10
CNR (dB)	50	50
Azimuth Beamwidth ($^\circ$)	-	1.7
Antenna Rotation Period (rpm)	-	40

For the sake of comparison, the frequency responses of the designs are presented first. Figure 4.3 indicates the frequency responses of the designed filters with Prinsen's filter for the stagger ratio of 36 : 45 : 39 : 48 : 42. Table 4.2 presents the performance measures. If the figure is examined, it is seen that the responses of the filters show similar passband characteristic except from the maximum deviation value and stopband responses.

In Figure 4.4 improvement factor for each filter in Figure 4.3 is plotted with the assumption of the Gaussian clutter PSD. It is seen that all the filters have almost identical improvement factor values in the passband. These values are given in Table 4.3. By comparing the improvement factors and performance measures, it is possible to conclude that mean stopband attenuation (*MSA*) criteria is closely linked to the improvement factor performance of the filters.

In Figure 4.5 improvement factors for all filters are plotted with different type of clutter model. In this case a Gaussian clutter with larger spread is used. For this case, the optimal filter response shows different characteristic compared to other filters. All the other filters achieve very similar improvement factors whereas the performance of them differs from the optimal filter considerably. Prinsen's filter and designed filters according to the performance measures do not provide an improvement factor close to the optimal case.

The decrease in the improvement factor values and associated performance measures constitute the possibility of designing another type of non-uniform MTI filter with better improvement

factor. The idea is investigated in the following subsection and another design method is developed by modifying the min-max design according to MTI improvement factor of optimal filter.

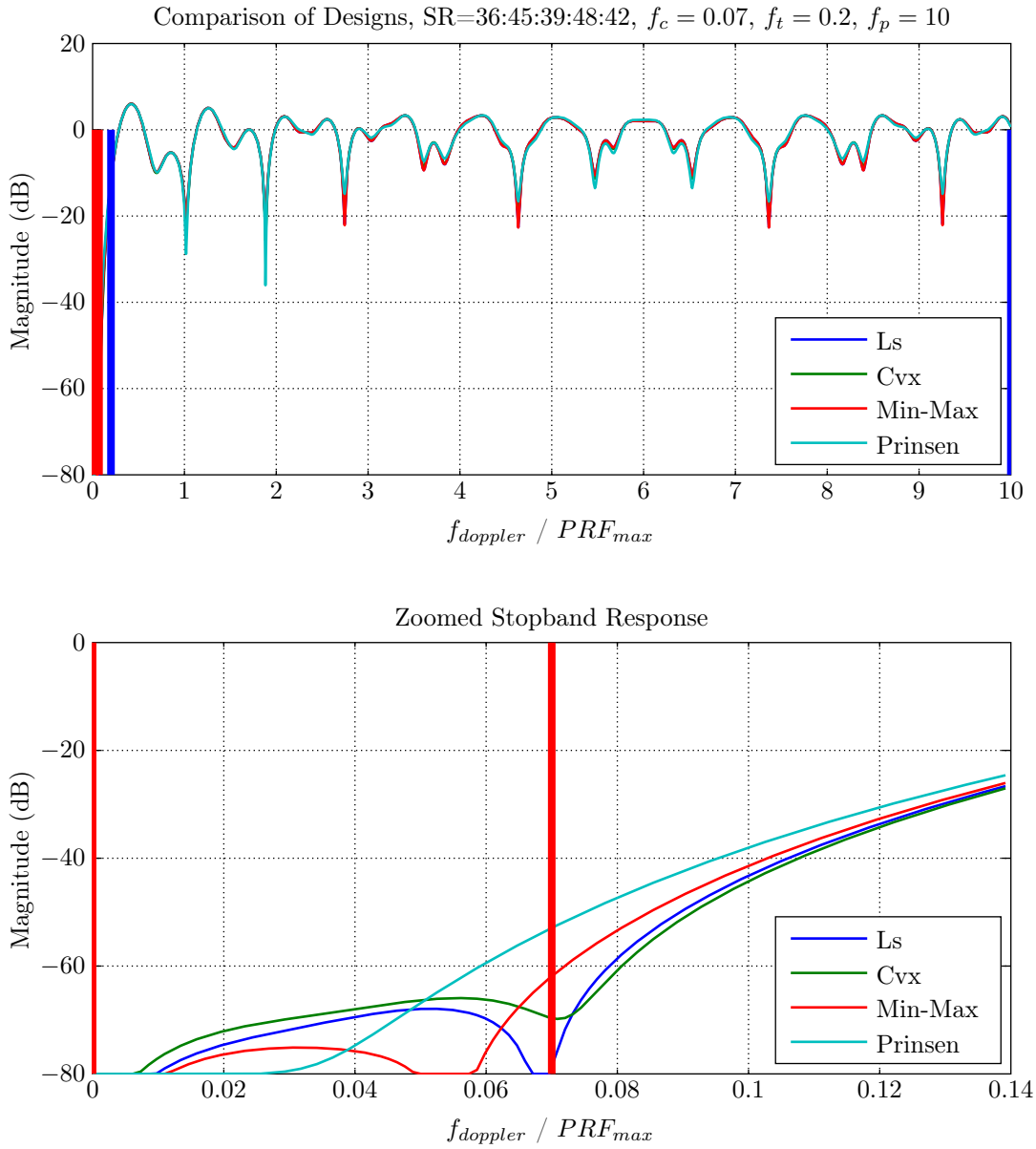


Figure 4.3: Frequency Response Comparison of Designed Filters with Prinsen's Filter

Table 4.2: Performance Measures for Comparison of Designed Filters with Prinsen's Filter

Designs	MSA (dB)	SA (dB)	MPE (dB)	MD (dB)
Ls	-72.682	-82.032	-0.532	22.603
Cvx	-69.843	-69.549	-0.529	25.691
Minmax	-75.708	-62.296	-0.533	22.670
Prinsen	-67.130	-53.172	-0.525	36.056

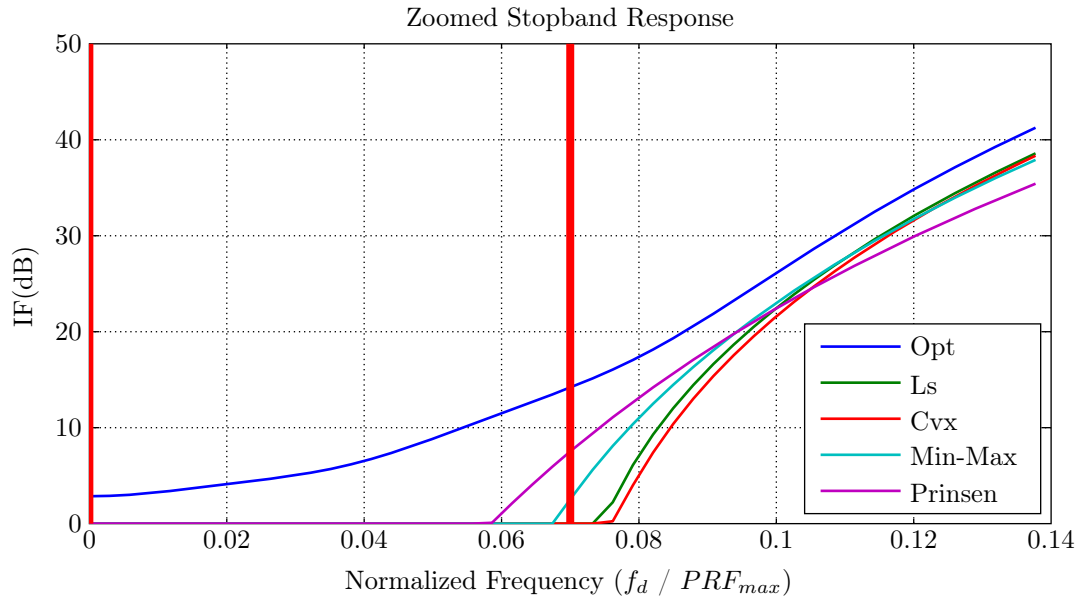
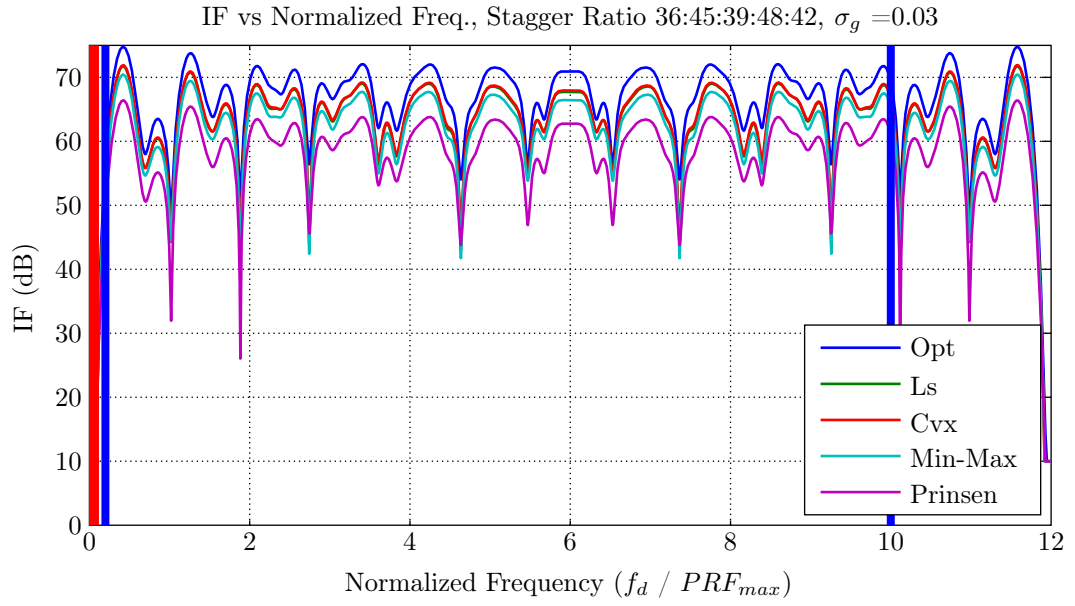


Figure 4.4: Improvement Factor Comparison of Designed Filters with Prinsen’s Filter with Gaussian Clutter PSD

Table 4.3: Improvement Factor Values for Comparison of Designed Filters with Prinsen’s Filter with Gaussian Clutter PSD

	Optimum	Ls	Cvx	Minmax	Prinsen
Improvement Factor (dB)	66.555	63.275	63.463	61.975	58.120

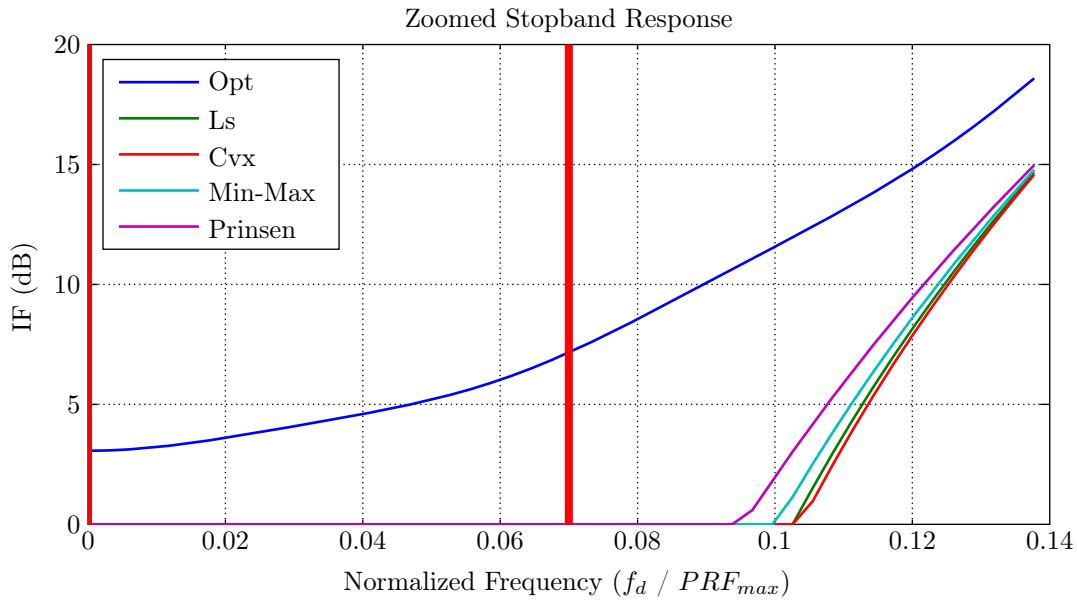
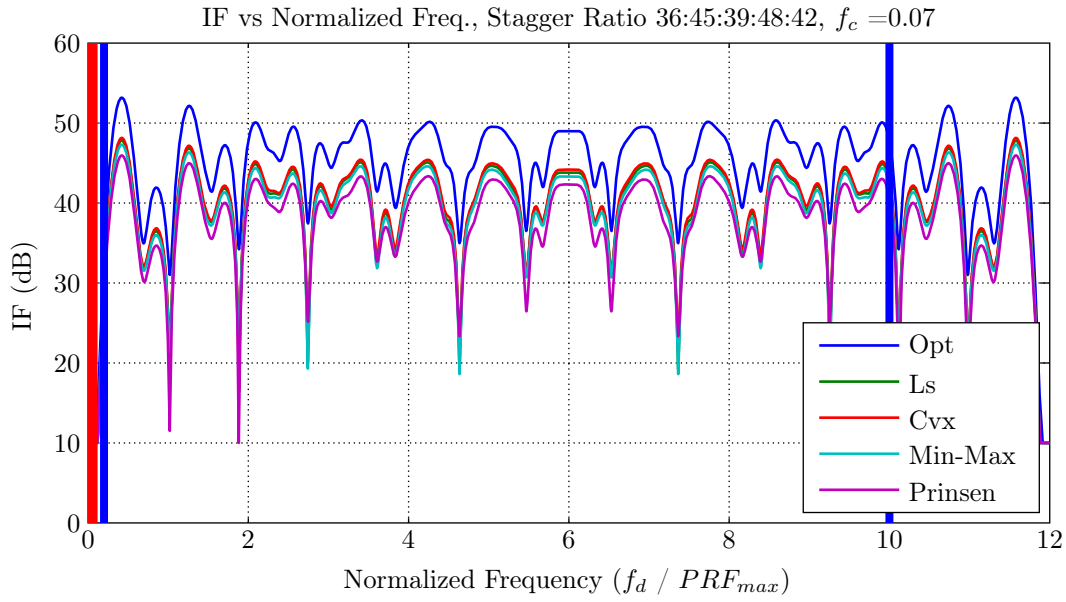


Figure 4.5: Improvement Factor Comparison of Designed Filters with Prinsen’s Filter with Gaussian Clutter PSD with Larger Doppler Spread

Table 4.4: Improvement Factor Values for Comparison of Designed Filters with Prinsen’s Filter with Gaussian Clutter PSD with Larger Doppler Spread

	Optimum	Ls	Cvx	Minmax	Prinsen
Improvement Factor (dB)	45.159	39.362	39.702	38.849	37.667

4.3 Min-Max Filter Design with Optimum Improvement Factor

In this section min-max filter design is modified for the purpose of obtaining a non-uniform MTI filter based on the MTI improvement factor of the optimum filter. First, a frequency interval is taken and the improvement factor of the optimum filter is calculated for each frequency value in the frequency interval of interest. Later, filter coefficients are optimized to provide the nearest improvement factor to optimum filter's using a min-max sense approach.

The optimization equation of the corresponding design is given in (4.5)

$$\min_{w_d, f} (I_{opt} - I_d) = \min_{w_d, f} \left(\frac{\mathbf{w}_{opt}^H \mathbf{R}_s \mathbf{w}_{opt}}{\mathbf{w}_{opt}^H \mathbf{R}_x \mathbf{w}_{opt}} - \frac{\mathbf{w}_d^H \mathbf{R}_s \mathbf{w}_d}{\mathbf{w}_d^H \mathbf{R}_x \mathbf{w}_d} \right) \quad (4.5)$$

where

- \mathbf{I}_{opt} : Optimum filter interference improvement factor
- \mathbf{I}_d : Designed filter interference improvement factor
- \mathbf{w}_{opt} : Optimum filter coefficient vector
- \mathbf{w}_d : Designed filter coefficient vector
- \mathbf{R}_x : Interference covariance matrix ($\mathbf{R}_x = \mathbf{R}_c + \mathbf{R}_n = \mathbf{R}_c + \sigma_n^2 \mathbf{I}$)
- \mathbf{R}_s : Signal covariance matrix ($\mathbf{R}_s = \mathbf{E}\{s(\theta)s^H(\theta)\}$)

The steps of near optimum filter design algorithm can be listed as follows

- Determine interpulse periods
- Calculate optimum filter improvement factor for each frequency value in the frequency interval of interest
- Determine initial value of filter coefficients for the near optimum filter design
- Calculate the filter coefficients that give the most near value to the optimum filter improvement factor

Min-max filter design with the optimum improvement factor is compared with previously designed filters for two cases. Figure 4.6 indicates the magnitude of the frequency responses of the filters. All the filters show same passband response whereas they have different stopband attenuation values. The new approach of min-max design named as, MinMax-IF, shows different behavior compared to others since it is designed according to improvement factor of optimum filter. Other filters provide better response when the performance measures in Table 4.5 are compared. The different behaviour is due to the value of the cutoff frequency of the Minmax-IF design. Since the weights are adjusted according to the optimum improvement factor, corresponding cutoff frequency value can be different than the other filters.

Figure 4.7 indicates the comparison of the improvement factors for the Gaussian clutter power spectral density. MinMax-IF design has better improvement factor value compared to other

filters. In Figure 4.8, the comparison of the improvement factors for the case of Gaussian clutter with larger spread is illustrated. For this case Minmax-IF filter has better improvement factor compared to others for this case also. As seen from the obtained results, this filter gives improved response compared to others. One of the disadvantage of this design is the requirement of the optimal filter coefficients that depends upon the clutter covariance matrix.

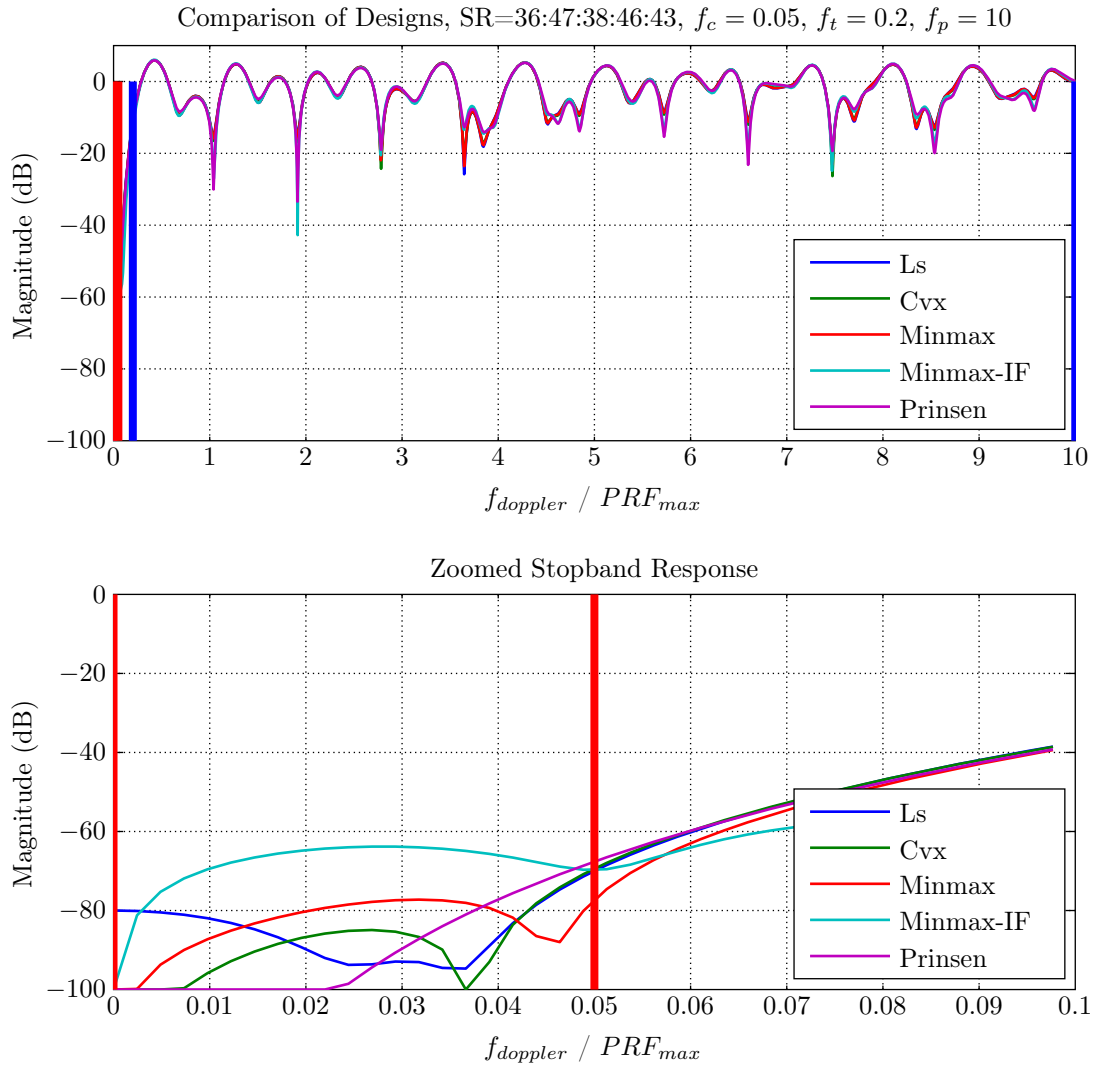


Figure 4.6: Frequency Response Comparison of Minmax-IF Filter with Other Filter Designs

Table 4.5: Performance Measures of the Comparison of Minmax-IF Filter with Other Filter Designs

Designs	MSA (dB)	SA (dB)	MPE (dB)	MD (dB)
Ls	-82.962	-71.403	-0.860	25.820
Cvx	-85.065	-70.810	-0.868	26.340
Minmax	-81.992	-80.121	-0.866	23.588
Minmax-IF	-67.136	-69.674	-0.909	42.753
Prinsen	-83.291	-68.616	-0.891	33.425

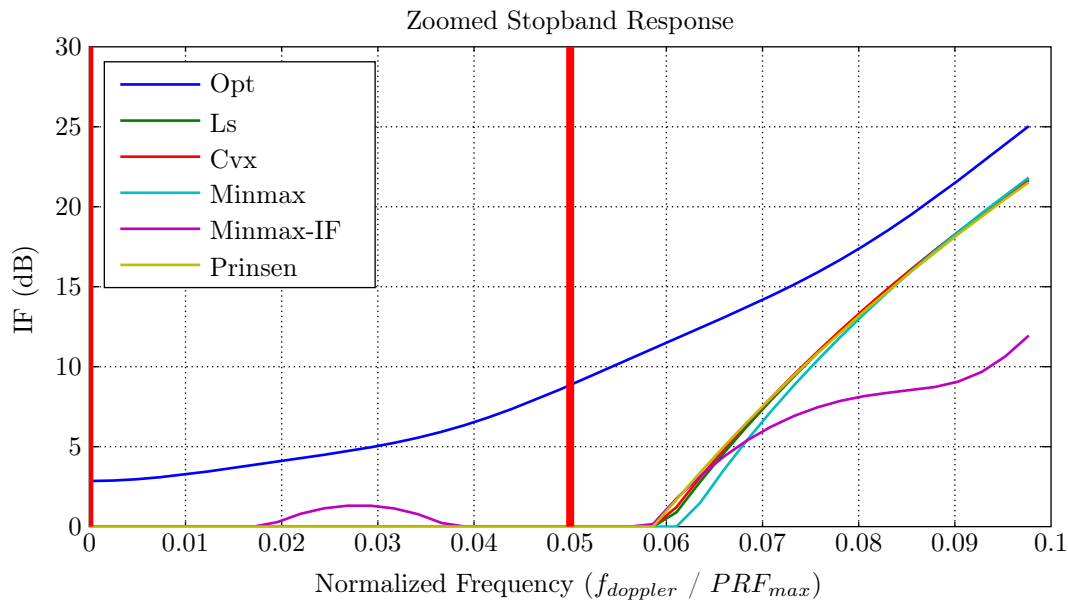
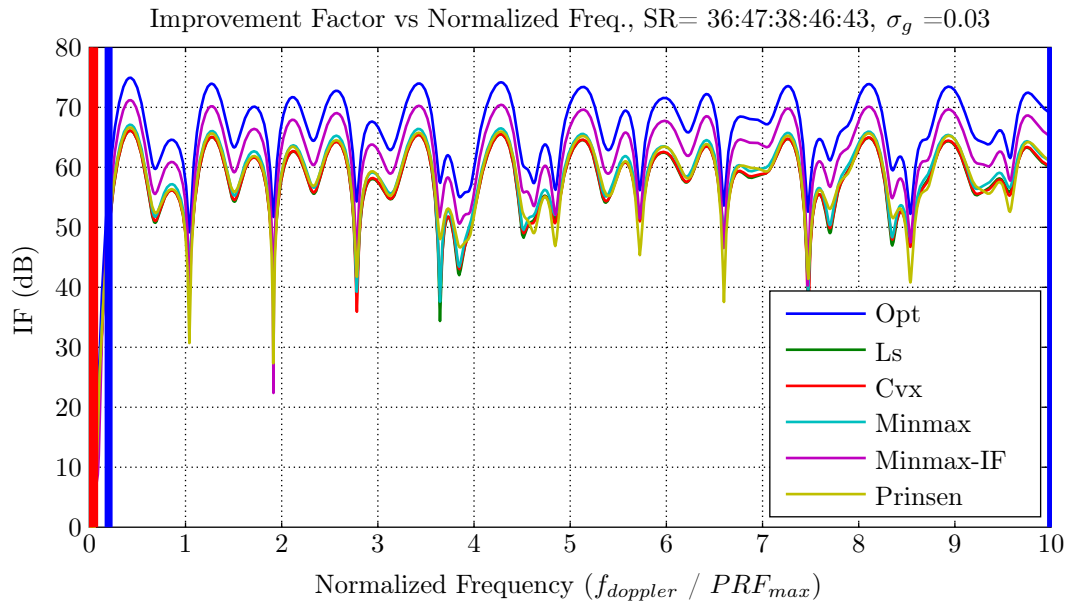


Figure 4.7: Improvement Factor Comparison of Designed Filters with Gaussian Clutter

Table 4.6: Improvement Factor Values for Comparison of Designed Filters with Gaussian Clutter

	Optimum	Ls	Cvx	Minmax	Minmax-IF	Prinsen
IF (dB)	65.969	57.155	57.126	58.137	61.929	57.469

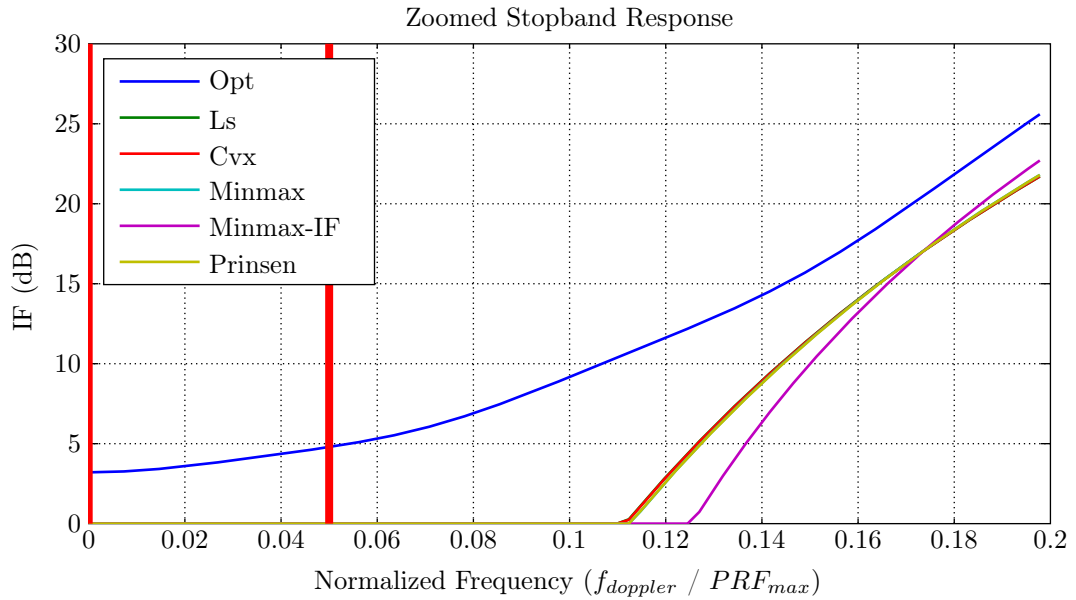
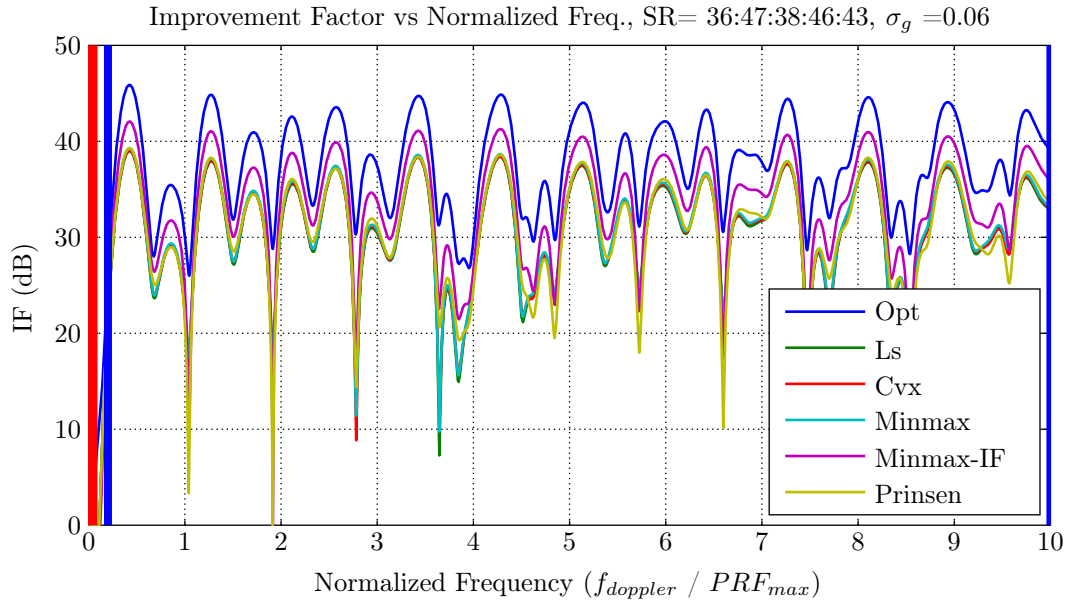


Figure 4.8: Improvement Factor Comparison of Designed Filters with Gaussian Clutter with Larger Doppler Spread

Table 4.7: Improvement Factor Values for Comparison of Designed Filters with Gaussian Clutter with Larger Doppler Spread

	Optimum	Ls	Cvx	Minmax	Minmax-IF	Prinsen
IF (dB)	37.193	30.051	30.055	30.309	32.785	30.092

4.4 Multiple Filter Design with Time Varying Coefficients

Multiple filter design is the use of time varying weights for the processing of successively transmitted pulses. Shrader [2] states that "The improvement factor limitation caused by pulse to pulse staggering can be avoided by the use of time varying weights in the canceller forward paths instead of binomial weights." Following multiple filter discussion considers this case and compares the responses with respect to time constant weights.

Multiple filter design can be described as the usage of more than one set of filter coefficients for the processing of transmitted pulses. In the previous chapters a single filter with $N + 1$ filter weights are used for processing of one period with N staggers. Usage of multiple filters means the processing of received pulses with more than one filters. Structure of the multiple filter processing is indicated in Figure 4.9.

Lets assume that $N + L$ pulses are transmitted for the MTI operation, when the stagger pattern includes N stagger periods. In time invariant single filter case, an MTI filter is designed with $N + 1$ coefficients and transmitted pulses are processed successively using this filter. In time varying weights case, multiple MTI filters are designed with $N + 1$ coefficients. That is pulses from 1 to N are processed by the first filter, 2 to $N + 1$ are processed by the second filter and so on. Processing of $N + L$ pulses with multiple filters can be thought as summing of the power outputs of the filters in order to obtain the total response of the multiple filter system. For L number of filters the total power output can be written as

$$|H(f)|^2 = |H_1(f)|^2 + |H_2(f)|^2 + |H_3(f)|^2 + \dots + |H_L(f)|^2 \quad (4.6)$$

where $|H_i(f)|^2$ represents the power output of each filter in multiple filter system. When the filter responses put in (4.6), following equation can be obtained.

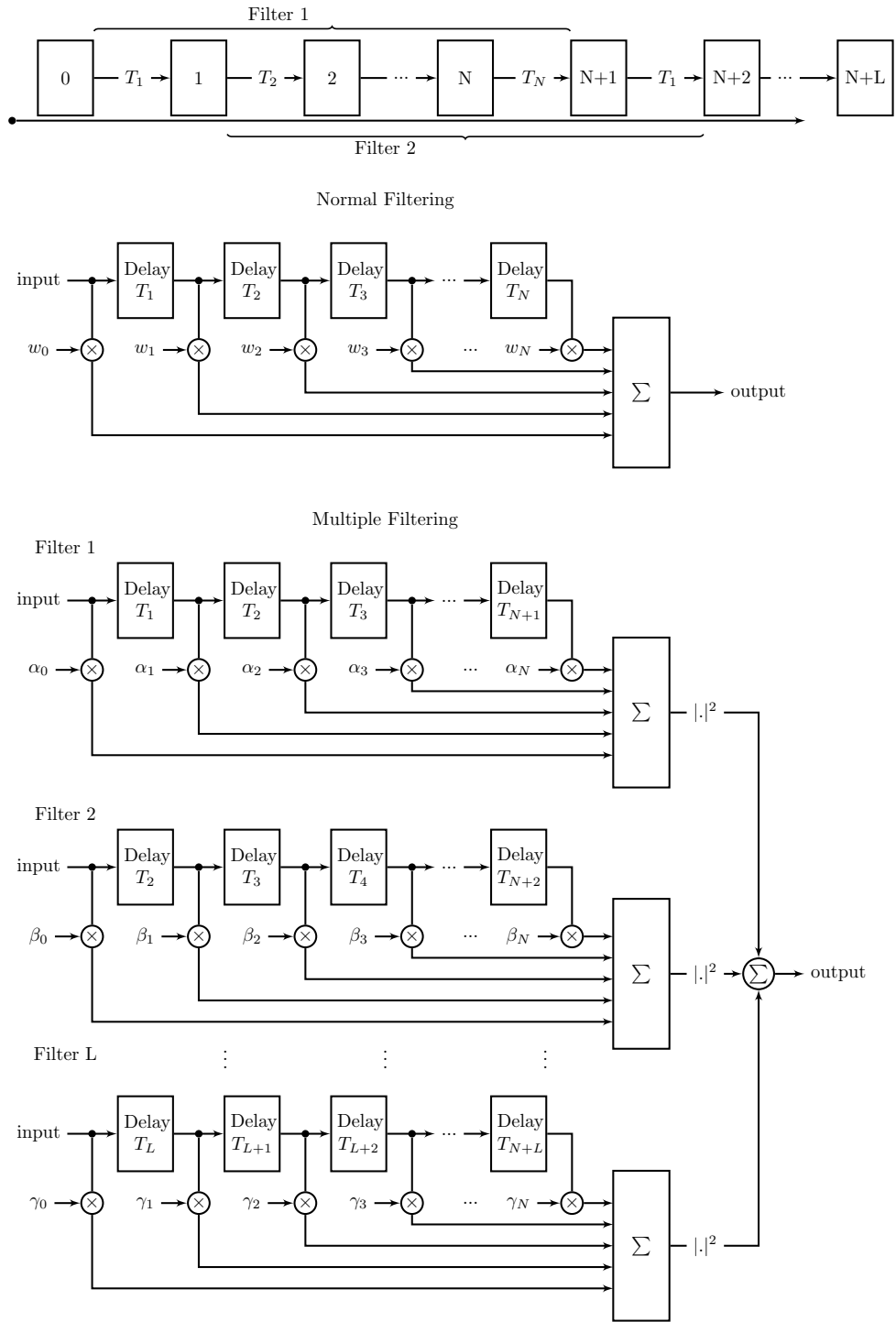


Figure 4.9: Processing of Received Pulses with Multiple Filter Structure with Time Varying Coefficients

$$\begin{aligned}
|H(f)|^2 = & \left| \sum_{i=1}^N \alpha_i \exp(-j2\pi ft_i) \right|^2 + \left| \sum_{i=2}^{N+1} \beta_i \exp(-j2\pi ft_i) \right|^2 + \dots \\
& \dots + \left| \sum_{i=L-N+1}^L \gamma_i \exp(-j2\pi ft_i) \right|^2 \quad (4.7)
\end{aligned}$$

where N is the number of staggers, L is the number of pulses processed, α_i 's are filter weights of the first filter, β_i 's are the filter weights of second filter, \dots , and γ_i 's are the filter weights of L th filter.

The main idea for the multiple filtering is the adaptation of the MTI filters for the specific stagger intervals. For example, lets consider the case when the stagger ratio of 8 : 9 : 10 is used and 7 pulses are transmitted with staggers 8 : 9 : 10 : 8 : 9 : 10. That is 8 : 9 : 10 sequence is repeated twice. According to the single filter approach, an MTI filter with 4 weights is designed with 8 : 9 : 10 stagger pattern. Let's assume that these weights are $\alpha_1, \alpha_2, \alpha_3$ and α_4 . Then, these are used as follows for the processing of 7 pulses. The group of successive staggers of 8 : 9 : 10, 9 : 10 : 8, 10 : 8 : 9, and 8 : 9 : 10 are processed by this filter. When the multiple filtering approach is used, 4 MTI filters are designed based on stagger sets of 8 : 9 : 10, 9 : 10 : 8 and 10 : 8 : 9 and 8 : 9 : 10. First MTI filter with weight vector α is used to process 8 : 9 : 10, second MTI filter with weight vector β is used to process 9 : 10 : 8, third MTI filter with weight vector γ is used to process 10 : 8 : 9 and fourth MTI filter with weight vector η is used to process 8 : 9 : 10. The matrix representation that gives the output of each MTI filter is indicated in (4.8)

$$\begin{bmatrix} O_1 \\ O_2 \\ O_3 \\ O_4 \end{bmatrix} = \begin{bmatrix} \alpha_1 & \alpha_2 & \alpha_3 & \alpha_4 & 0 & 0 & 0 \\ 0 & \beta_1 & \beta_2 & \beta_3 & \beta_4 & 0 & 0 \\ 0 & 0 & \gamma_1 & \gamma_2 & \gamma_3 & \gamma_4 & 0 \\ 0 & 0 & 0 & \eta_1 & \eta_2 & \eta_3 & \eta_4 \end{bmatrix} \begin{bmatrix} P_1 \\ P_2 \\ P_3 \\ P_4 \\ P_5 \\ P_6 \\ P_7 \end{bmatrix} \quad (4.8)$$

where P_1 to P_7 are the input pulses and O_1 to O_4 are MTI filter outputs. O_1 is the output of MTI using the first 4 pulses. These pulses are separated by T_1, T_2, T_3 seconds as shown in top part of Figure 4.9. O_2 is the output using the successive 4 pulses starting from 2nd pulse. These pulses are separated by T_2, T_3, T_4 seconds.

Assuming the target has a Doppler of frequency of f_d , then P_k in equation (4.8) becomes as $P_k = e^{j2\pi f_d t_k}$, as before. Then $O_1 = \sum_{k=1}^N \alpha_k e^{j2\pi f_d t_k}$, $O_2 = \sum_{k=2}^{N+1} \beta_{k-1} e^{j2\pi f_d t_k}$, $O_3 = \sum_{k=3}^{N+2} \gamma_{k-2} e^{j2\pi f_d t_k}$ and $O_4 = \sum_{k=4}^{N+3} \eta_{k-3} e^{j2\pi f_d t_k}$.

To investigate the performance of multiple filtering, firstly non-uniform filter designs are implemented as time invariant filters. Figure 4.10 indicates the single filters for the stagger ratio of 16 : 20 : 17 : 22. Response of the designed filters is similar to each other and they exhibit 60 dB average stopband attenuation and 20 dB maximum deviation in the passband. Table 4.8 indicates the performance measures.

Figure 4.11 illustrates the improvement factors of the designed filters in Figure 4.10. All the

filters achieve similar improvement factors. These are given in Table 4.9. Up to this point, there is no difference with respect to the earlier comparisons. Now these designed filters will be used for multiple filtering.

Figure 4.12 indicates the power response of the multiple filters when the designed filters in Figure 4.10 are used for to set-up of multiple filtering. Figure 4.13 indicates the improvement factor for multiple filters. The stagger ratio utilized is $16 : 20 : 17 : 22 : 16 : 20 : 17$. It is seen from the figure that, all the filters exhibit same response. Table 4.10 shows the performance parameters and they are nearly same for all the filters. It must be noted here that filters have better frequency responses for the stagger ratio of $16 : 20 : 17 : 22$. However when they are used for stagger ratios $20 : 17 : 22 : 16$, $17 : 22 : 16 : 20$ and $22 : 16 : 20 : 17$, the response become worse and all the filters show the same power response. The effect can be seen more clearly if the filter responses are examined individually. Figure 4.14 and 4.15 indicate the filter responses for passband and stopband for each stagger pattern cases. As it is seen, the performance of the filters is satisfactory for the first sub plot. However, the performance of the filters decrease in terms of stopband attenuation for other sub-plots. Table 4.12, 4.13, 4.14 and 4.15 indicate the performance parameters for single filters with stagger ratios of $16 : 20 : 17 : 22$, $20 : 17 : 22 : 16$, $17 : 22 : 16 : 20$ and $22 : 16 : 20 : 17$ respectively.

Figure 4.16 and 4.17 indicate the passband and stopband of the filters designed for each specific stagger ratios. It is seen from the Tables 4.16, 4.17, 4.18 and 4.19 that better stopband attenuation values are obtained (nearly 60 dB) when the time varying filters are designed for each stagger pattern.

Figure 4.18 and 4.19 indicate power response and improvement factors of multiple filters with time varying coefficients for the stagger ratio of $16 : 20 : 17 : 22 : 16 : 20 : 17$. As it is observed, stopband attenuation of the multiple filters is greater than time invariant coefficient filters. In other words, if a single MTI filter is designed for each sub-stagger group and used in multiple filter structure, stopband attenuation performance do not degrade as compared to the single time invariant MTI filter.

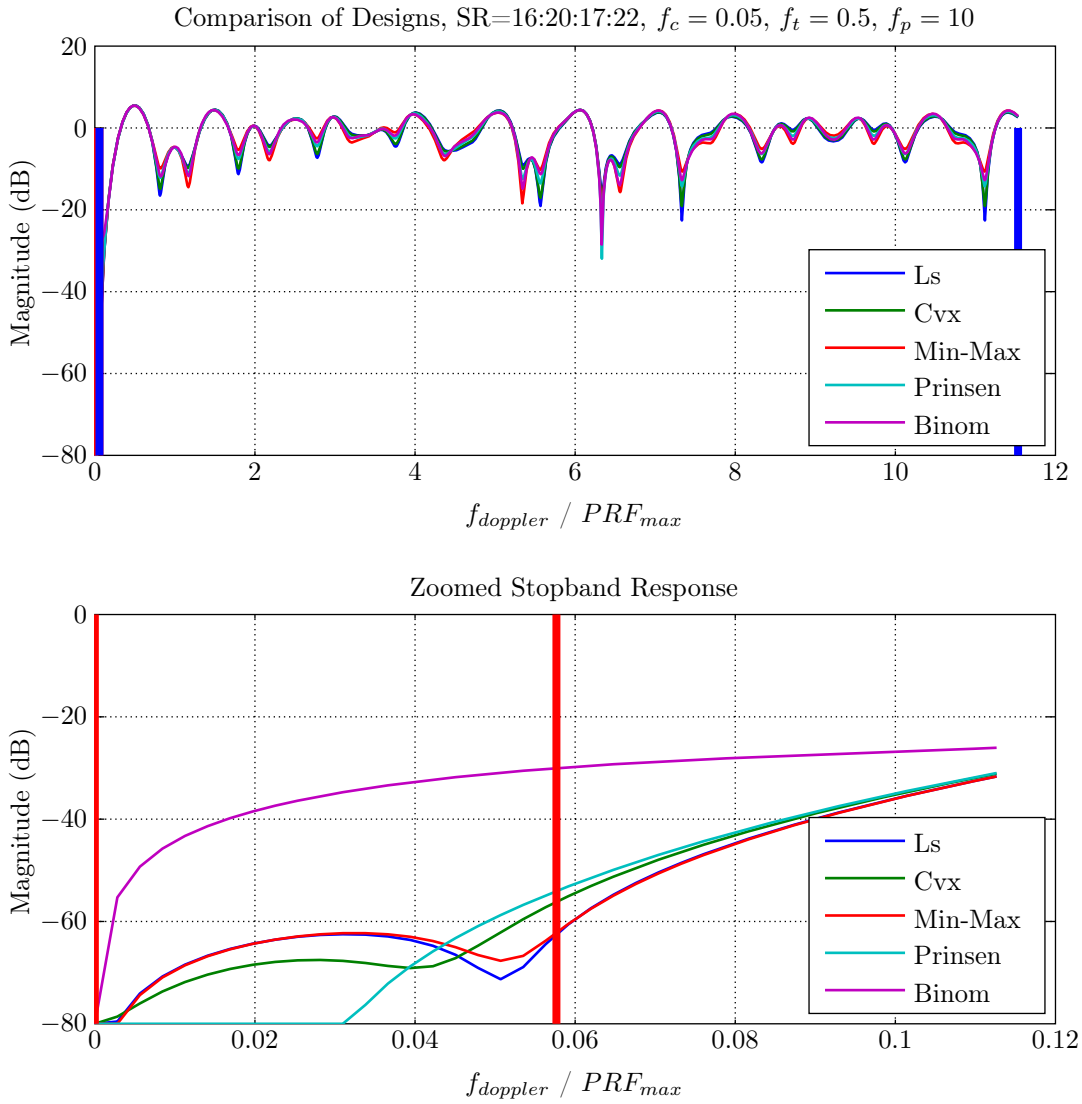


Figure 4.10: Frequency Response of Designed Filters for Stagger Ratio 16:20:17:22 (Single Filter)

Table 4.8: Performance Measures of Designed Filters for Stagger Ratio 16:20:17:22

Designs	MSA (dB)	SA (dB)	MPE (dB)	MD (dB)
Ls	-65.480	-64.418	-0.023	22.601
Cvx	-65.520	-57.212	-0.020	19.102
Min-Max	-65.004	-63.755	-0.009	19.804
Prinsen	-63.915	-54.892	-0.016	31.950
Binom	-34.498	-30.181	-0.013	28.499

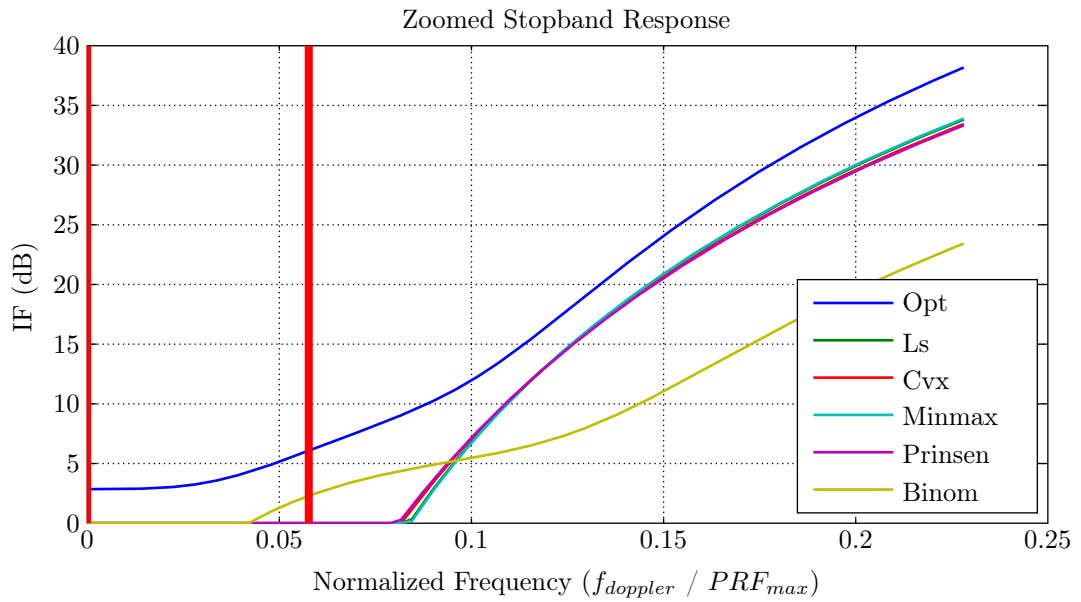
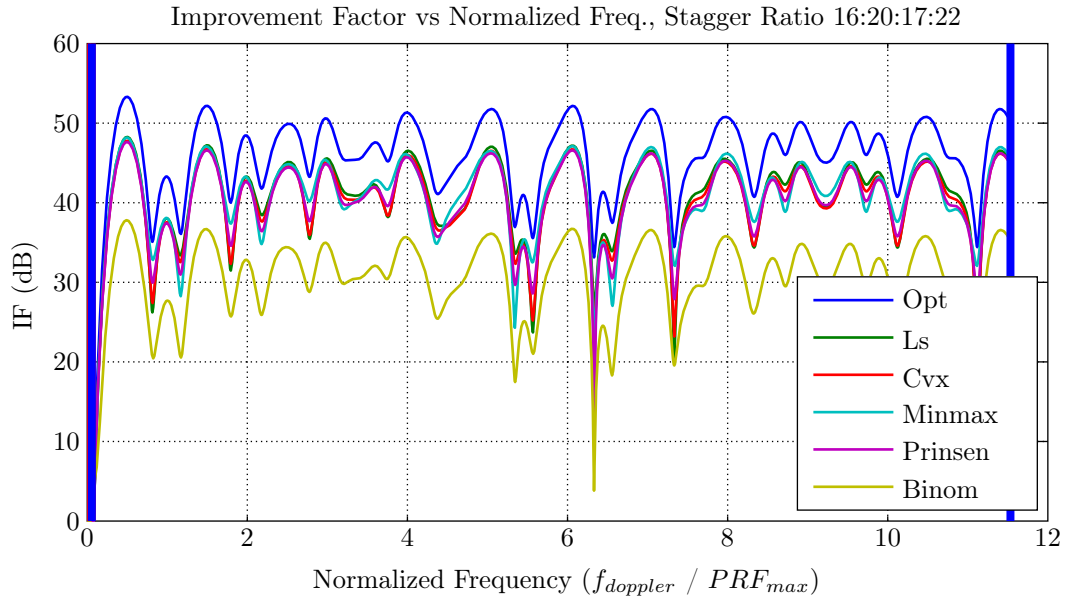


Figure 4.11: Improvement Factor Plots of Designed Filters for Stagger Ratio 16:20:17:22 (Single Filter)

Table 4.9: Improvement Factor Values of Designed Filters for Stagger Ratio 16:20:17:22

	Optimum	Ls	Cvx	Minmax	Prinsen	Binom
IF (dB)	45.769	40.487	40.061	40.530	39.921	30.329

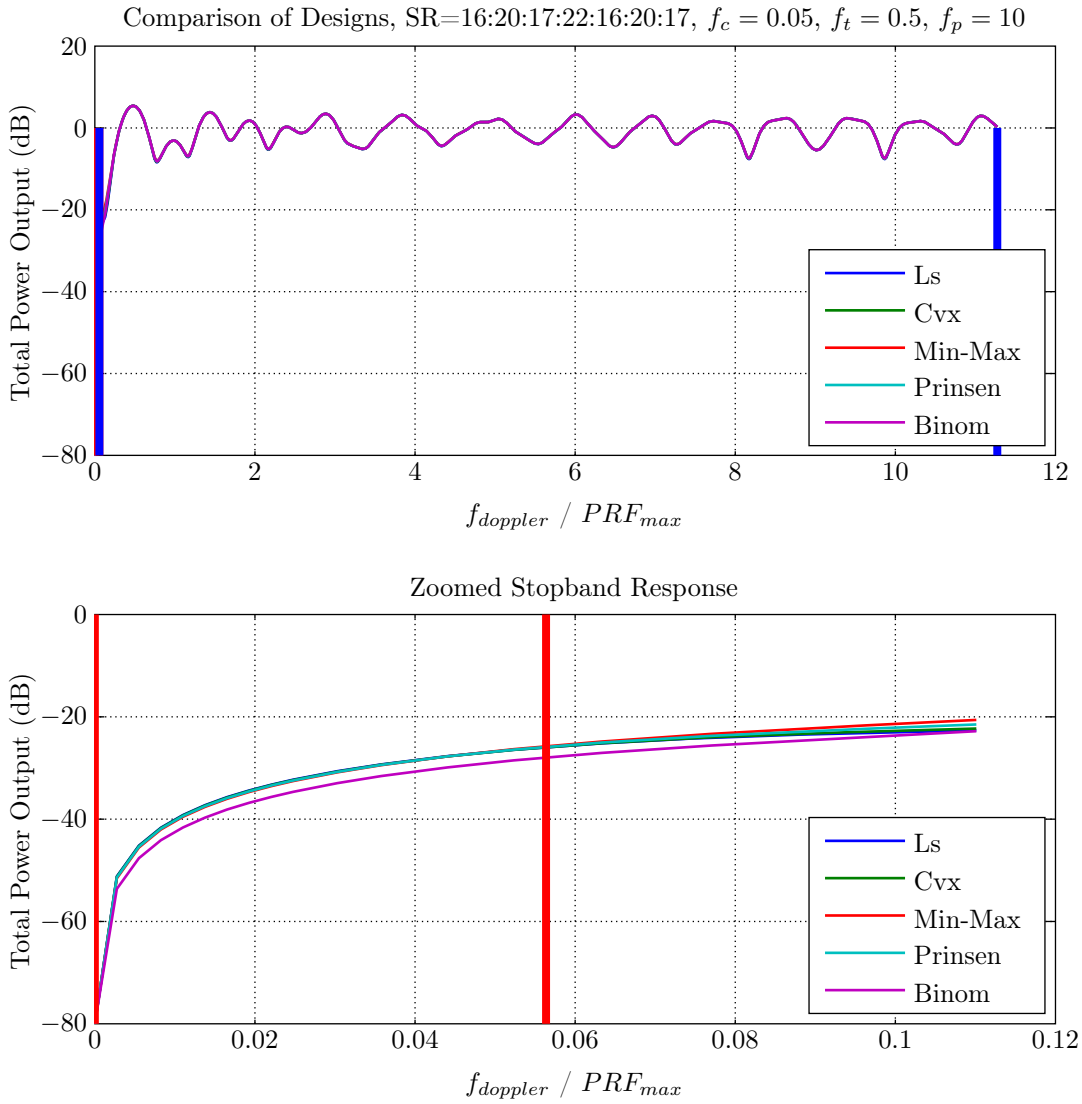


Figure 4.12: Total Power Response of Designed Time Invariant Single Filters for Stagger Ratio 16:20:17:22:16:20:17 (Multiple Filter)

Table 4.10: Performance Measures of Total Power Response of Designed Filters for Stagger Ratio 16:20:17:22:16:20:17

Designs	MSA (dB)	SA (dB)	MPE (dB)	MD (dB)
Ls	-30.399	-26.089	-0.025	8.422
Cvx	-30.437	-26.097	-0.024	8.337
Min-Max	-30.440	-25.920	-0.024	8.027
Prinsen	-30.449	-26.031	-0.024	8.191
Binom	-32.598	-28.116	-0.024	8.191

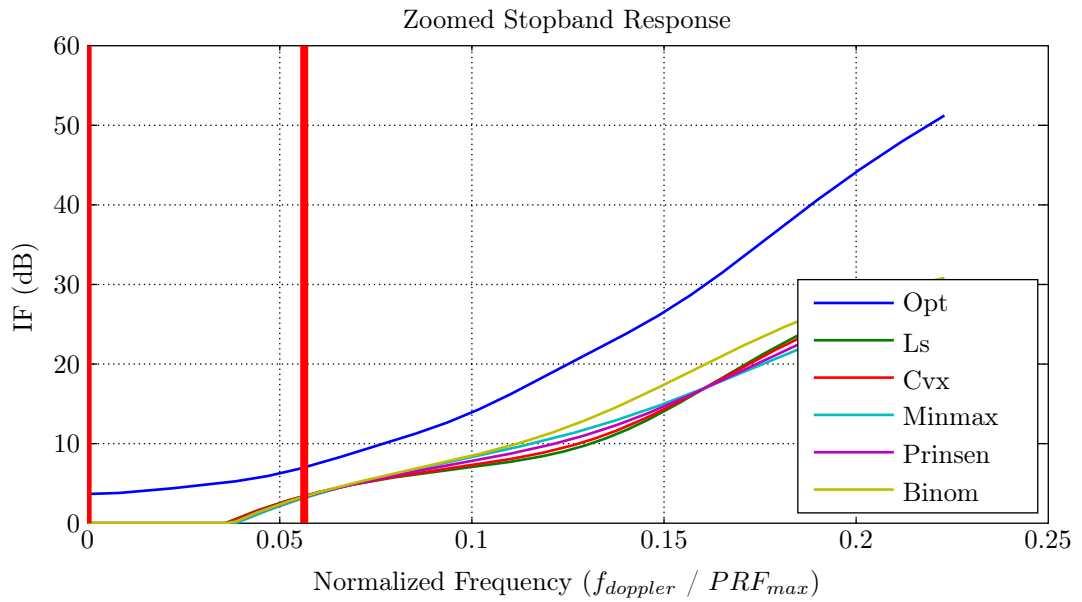
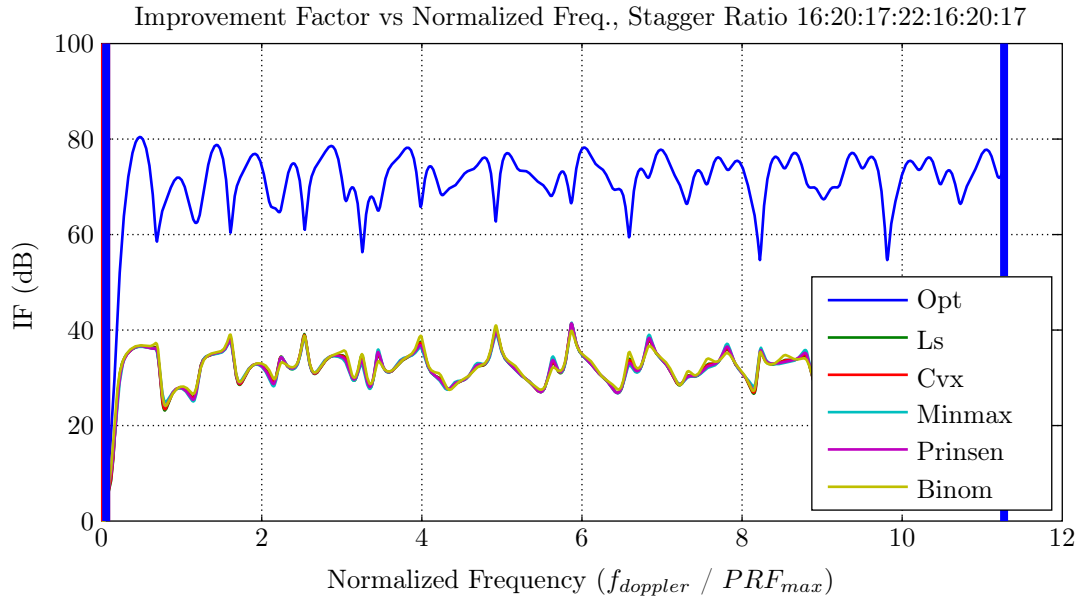


Figure 4.13: Improvement Factor Plots of Designed Time Invariant Single Filters for Stagger Ratio 16:20:17:22:16:20:17 (Multiple Filter)

Table 4.11: Improvement Factor Values of Designed Single Filters for Stagger Ratio 16:20:17:22:16:20:17

	Optimum	Ls	Cvx	Minmax	Prinsen	Binom
IF (dB)	70.800	31.799	31.837	31.840	31.864	32.070

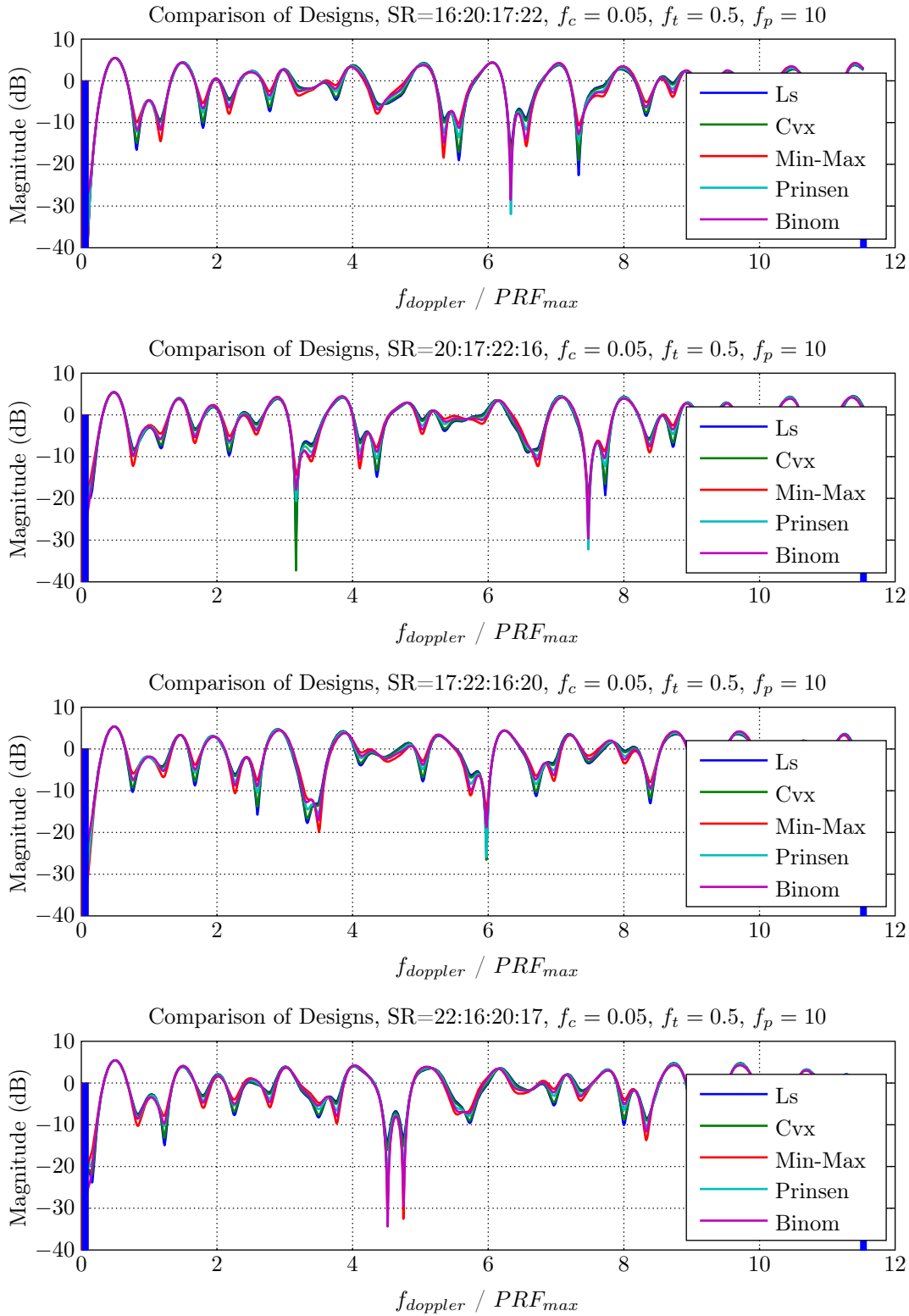


Figure 4.14: Passband Response of Designed Single Filters for Stagger Ratios 16:20:17:22, 20:17:22:16, 17:22:16:20, 22:16:20:17

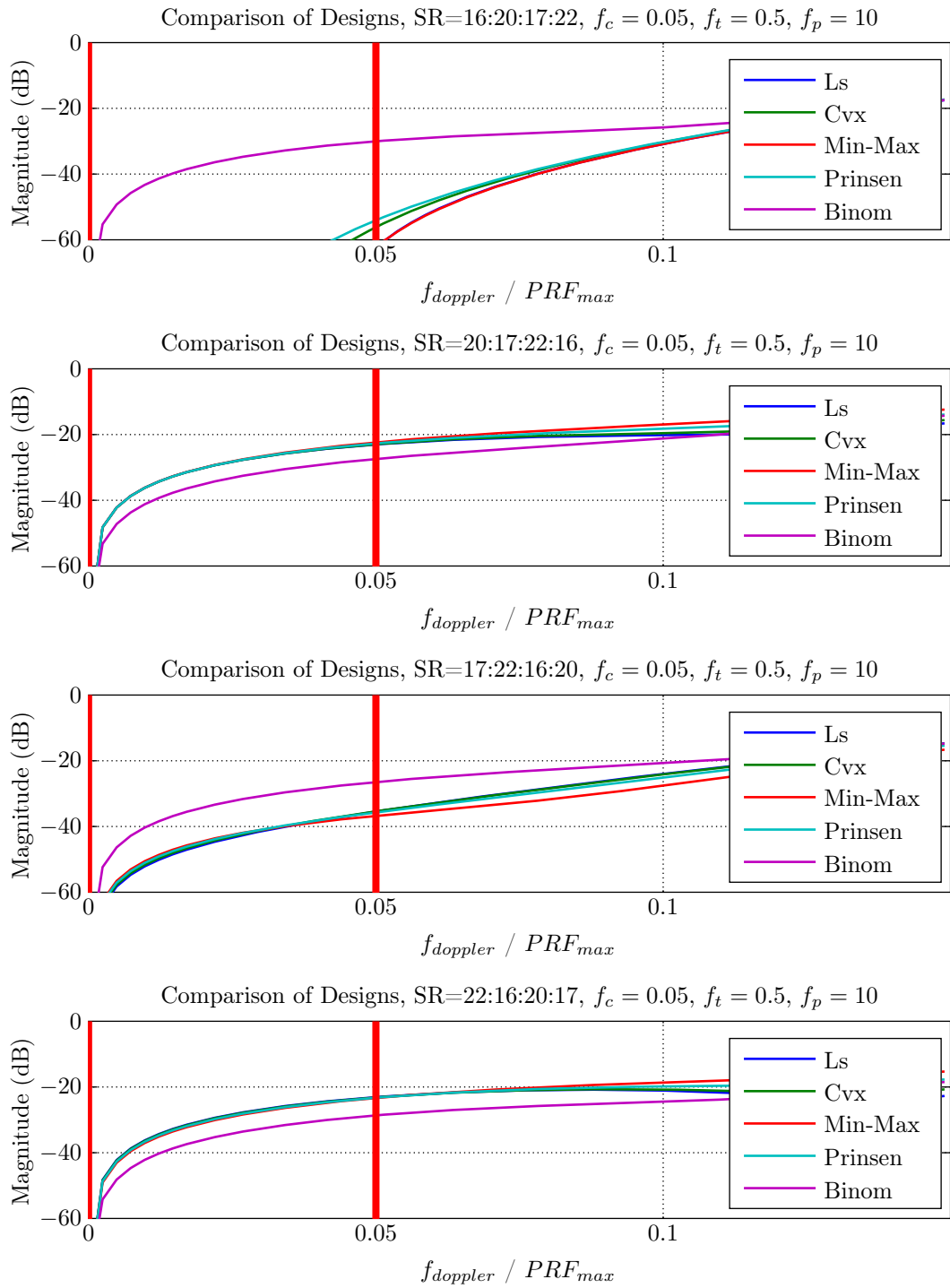


Figure 4.15: Stopband Response of Designed Single Filters for Stagger Ratios 16:20:17:22, 20:17:22:16, 17:22:16:20, 22:16:20:17

Table 4.12: Performance Measures of Designed Filters for Stagger Ratio 16:20:17:22

Designs	MSA (dB)	SA (dB)	MPE (dB)	MD (dB)
Ls	-65.480	-64.418	-0.023	22.601
Cvx	-65.520	-57.212	-0.020	19.102
Min-Max	-65.004	-63.755	-0.009	19.804
Prinsen	-63.915	-54.892	-0.016	31.950
Binom	-34.498	-30.181	-0.013	28.499

Table 4.13: Performance Measures of Designed Filters for Stagger Ratio 20:17:22:16

Designs	MSA (dB)	SA (dB)	MPE (dB)	MD (dB)
Ls	-27.455	-23.170	0.009	31.521
Cvx	-27.426	-23.102	0.009	37.258
Min-Max	-27.098	-22.558	0.003	23.187
Prinsen	-27.290	-22.868	0.007	32.223
Binom	-32.134	-27.602	0.004	29.589

Table 4.14: Performance Measures of Designed Filters for Stagger Ratio 17:22:16:20

Designs	MSA (dB)	SA (dB)	MPE (dB)	MD (dB)
Ls	-41.224	-35.736	-0.031	21.172
Cvx	-41.054	-35.675	-0.032	26.559
Min-Max	-41.495	-36.941	-0.039	19.923
Prinsen	-41.051	-35.948	-0.035	25.847
Binom	-31.211	-26.658	-0.038	18.769

Table 4.15: Performance Measures of Designed Filters for Stagger Ratio 22:16:20:17

Designs	MSA (dB)	SA (dB)	MPE (dB)	MD (dB)
Ls	-41.224	-35.736	-0.031	21.172
Cvx	-41.054	-35.675	-0.032	26.559
Min-Max	-41.495	-36.941	-0.039	19.923
Prinsen	-41.051	-35.948	-0.035	25.847
Binom	-31.211	-26.658	-0.038	18.769

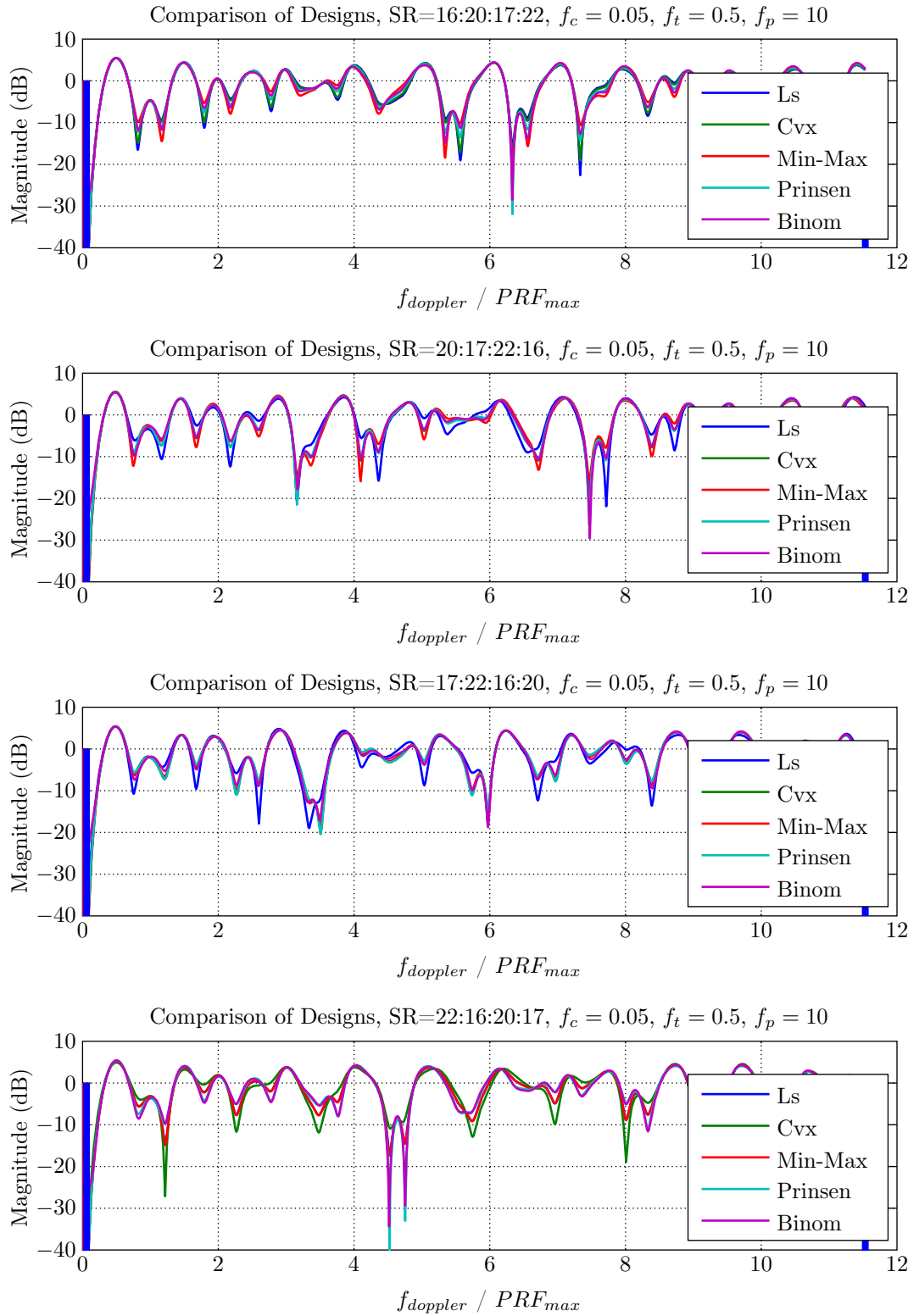


Figure 4.16: Passband Response of Designed Filters for Stagger Ratios 16:20:17:22, 20:17:22:16, 17:22:16:20, 22:16:20:17

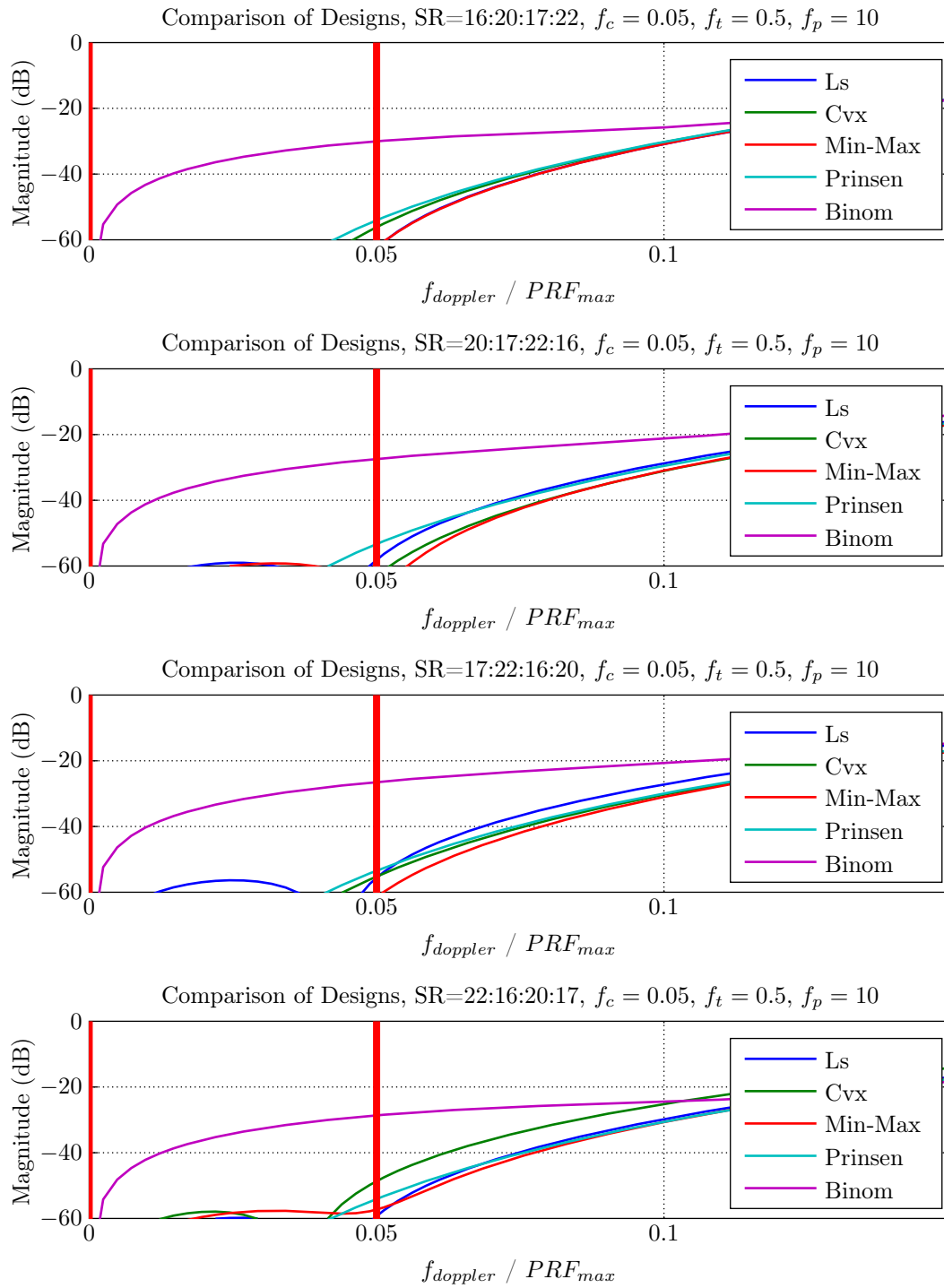


Figure 4.17: Stopband Response of Designed Filters for Stagger Ratios 16:20:17:22, 20:17:22:16, 17:22:16:20, 22:16:20:17

Table 4.16: Performance Measures of Designed Filters for Stagger Ratio 16:20:17:22

Designs	MSA (dB)	SA (dB)	MPE (dB)	MD (dB)
Ls	-65.480	-64.418	-0.023	22.601
Cvx	-65.520	-57.212	-0.020	19.102
Min-Max	-65.004	-63.755	-0.009	19.804
Prinsen	-63.915	-54.892	-0.016	31.950
Binom	-34.498	-30.181	-0.013	28.499

Table 4.17: Performance Measures of Designed Filters for Stagger Ratio 20:17:22:16

Designs	MSA (dB)	SA (dB)	MPE (dB)	MD (dB)
Ls	-62.002	-59.908	0.008	21.895
Cvx	-73.857	-64.717	0.001	23.140
Min-Max	-61.981	-64.872	-0.003	15.921
Prinsen	-63.141	-54.137	0.001	26.344
Binom	-32.134	-27.602	0.004	29.589

Table 4.18: Performance Measures of Designed Filters for Stagger Ratio 17:22:16:20

Designs	MSA (dB)	SA (dB)	MPE (dB)	MD (dB)
Ls	-59.469	-57.416	-0.029	18.961
Cvx	-65.220	-56.106	-0.038	20.367
Min-Max	-70.287	-63.068	-0.037	18.191
Prinsen	-63.020	-54.227	-0.038	20.395
Binom	-31.211	-26.658	-0.038	18.769

Table 4.19: Performance Measures of Designed Filters for Stagger Ratio 22:16:20:17

Designs	MSA (dB)	SA (dB)	MPE (dB)	MD (dB)
Ls	-59.469	-57.416	-0.029	18.961
Cvx	-65.220	-56.106	-0.038	20.367
Min-Max	-70.287	-63.068	-0.037	18.191
Prinsen	-63.020	-54.227	-0.038	20.395
Binom	-31.211	-26.658	-0.038	18.769

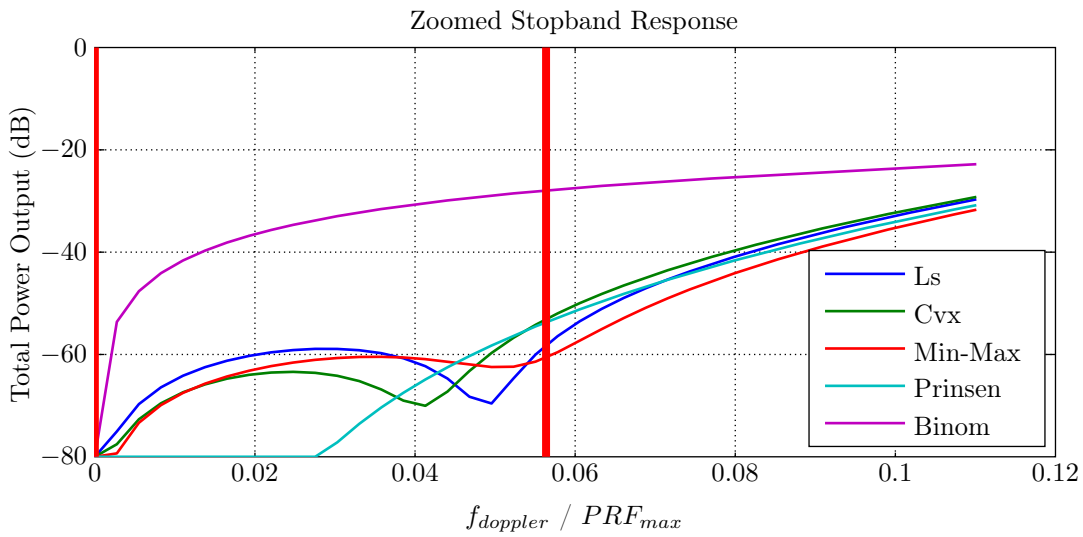
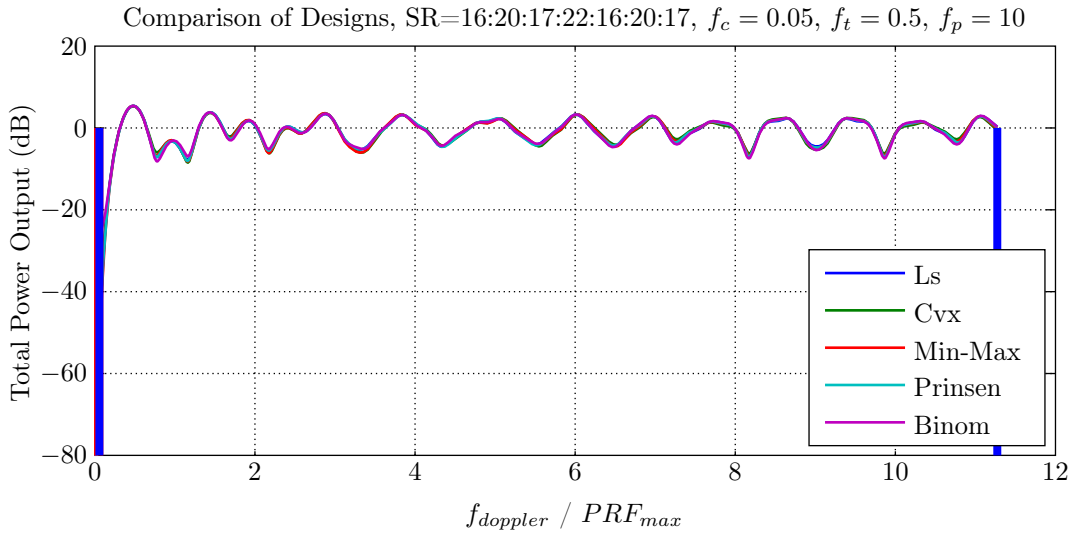


Figure 4.18: Total Power Response of Designed Multiple Filters used for Stagger Ratio 16:20:17:22:16:20:17 (Multiple Filter)

Table 4.20: Performance Measures of Designed Multiple Filters used for Stagger Ratio 16:20:17:22:16:20:17

Designs	MSA (dB)	SA (dB)	MPE (dB)	MD (dB)
Ls	-61.905	-60.008	-0.022	7.767
Cvx	-62.623	-54.198	-0.024	8.478
Min-Max	-62.772	-61.397	-0.024	8.205
Prinsen	-63.421	-54.519	-0.025	8.080
Binom	-32.598	-28.116	-0.024	8.191

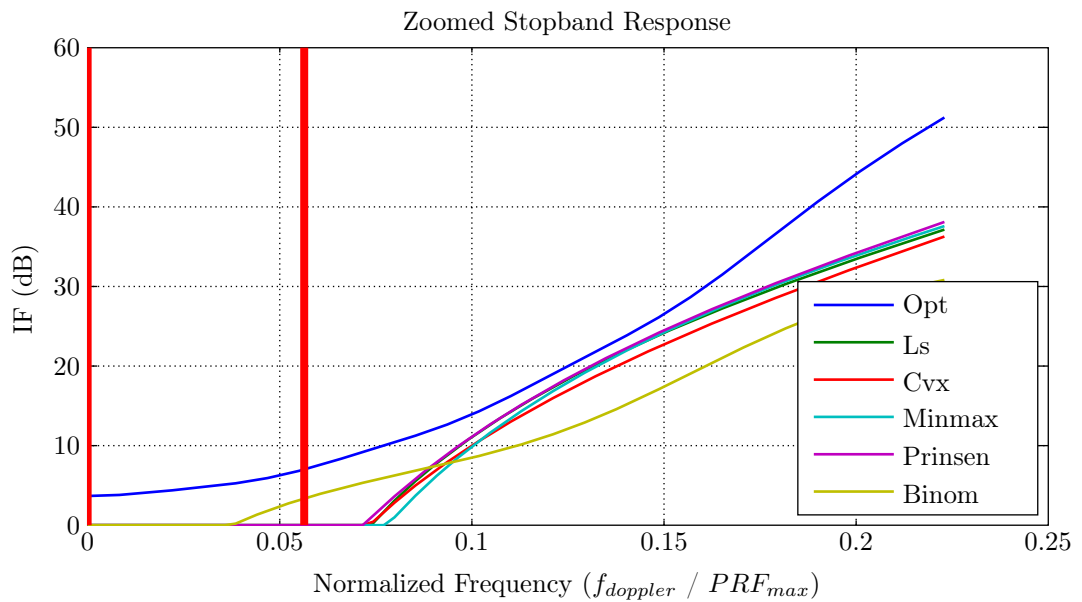
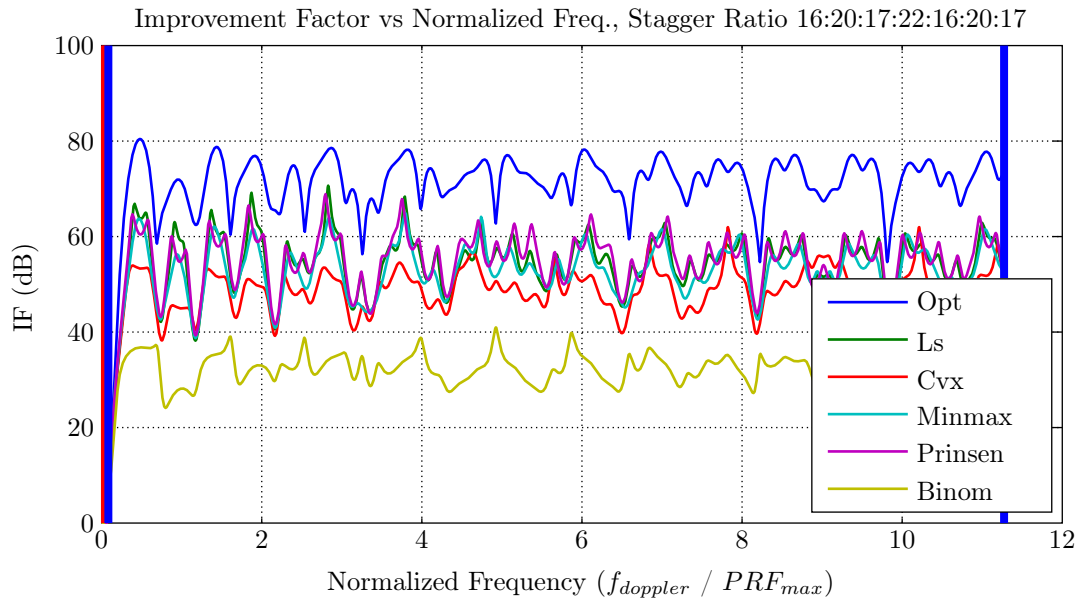


Figure 4.19: Improvement Factor Plots of Designed Multiple Filters used for Stagger Ratio 16:20:17:22:16:20:17

Table 4.21: Improvement Factor Values of Designed Multiple Filters used for Stagger Ratio 16:20:17:22:16:20:17

	Optimum	Ls	Cvx	Minmax	Prinsen	Binom
IF (dB)	70.800	53.764	48.180	52.179	54.390	32.070

CHAPTER 5

COMPARISON OF FILTER DESIGNS WITH SELECTED STUDIES

In this chapter comparison of the design methods with four specific non-uniform MTI filter designs are presented. For each case, summary of the design approach is given and a comparison between the proposed designs in this study are made according to the improvement factor performance and the magnitude of the frequency response of the filter's.

The specific reference designs taken from literature are [19], [20], [25] and [6]. Each design has its own notation, different pulse intervals and design approach. In order to present comparisons with these designs, interpulse durations are converted into stagger ratios. The constraints, frequency boundaries and the clutter models are kept same and expressed with the parameters used in this work.

5.1 Hsiao's Design

One of the first studies related to stagger MTI filter design is Hsiao's non-uniform MTI filter design [19]. In his study, the optimization procedure based on the maximum attenuation in the stopband and minimum ripple in the passband. Different from the proposed designs in this work, maximum attenuation and the minimum ripple objectives are considered separately. To obtain maximum stopband attenuation, the coefficients of the filter are calculated using the clutter covariance matrix and solving the eigenvalue problem given in (5.1).

$$\sum_j \alpha_j \rho_{ij} - \lambda \alpha_i = 0 \quad i = 0, \dots, N, \quad j = 0, \dots, N \quad (5.1)$$

Here, α_i 's are the filter coefficients, λ is eigenvalues of the clutter covariance matrix, N is the number of pulses and ρ_{ij} are the elements of the clutter covariance matrix. The solution is finding the eigenvector associated with the minimum eigenvalue λ .

For minimum passband ripple, selection of the stagger intervals is considered. Selection of intervals is based on the calculation of the mean squared deviation in the passband and selecting the stagger intervals that result in the minimum mean squared deviation. The mean squared deviation is stated as

$$\epsilon^2 = \frac{1}{f_r/2 - f_u} \int_{f_u}^{f_r/2} \left[\sum_{i \neq j} \alpha_i \alpha_j \cos 2\pi(T_i - T_j) \right]^2 df \quad (5.2)$$

Here, f_r is the first blind Doppler frequency, f_u is the upper bound of the stopband, α_i 's are the filter coefficients and T 's are the sampling times. To get minimum ripple in the passband this error function must be minimized. In least square sense this can be achieved as

$$\frac{\partial \epsilon^2(T_i)}{\partial T_i} = 0 \quad i = 0, \dots, N \quad (5.3)$$

Approximate solution to this problem is stated and a search technique is presented for stagger selection which provides locally optimal solutions with the given constraints. Presented technique considers the calculation of the mean squared deviation in the passband iteratively and selecting the stagger intervals that gives the minimum mean squared deviation.

In the study, normalized interpulse periods are given as (1.1, 1.1, 1.0, 1.2, 1.4, 1.1). PSD of the clutter is assumed to have uniform distribution that is given by

$$C(f) = \begin{cases} \frac{1}{f_u - f_l} & f_l \leq f \leq f_u, \\ 0 & otherwise \end{cases} \quad (5.4)$$

Frequency response and the improvement factor comparison for Hsiao's design are given in Figure 5.1 and 5.2 respectively. Performance measures and the improvement factors are given in Table 5.1 and 5.2. Comparison of the filters shows that, improvement in the *SA*, *MPE* and *MD* parameters are achieved, whereas *MSA* of Hsiao is greater from all other designs. Also the improvement factor of Hsiao is greater from all other designs. There are several reasons for the obtained results. The first reason is the design methodology of Hsiao. In the design, two independent optimizations are carried out for stopband and passband improvements. Best values for attenuation and mean squared deviation are selected in the context of adjusting the filter coefficients and the stagger intervals. One of the other reasons is the usage of uniformly distributed clutter PSD model. For defined frequency bands, solution of the minimum eigenvalue problem gives the best response in the mean stopband attenuation value. Another reason is related to the objectives of the proposed methods. If the response of each design is considered individually, objectives are achieved whereas Hsiao's improvement factor does not attained. For example, minimum mean stopband error is achieved with LS design and improvement in maximum deviation is obtained with respect to Hsiao's design.

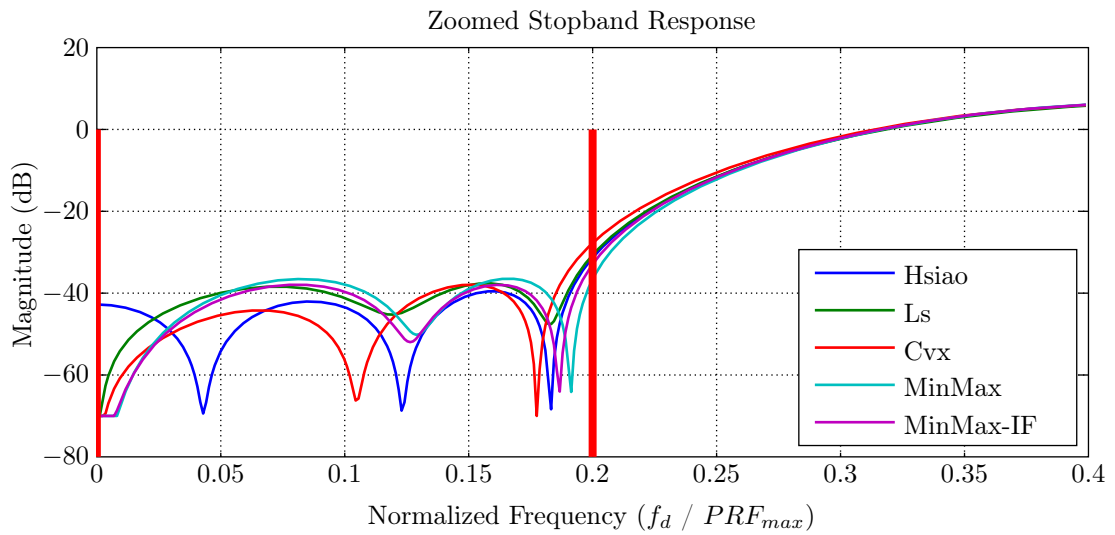
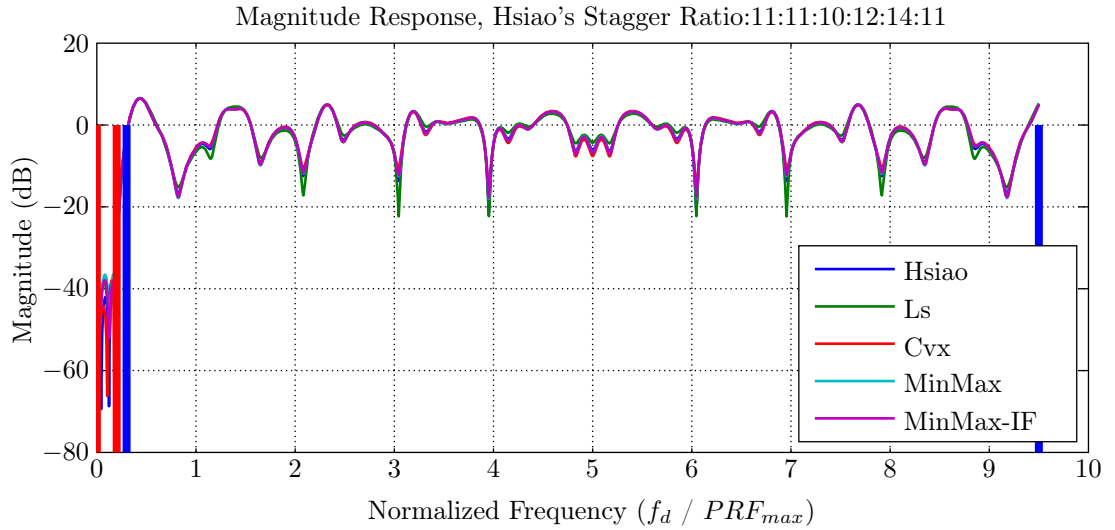


Figure 5.1: Magnitude Response Comparison of Designed Filters with Hsiao's Filter

Table 5.1: Performance Measures for Magnitude Response Comparison of Designed Filters with Hsiao's Filter

	MSA (dB)	SA (dB)	MPE (dB)	MD (dB)
Hsiao	-44.326	-31.686	-0.684	21.377
Ls	-40.940	-30.994	-0.699	22.316
Cvx	-43.347	-28.027	-0.669	17.587
Minmax	-41.155	-37.148	-0.686	17.951
Minmax-IF	-42.282	-33.348	-0.682	17.714

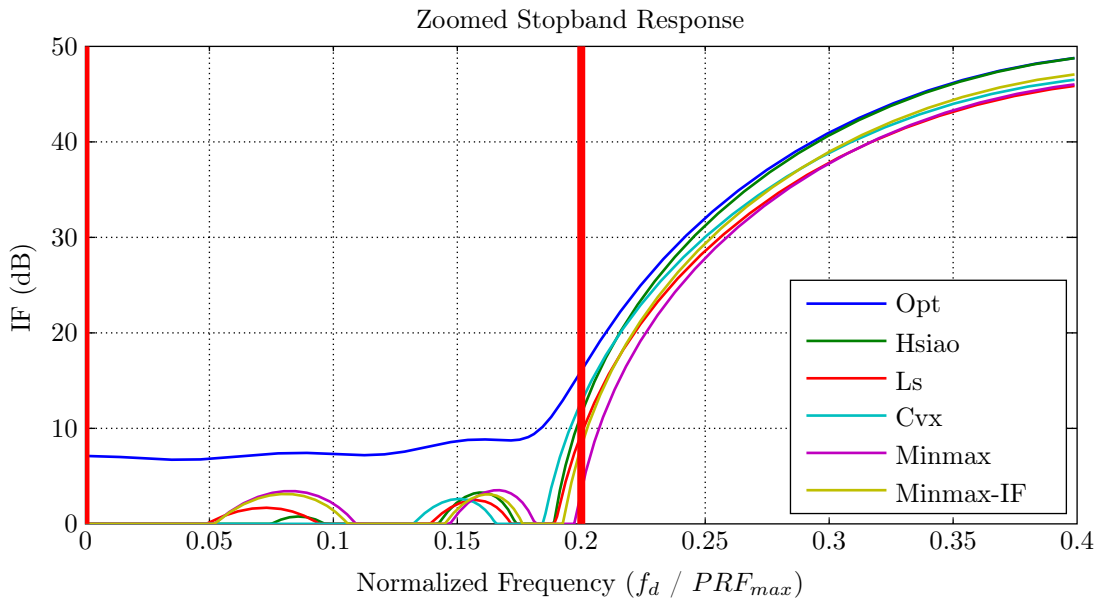
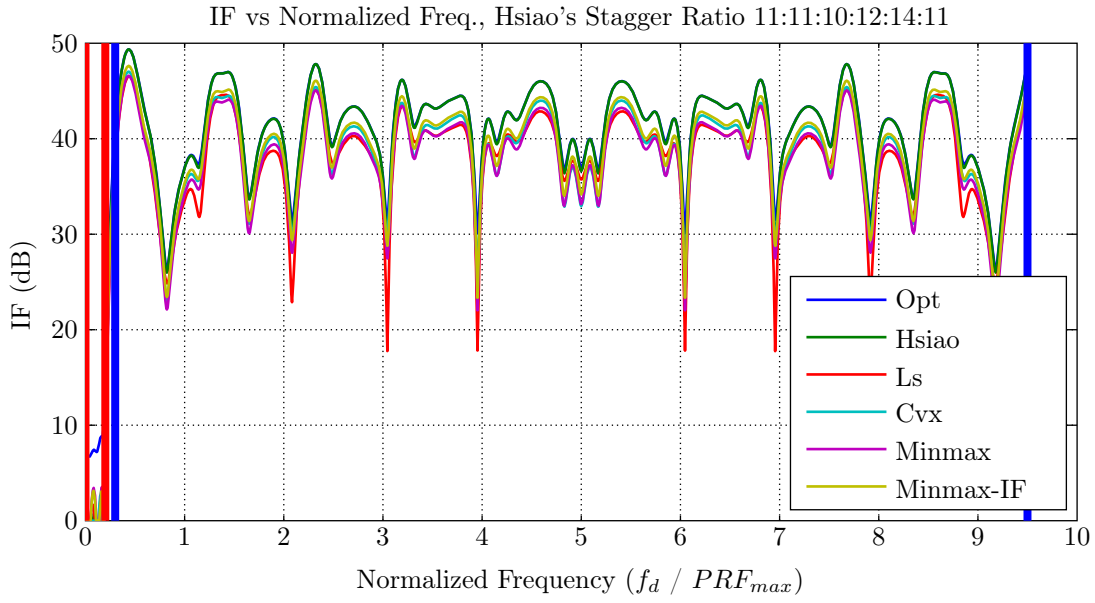


Figure 5.2: Improvement Factor Plots of Designed Filters with Hsiao's Filter

Table 5.2: Improvement Factor Values of Designed Filters with Hsiao's Filter

	Optimum	Hsiao	Ls	Cvx	Minmax	Minmax-IF
IF (dB)	40.462	40.041	37.306	37.840	37.259	38.335

5.2 Jacomini's Design

In this design also minimum ripple in the passband and maximum clutter attenuation in the stopband criteria are considered [20]. Different from the Hsiao's design optimization problem stated differently. The equation to be minimized is given as

$$P_T = P_C + WP_r \quad (5.5)$$

where P_C is the output clutter power and P_r is the power obtained by summation of the squared filter magnitude in passband. These values are given by

$$P_C = \int_0^{2\pi f_i} F_C(w)H(w)dw \quad (5.6)$$

$$P_r = \int_{f_l}^{f_u} H_p(w)dw \quad (5.7)$$

W is the design parameter used to determine the relative importance between the passband ripple and stopband clutter attenuation.

Since the optimization problem is a non-linear problem, the design aims to find a local solution. Two solution methods are used namely Gradient Method and Quadratic Method. Both methods tries to minimize the value of P_T to obtain better performance.

Normalized sampling durations for the selected filter are given as (0.0, 0.279, 0.483, 0.633, 0.808, 1.047). Corresponding normalized interpulse durations are calculated as (0.279, 0.204, 0.150, 0.175, 0.239) by subtracting consecutive sampling durations. Similar to the Hsiao's case, uniformly distributed clutter PSD is used. Frequency response and improvement factor comparison are given in Figure 5.3 and 5.4 respectively. Performance measures and the improvement factors are given in Table 5.3 and 5.4.

If the responses of the filters are examined, the first notable result is the similarity between the performances of the Jacomini's and the least square filter. This result is expected since the cost functions of the designs consider the same objectives with a weight factor. Despite the difference between the underlying analytical formulations, boundaries on the constraints lead to similar results.

If MSA , SA and MPE are considered, CVX and Min-max designs achieve better responses compared to the Jacomini's and least square filter, whereas they do not improve the MD value.

Another notable difference is seen in the improvement factor performances of the filters. Min-max design with optimum filter improvement factor achieves the best improvement factor compared to other designs. This is due to use of smaller cutoff frequency, uniform clutter PSD model and suitable stagger periods.

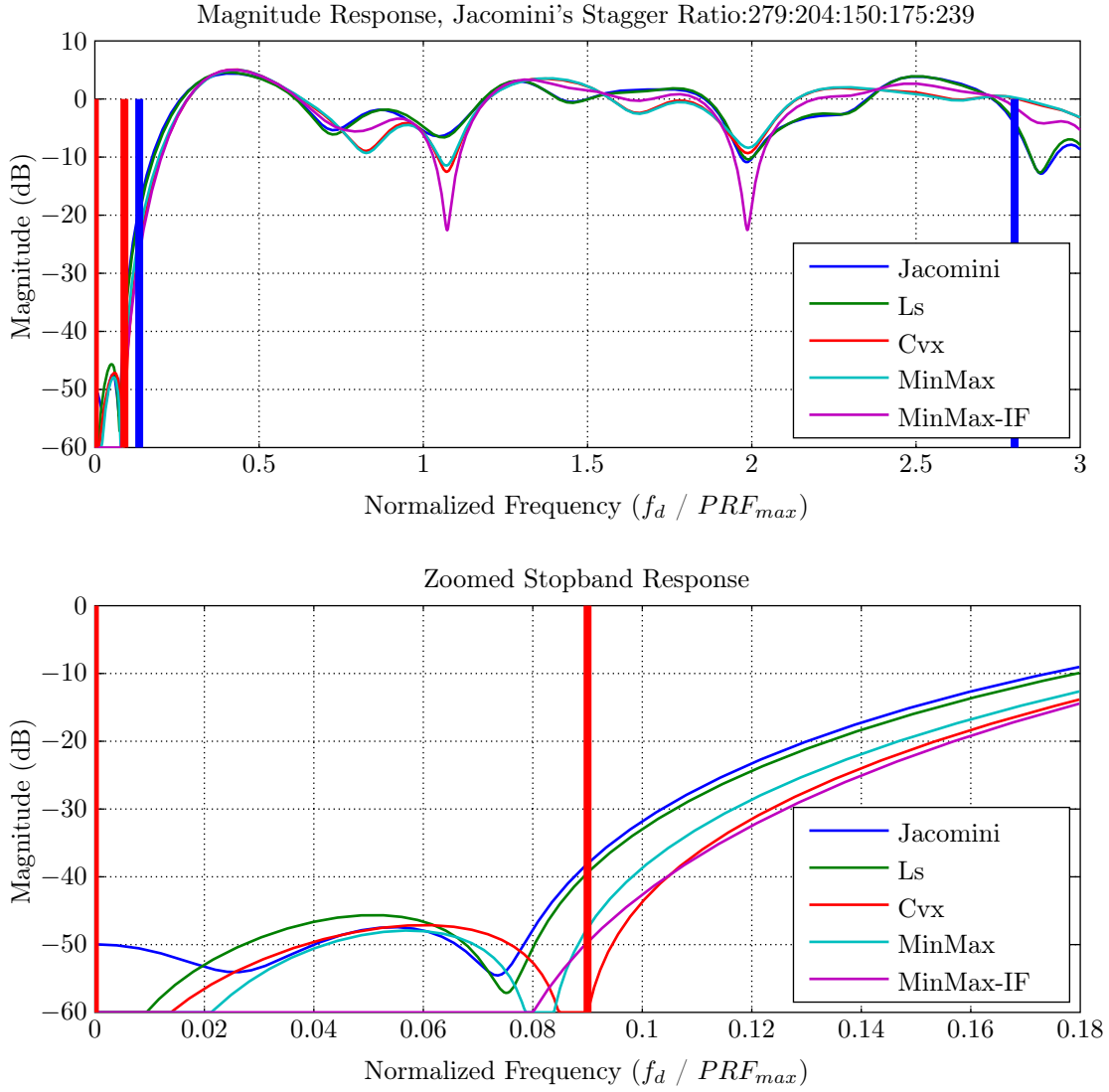


Figure 5.3: Magnitude Response Comparison of Designed Filters with Jacomini's Filter

Table 5.3: Performance Measures for Magnitude Response Comparison of Designed Filters with Jacomini's Filter

	MSA (dB)	SA (dB)	MPE (dB)	MD (dB)
Jacomini	-49.075	-38.247	-0.014	10.879
Ls	-49.167	-39.605	-0.026	10.409
Cvx	-51.915	-61.130	-0.252	13.840
Minmax	-53.506	-47.909	-0.251	12.645
Minmax-IF	-64.008	-49.876	-0.205	22.598

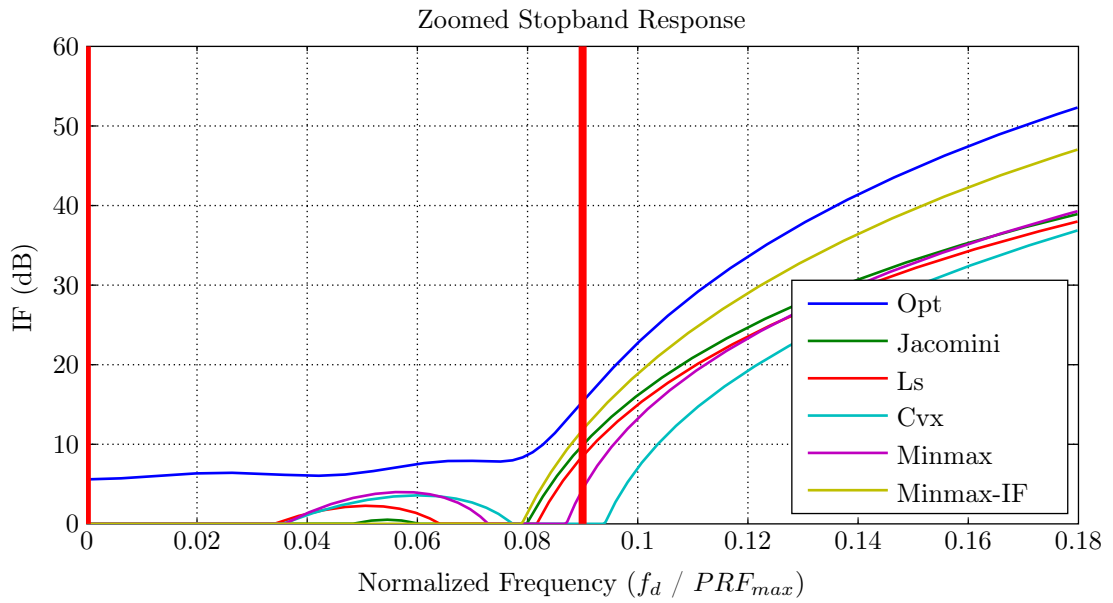
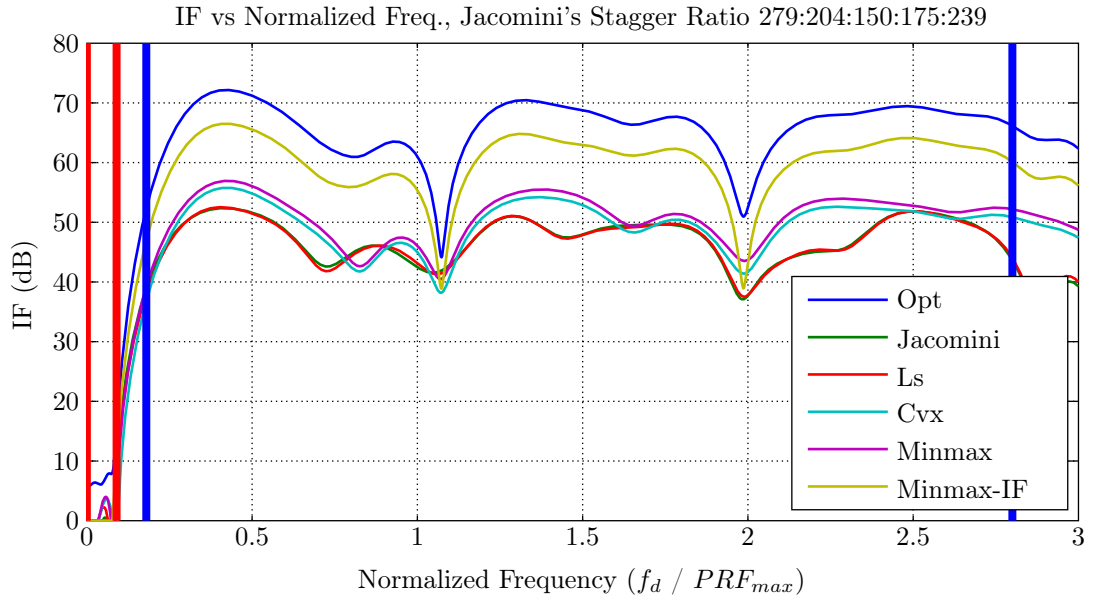


Figure 5.4: Improvement Factor Plots of Designed Filters with Jacomini's Filter

Table 5.4: Improvement Factor Values of Designed Filters with Jacomini's Filter

	Optimum	Jacomini	Ls	Cvx	Minmax	Minmax-IF
IF (dB)	63.123	44.660	44.575	47.193	48.447	57.257

5.3 Ewell's Design

In [25], Ewell designed *Constrained Improvement Processors* named as CIPs. Design constraints of these are different from previous cases. The improvement factor to be satisfied is specified firstly and then ripples in passband is minimized according to the improvement factor constraint. Two categories of designs are presented. First approach considers the optimization of filter weights for a fixed stagger pattern whereas stagger periods are also optimized along with the filter coefficients in the second approach.

The power response of the processors is given by

$$G(f) = \sum_{i=1}^N X_i^2 + \sum_{k=1}^{N-1} \sum_{i=1}^{N-k} 2X_i X_{i+k} \times \cos \{2\pi f [k - \Delta(i) + \Delta(i+k)]\} \quad (5.8)$$

Here, X 's are filter coefficients, Δ 's are normalized interpulse duration differences and N is the number of pulses.

Mean square error of the design is defined in [25] as

$$mse = \frac{1}{f'} \int_0^{f'} [1 - G(f)]^2 df \quad (5.9)$$

Here, f' is the highest interested normalized frequency. Design of the processors is based on placing the $G(f)$ into mse equation and solving for the minimum mean-square deviation of the frequency response according to specified MTI improvement.

For comparison, CIP design with %20 variation is taken with stagger ratio of 8 : 9 : 10. Gaussian clutter PSD is used with $\sigma = 0.01$. Frequency response and improvement factor comparison are given in Figure 5.5 and 5.6 respectively. Performance measures and the improvement factors are given in Table 5.5 and 5.6.

Different observations can be obtained from the performance of the filters. It must be noted that the constraint of the Ewell's design is different from the proposed designs. As seen from the results, nearly 60 dB attenuation is possible to achieve with the proposed designs whereas the Ewell's filter is constrained to 30 dB attenuation. Since the maximum attenuation is constrained to these value, minimum ripple in the passband is obtained. However, CVX and Min-max designs achieve close performance to the Ewell's, in terms of passband performance. In addition, these designs accomplish better stopband attenuation performance (20-45 dB further attenuation).

The limitation on the performance of Ewell's filter is clearly seen from Figure 5.6. Minmax-IF method accomplishes the best improvement factor between all designs (75.435 dB). Other proposed designs also achieve better improvement factors. Ewell's filter improvement factor is the smallest one since it is constrained to 30 dB.

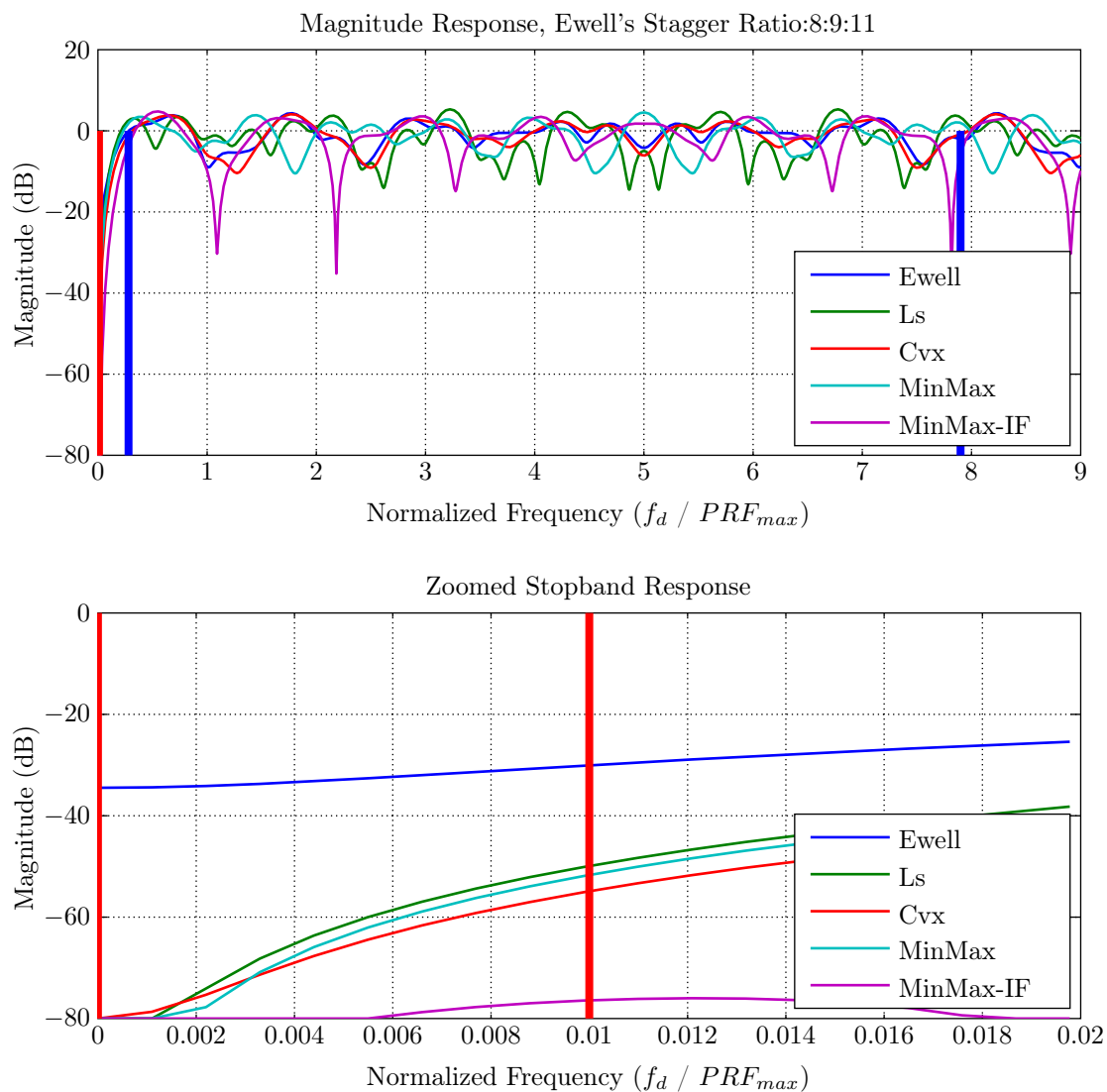


Figure 5.5: Magnitude Response Comparison of Designed Filters with Ewell's Filter

Table 5.5: Performance Measures for Magnitude Response Comparison of Designed Filters with Ewell's Filter

	MSA (dB)	SA (dB)	MPE (dB)	MD (dB)
Ewell	-32.534	-30.088	-0.370	9.020
Ls	-58.974	-50.102	-0.857	14.515
Cvx	-63.390	-55.077	-0.456	10.430
Minmax	-60.927	-51.876	-0.388	10.503
Minmax-IF	-81.470	-76.458	-0.620	35.194

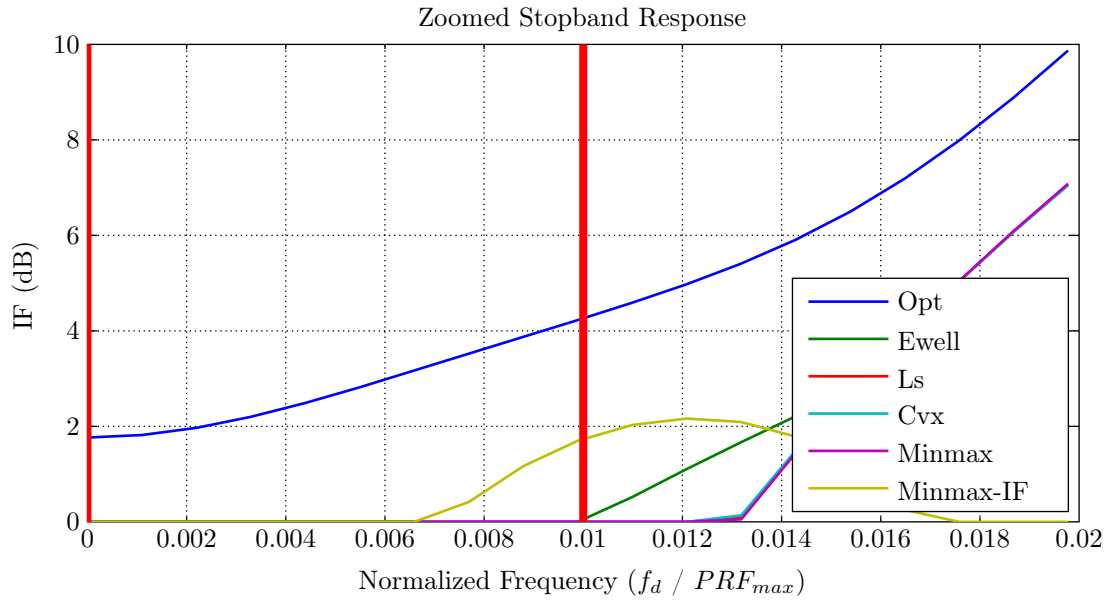
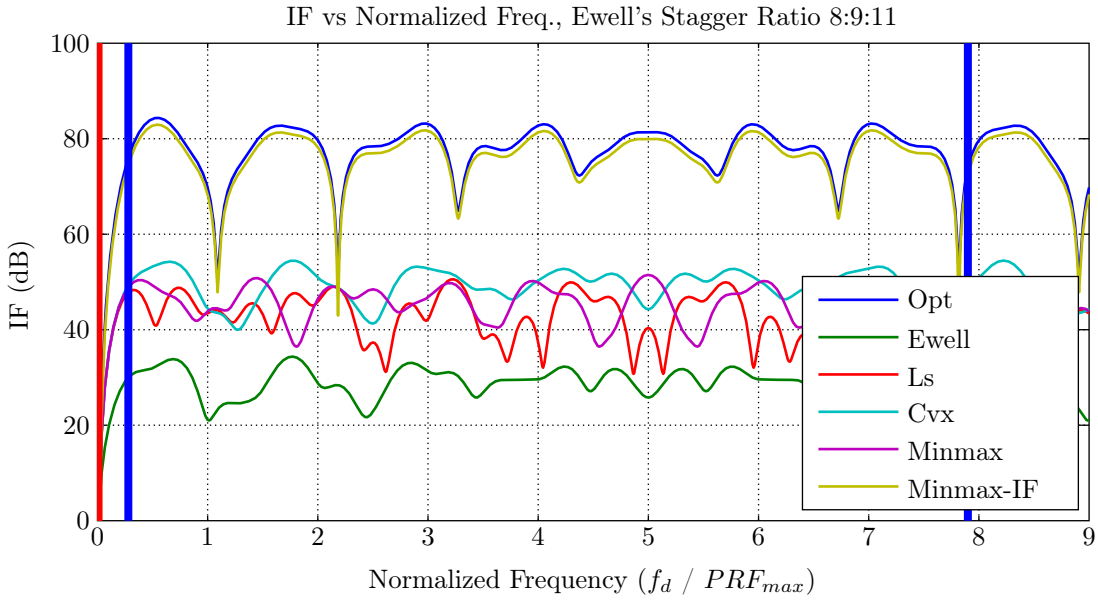


Figure 5.6: Improvement Factor Plots of Designed Filters with Ewell's Filter

Table 5.6: Improvement Factor Values of Designed Filters with Ewell's Filter

	Optimum	Ewell	Ls	Cvx	Minmax	Minmax-IF
IF (dB)	76.936	28.780	43.061	48.711	45.450	75.435

5.4 Zuyin's Design

In [6], Zuyin proposes a new analytical method for the non-uniform MTI filter design. Design criteria of the proposed approach are similar to the previous designs. Interpulse durations are selected according to minimum passband ripple and the filter coefficients are selected to increase the clutter suppression capability.

The design focuses on the approximation of the offered filter transfer functions into transversal type of transfer functions of MTI filters. The suggested filters called as prototype highpass filters whose transfer function is given by

$$H_{N-1}^*(jw) = \frac{jwT_l}{jwT_l + 1} \quad (5.10)$$

Zuyin states that "When N received pulse signals are used for the MTI processing, it is possible to get the approximated transfer function of transversal MTI filters through rational fractions" [6]. Corresponding approximation is given by

$$H_{N-1}^*(jw) = \sum_{n=0}^{N-1} \alpha_n e^{-jw t_n} \quad (5.11)$$

For numerical comparison, taken stagger intervals are given by (0.838T, 1.135T, 0.892T, 1.108T, 1.027T). These values are rewritten as a stagger ratio of 838 : 1135 : 892 : 1108 : 1027. Frequency response and improvement factor comparison are given in Figure 5.7 and 5.8 respectively. Performance measures and the improvement factors are given in Table 5.7 and 5.8.

To consider the improvement in passband ripple, mean stopband attenuation of the proposed designs are selected close to the Zuyin's (~ 66 dB). In this comparison, improvement capability of the designs in passband ripple is seen clearly. If Table 5.7 is examined, MPE values of the designs are close to each other whereas the MD values are improved by 2 dB to 10 dB compared to the Zuyin's. The improvement in SA and MD values also provides better improvement factors as seen from Table 5.8.

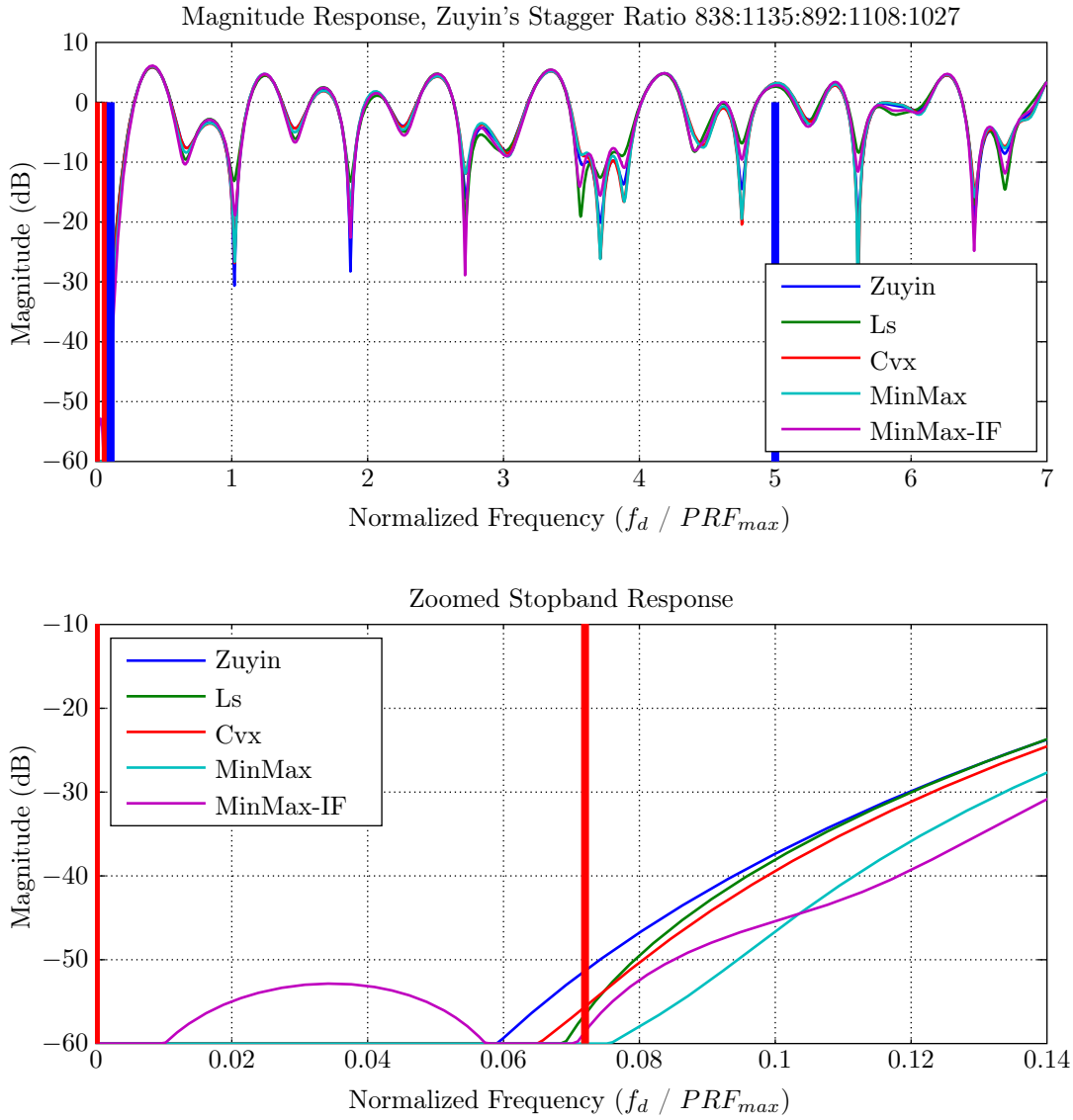


Figure 5.7: Magnitude Response Comparison of Designed Filters with Zuyin's Filter

Table 5.7: Performance Measures for Magnitude Response Comparison of Designed Filters with Zuyin's Filter

	MSA (dB)	SA (dB)	MPE (dB)	MD (dB)
Zuyin	-66.987	-51.426	-1.154	37.362
Ls	-66.888	-56.710	-1.108	38.047
Cvx	-66.547	-55.745	-1.152	39.402
Minmax	-66.386	-62.051	-1.175	46.620
Minmax-IF	-57.013	-58.791	-1.201	45.407

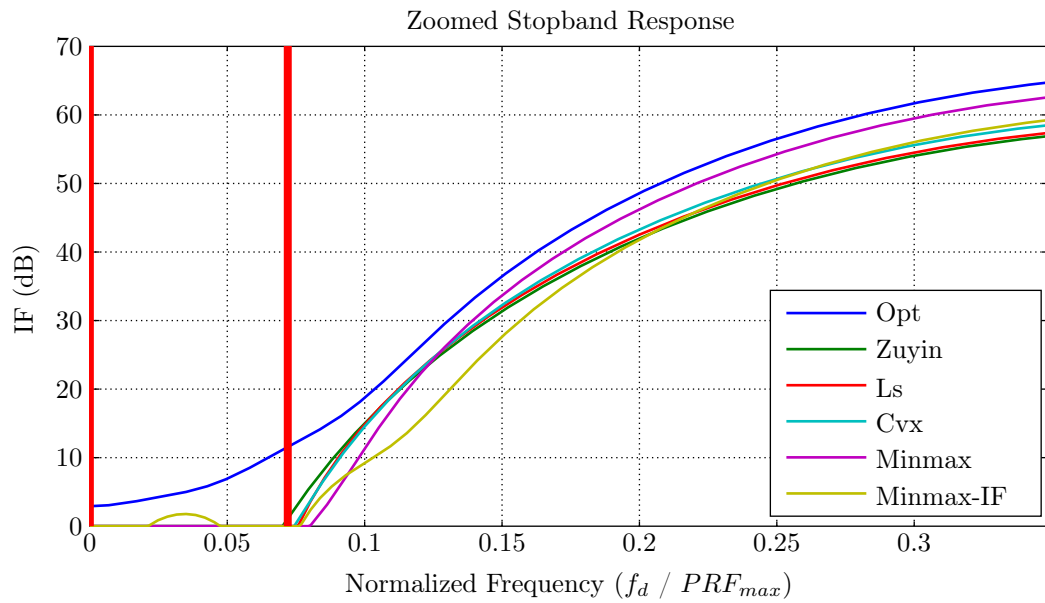
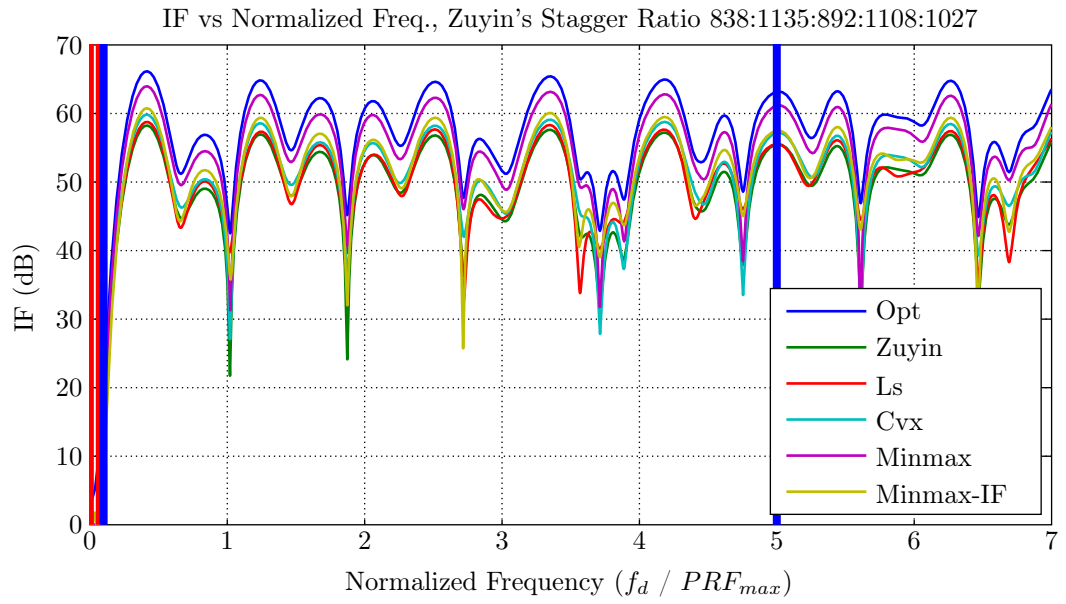


Figure 5.8: Improvement Factor Plots of Designed Filters with Zuyin's Filter

Table 5.8: Improvement Factor Values of Designed Filters with Zuyin's Filter

	Optimum	Zuyin	Ls	Cvx	Minmax	Minmax-IF
IF (dB)	56.887	48.701	49.525	50.375	54.297	51.071

CHAPTER 6

CONCLUSION

6.1 Results and Conclusion

In this work, we apply classical filter design frameworks to the staggered PRI MTI filter and present the results with comparisons. The goal of the MTI filter design is providing maximum clutter attenuation in stopband and minimum ripple in passband. The presented design techniques are based upon these goals. The weighted least square, convex and min-max techniques are utilized to design filters with non-uniform sampling. It has been shown that with a proper selection of the weight parameter, a good compromise between clutter attenuation and flat passband response can be attained.

Two additional approaches are considered in order to increase the signal-to-clutter ratio improvement. First approach implements the modified min-max design by considering the optimum filter's improvement factor. This methodology has an advantage to improve the performance when the clutter power spectrum density corresponds to a scan radar clutter power spectrum density. This design can be used when other designs do not provide the required MTI improvement factor. Second approach focuses on the implementation of the designed filters as multiple filters that have time varying coefficients. Multiple filter structure is examined in detail and related performance comparison with the filters with time constant weights are made.

Here, it must be noted that, usage of optimal MTI filters can provide better clutter attenuation and passband performance compared to the designed filters. Also the analysis and implementations of these are well established for uniform and non-uniform PRF cases. However, these optimal filters have different disadvantages. For example, the optimal filter that is based on eigen filter method, focuses on maximizing clutter attenuation and improvement factor. Since the maximum deviation in passband is not considered, higher ripples can form that forms extra blind speeds. The other optimal filter, that is based on match filtering, considers the best achievable response in return for higher processing power. Also there can be conditions that do not require highest improvement factor. At the beginning of this study, these cases are considered and a flexible solution for different scenarios are thought. Therefore, possible novelty of this work is the flexibility of the design parameters and the usage of different methods for the solution of the staggered PRI MTI filtering. Reasonable values can be obtained for the given stagger ratios without the need of optimization of the stagger periods.

Obtained results throughout the thesis work illustrate the effectiveness of the design techniques. Most of the time, required constraints can be achieved with the designs and better

responses are obtained generally for different performance measures as compared to the designs in the literature.

6.2 Future Work

We will plan to widen the MTI filter design into pulse-Doppler radars by changing the highpass filtering characteristics into bandpass characteristics and design filters for the staggered pulse-Doppler Radars. In addition, these type of bandpass filtering can be implemented in non-uniform Airborne MTI Radars.

By improving run time of the algorithms, it is possible to implement staggered MTI filters in an adaptive manner with the estimation of the clutter covariance matrix. Since the designs present flexible solutions to different cutoff frequency and velocity band requirements.

It is our another plan to implement the techniques in a real time radar simulator by employing the hardware implementations of the proposed non-uniform MTI filter designs.

REFERENCES

- [1] H. Meikle, *Modern Radar Systems*. Artech House, 2001.
- [2] M. Skolnik, *Radar Handbook*, 3rd ed. McGraw-Hill, 2008.
- [3] D. Schleher, *MTI and Pulsed Doppler Radar with MATLAB*. Artech House, 2010.
- [4] D. Barton and S. Leonov, *Radar Technology Encyclopedia*. Artech House, 1998.
- [5] M. Skolnik, *Introduction to Radar Systems*, 3rd ed. McGraw-Hill, 2001.
- [6] W. Zuyin, "Optimal design of clutter rejection filters for MTI system," in *Radar, 2001 CIE International Conference on, Proceedings*, 2001, pp. 475–478.
- [7] "IEEE standard radar definitions," *IEEE Std 686-2008 (Revision of IEEE Std 686-1997)*, pp. c1–41, 21 2008.
- [8] S. Jie, H. You, and T. Xiao-ming, "Adaptive radar clutter suppression based on real data," in *Radar, 2006. CIE '06. International Conference on*, Oct. 2006, pp. 1–4.
- [9] M. Richards, *Fundamentals of Radar Signal Processing*. McGraw-Hill, 2005.
- [10] D. Schleher and D. Schulkind, "Optimization of digital MTI using quadratic programming," in *Acoustics, Speech, and Signal Processing, IEEE International Conference on ICASSP '77.*, vol. 2, May 1977, pp. 849–853.
- [11] P. Prinsen, "A class of high-pass digital MTI filters with nonuniform PRF," *Proc. IEEE*, vol. 61, no. 8, pp. 1147–1148, Aug. 1973.
- [12] H. Hang, "The parameters design method of recursive MTI filter based on pole-zero analyses," in *Microwave and Millimeter Wave Technology, 2004. ICMMT 4th International Conference on, Proceedings*, Aug. 2004, pp. 651–654.
- [13] J. Hsiao, "On the optimization of MTI clutter rejection," *Aerospace and Electronic Systems, IEEE Transactions on*, vol. AES-10, no. 5, pp. 622–629, Sept. 1974.
- [14] M. Arbabian, M. Bastani, and M. Tabesh, "Optimization of PRF staggering in MTI radar," in *Radar Conference, 2005 IEEE International*, May 2005, pp. 602–607.
- [15] M. Ahmadi and K. Mohamedpour, "PRI modulation type recognition using level clustering and autocorrelation," *American Journal of Signal Processing*, vol. 2, no. 5, pp. 83–91, 2012.
- [16] L. Vergara-Dominguez, "Analysis of the digital MTI filter with random PRI," *Radar and Signal Processing, IEE Proceedings F*, vol. 140, no. 2, pp. 129–137, Apr 1993.
- [17] J. Coleman, "Choosing nonuniform tap spacings for a tapped-delay-line filter," *Circuits and Systems II: Analog and Digital Signal Processing, IEEE Transactions on*, vol. 43, no. 4, pp. 298–303, Apr 1996.

- [18] P. Prinsen, "Elimination of blind velocities of MTI radar by modulating the interpulse period," *IEEE Trans. Aerosp. Electron. Syst.*, vol. AES-9, no. 5, pp. 714–724, Sept. 1973.
- [19] J. Hsiao and F. Kretschmer Jr, "Design of a staggered-PRF MTI filter." DTIC Document, Tech. Rep., 1973.
- [20] O. Jacomini, "Weighting factor and transmission time optimization in video MTI radar," *IEEE Trans. Aerosp. Electron. Syst.*, vol. AES-8, no. 4, pp. 517–527, July 1972.
- [21] H. Tao, G. Liao, and L. Wang, "Integer coded genetic algorithm design of staggered sampling MTI," in *Neural Networks and Signal Processing, 2003. Proceedings of the 2003 International Conference on*, vol. 1, Dec. 2003, pp. 558–562 Vol.1.
- [22] T. Haihong, L. Nintao, and L. Guisheng, "Novel filter design for detecting weak targets of slow speed out of multi-mode clutters," in *Radar, 2006. CIE '06. International Conference on*, Oct. 2006, pp. 1–4.
- [23] K. Arora, "Class of optimum design of MTI filters for clutter rejection," *IEEE Trans. Aerosp. Electron. Syst.*, vol. 126, no. 12, pp. 517–527, December 1979.
- [24] S. Prasad, "Class of min-max digital m.t.i. filters for clutter rejection," *Electronic Circuits and Systems, IEE Journal on*, vol. 1, no. 6, pp. 217–223, November 1977.
- [25] G. Ewell and A. Bush, "Constrained improvement MTI radar processors," *IEEE Trans. Aerosp. Electron. Syst.*, vol. AES-11, no. 5, pp. 768–780, Sept. 1975.
- [26] B. Bidégaray-Fesquet, L. Fesquet *et al.*, "A fully non-uniform approach to FIR filtering," in *SAMPTA'09, International Conference on Sampling Theory and Applications*, 2009.
- [27] K. Busawon and W. Ng, "Digital filter design using non-uniform sampling," in *Proceedings of the 6th conference on Applications of electrical engineering*. World Scientific and Engineering Academy and Society (WSEAS), 2007, pp. 120–124.
- [28] H. Dammak, M. Ben-Romdhane, and K. Grati, "Software embedded implementation of real time non uniform sampling filter," in *Design Technology of Integrated Systems in Nanoscal Era, 2009. DTIS '09. 4th International Conference on*, April 2009, pp. 86–89.
- [29] E. Angelidis and J. Diamessis, "A novel method for designing FIR digital filters with nonuniform frequency samples," *Signal Processing, IEEE Transactions on*, vol. 42, no. 2, pp. 259–267, Feb. 1994.
- [30] L. Fesquet and B. Bidégaray-Fesquet, "IIR digital filtering of non-uniformly sampled signals via state representation," *Signal Process.*, vol. 90, no. 10, pp. 2811–2821, Oct 2010.
- [31] L. Fesquet, G. Sicard, and B. Bidégaray-Fesquet, "Targeting ultra-low power consumption with non-uniform sampling and filtering," in *Circuits and Systems (ISCAS), Proceedings of 2010 IEEE International Symposium on*, June 2010, pp. 3585–3588.
- [32] D. Marimon, "Fast non-uniform filtering with symmetric weighted integral images," in *Image Processing (ICIP), 2010 17th IEEE International Conference on*, Sept. 2010, pp. 3305–3308.

- [33] D. Scholnik and J. Coleman, "Periodically nonuniform bandpass sampling as a tapped-delay-line filtering problem," in *Acoustics, Speech, and Signal Processing, 1999. Proceedings., 1999 IEEE International Conference on*, vol. 3, Mar 1999, pp. 1721–1724 vol.3.
- [34] Z. Jin, X.-D. Li, and J. King, "Non-uniform time sampling FIR filter design based on least-squares criterion," *Electronics Letters*, vol. 46, no. 23, pp. 1544–1545, 11 2010.
- [35] S. Haykin and J. Boulter, "Response of a recursive M.T.I. filter to inputs with staggered P.R.F." *Electronics Letters*, vol. 7, no. 14, pp. 415–416, 1971.
- [36] S. Gilon and A. Venetsanopoulos, "Design of MTI radar on the basis of detection probability," *Aerospace and Electronic Systems, IEEE Transactions on*, vol. AES-15, no. 1, pp. 106–118, Jan. 1979.
- [37] S.-P. Wu, S. Boyd, and L. Vandenberghe, *Applied Computational Control Signal and Communications*. Birkhauser, 1997, ch. 1: FIR Filter Design via Spectral Factorization and Convex Optimization, pp. 1–33.
- [38] H. Thomas and T. Abram, "Stagger period selection for moving-target radars," *Electrical Engineers, Proceedings of the Institution of*, vol. 123, no. 3, pp. 195–199, March 1976.

APPENDIX A

FILTER WEIGHTS FOR COMPARISON WITH SELECTED STUDIES

Table A.1: Staggered MTI Filter Weights for Comparison with Hsiao's Study

	\mathcal{W}	Normalized Filter Coefficients
Hsiao	-	0.0809, -0.3011, 0.5846, -0.6173, 0.3796, -0.1795, 0.0600
Ls	48800	0.1003, -0.3418, 0.6104, -0.6036, 0.3382, -0.1424, 0.0390
Cvx	3.031e14	-0.0616, 0.2717, -0.5692, 0.6293, -0.4009, 0.1939, -0.0633
MinMax	7510	0.0793, -0.2969, 0.5753, -0.6174, 0.3872, -0.1967, 0.0693
MinMax-IF	-	-0.0760, 0.2924, -0.5753, 0.6204, -0.3886, 0.1936, -0.0665

Table A.2: Staggered MTI Filter Weights for Comparison with Jacomini's Study

	\mathcal{W}	Normalized Filter Coefficients
Jacomini	-	0.0625, -0.3517, 0.7363, -0.5658, 0.0975, 0.0244
Ls	148500	0.0760, -0.3731, 0.7290, -0.5562, 0.1188, 0.0054
Cvx	1000	0.0093, -0.1388, 0.5435, -0.7270, 0.3887, -0.0756
MinMax	10000	0.0018, -0.1200, 0.5317, -0.7355, 0.3956, -0.0737
MinMax-IF	-	-0.0347, 0.2386, -0.6404, 0.6747, -0.2743, 0.0362

Table A.3: Staggered MTI Filter Weights for Comparison with Ewell's Study

	\mathcal{W}	Normalized Filter Coefficients
Ewell	-	0.3547, -0.8649, 0.2982, 0.1930
Ls	65790	0.5899, -0.6651, -0.2840, 0.3592
Cvx	18740000	0.4913, -0.8301, 0.2476, 0.0913
MinMax	6000	-0.2166, -0.1616, 0.8431, -0.4649
MinMax-IF	-	0.2733, -0.7196, 0.6155, -0.1692,

Table A.4: Staggered MTI Filter Weights for Comparison with Zuyin's Study

	\mathcal{W}	Normalized Filter Coefficients
Zuyin	-	0.0828, -0.3096, 0.6440, -0.6355, 0.2748, -0.0564
Ls	4055000	0.1305, -0.4080, 0.6774, -0.5640, 0.1961, -0.0320
Cvx	1000	-0.0728, 0.2819, -0.6228, 0.6533, -0.3093, 0.0698
MinMax	10000	0.0833, -0.2957, 0.6182, -0.6454, 0.3175, -0.0780
MinMax-IF	-	-0.1282, 0.3837, -0.6489, 0.5886, -0.2554, 0.0601